FHWA-NJ-2007-007

Concrete Shrinkage Analysis for Bridge Deck Concrete

FINAL REPORT
December 2007

Submitted by

Hani Nassif [1]
Associate Professor

Kagan Aktas[1]
Research Assistant

Nakin Suksawang[2]
Assistant Professor

Husam Najm [1]
Associate Professor

[1]Dept. of Civil & Environmental Engineering
Rutgers, The State University
Piscataway, NJ 08854-8014

[2]Dept. of Civil Engineering and Construction
Florida International University
1501 West Bradley Ave.
Miami, FL 61625

NJDOT Research Project Manager
Mr. Edward S. Kondrath

In cooperation with

New Jersey
Department of Transportation
Bureau of Research
And
U. S. Department of Transportation
Federal Highway Administration

DISCLAIMER STATEMENT

"The contents of this report reflect the views of the author(s) who is (are) responsible for the facts and the accuracy of the data presented herein. The contents do not necessarily reflect the official views or policies of the New Jersey Department of Transportation or the Federal Highway Administration. This report does not constitute a standard, specification, or regulation."

This document is disseminated under the sponsorship of the Department of Transportation, University Transportation Centers Program, in the interest of information exchange. The U.S. Government assumes no liability for the contents or use thereof.

TECHNICAL REPORT
STANDARD TITLE PAGE

1. Report No. FHWA NJ-2007-007	2.Government Accession No.	3. Recipient's Catalog No.
4. Title and Subtitle Concrete Shrinkage Analysis of Bridge Deck Concrete		5. Report Date December 2007 6. Performing Organization Code CAIT/Rutgers
7. Author(s) Hani Nassif, Kagan Aktas, Husam Najm, and Nakin Suksawang		8. Performing Organization Report No.
9. Performing Organization Name and Address Dept. of Civil & Environmental Engineering Center for Advanced Infrastructure & Transportation (CAIT) Rutgers, The State University Piscataway, NJ 08854-8014		10. Work Unit No. 11. Contract or Grant No.
12. Sponsoring Agency Name and Address New Jersey Department of Transportation PO 600 Trenton, NJ 08625 Federal Highway Administration U.S. Department of Transportation Washington, D.C.		13. Type of Report and Period Covered Final Report 01/31/05 – 06/30/2007 14. Sponsoring Agency Code

15. Supplementary Notes

16. Abstract

Infrastructure facilities constitute a major part of the national investment. According to the National Bridge Inventory (NBI) (Federal Highway Administration, 2004) [1] there are more than 594,470 bridges and about 150,981 (25.4%) of them are structurally deficient or obsolete. Major decisions are needed to allocate the limited funds available for repair, rehabilitation, and replacement. Over the last decade, the use of High Performance Concrete (HPC) has emerged as an important alternative to deal with deteriorating infrastructure. The concept of HPC in the USA was developed under the Strategic Highway Research Program (SHRP) contract C205. At the end of SHRP program, a major thrust was made for implementation of results. The Federal Highway Administration (FHWA) has initiated programs for the design and construction of HPC bridges and pavements with the aim of reducing both initial construction costs and long-term maintenance costs.

A test has been developed by AASHTO (PP 34-99, The Passive or Restrained Ring Test) that compares the relative cracking potentials of concrete mixtures. This cracking tendency was performed on 16 concrete mixes used for bridge decks by NJDOT to identify those that would exhibit high potential for cracking. Although cracking of bridge decks can be attributed to various causes, this study provided a comparative classification of the cracking potential of each mix. A correlation of cracking potential with various parameters is also established. Results show that mixes with high Coarse Aggregate (CA) to Fine Aggregate (FA) ratio (i.e., CA/FA >1.48) and a CA minimum weight of 1800 lb/cu.yd have lower potential for cracking. It is also shown that rate of free shrinkage correlates directly with the rate of restrained shrinkage, and a limit of 450 micro strain for free shrinkage at 56 days is recommended to reduce the cracking potential of concrete mixes.

17. Key Words Bridge Deck Cracking, Restrained Shrinkage, HPC,	18. Distribution Statement		
19. Security Classif (of this report) Unclassified	20. Security Classif. (of this page) Unclassified	21. No of Pages	22. Price

Form DOT F 1700.7 (8-69)

Acknowledgements

The authors would like to thank the New Jersey Department of Transportation (NJDOT) and staff for their help and support of this project: Camille Crichton-Sumners, Research Bureau Manager, Edward S. Kondrath and Tony Chmeil (Retired), NJDOT project manager(s), Jose Lopez and Richard Dunne, from the Bureau of Structural Design, Eileen Sheehy, Bob Skalla, and Fred Lovett, from the Bureau of Materials, for their help and assistance throughout the project. Also, the assistance of students Chris Ericsson, Michael Boxer, Eric Rundstrom, Kyle Kelly, Wai Wah (Derek) Lam, John Montemarano, and Michael Yu are thankfully acknowledged.

TABLE OF CONTENTS

LIST OF FIGURES

LIST OF TABLES

EXECUTIVE SUMMARY

Concrete cracking remains to be one of the most critical issues that lead to deterioration of bridge decks, increasing maintenance costs and shortening the overall service life. Cracks allow water and chemicals to penetrate into the concrete which increases the damage from freeze and thaw cycles, leaving the reinforcing steel exposed to corrosion. Cracking in bridge decks takes place due to a combination of several factors. These include but are not limited to the concrete mix design and its properties, actual design of the bridge, magnitude of loads on the bridge, construction practices, and temperature effects.

Concrete, by its nature, undergoes volume changes during the course of its life time. These changes are a result of its chemical and physical composition, curing history, and environmental conditions under drying. If concrete is not restrained, these volume changes do not create any stress in the concrete leading to a length change only. If, however, concrete is restrained from shrinking freely, internal tensile stresses will develop. When the level of restraint is high enough, it will induce stresses that exceed the tensile capacity of concrete which will lead to cracking.

Minimizing the factors that lead to cracking of concrete is one of the easiest ways of extending service life of bridges. Since control over loading, temperature cycles and restraints in a deck are not easily controllable, choosing concrete mixes that have less potential to crack under restrained conditions remains one of the best alternatives for reducing cracking. The amount of cement and cementitious materials, type and amount of aggregates used, water to cementitious materials ratio, and various chemicals used all have effects on properties of concrete that affect its behavior under restrained conditions. Therefore, identifying these effects and accurately defining the potential of cracking of concrete mixes are vital for controlling cracking.

The primary purpose of this research is to define and compare the cracking potential of common high performance concrete (HPC) mixes used in bridge decks by the New Jersey Department of Transportation (NJDOT). This study will provide guidance and recommendations to selecting HPC mixes with lower cracking potentials. Basic properties to be investigated include compressive strength, tensile splitting strength, modulus of elasticity, unrestrained (i.e., free) drying shrinkage and restrained shrinkage. A total of 16 mixes from various bridge deck projects were selected and provided by NJDOT. The water to binder ratio ranges between 0.34 – 0.40 and the majority of the mixes have slag as a replacement for cement. Mixes are grouped according to the cement replacement percentages. Two main groups are 30% and 40% slag replacement. Remaining mixes have varying percentages of slag, silica fume and fly ash as cementitious replacements. Also, the source of coarse and fine aggregates, as well as the type and manufacturer of chemical admixtures are varied within groups of

mixes. This forms a complex matrix of variables by which the effects of the most sensitive parameters can be determined.

To determine the mechanical properties of the mixes, standard ASTM tests were conducted. To measure the cracking potential of each mix a modified version of the AASHTO PP34-99, restrained shrinkage ring test, was utilized. The raw materials needed for the mixes were provided by NJDOT Materials Laboratory from various suppliers. The mixes were mixed in the laboratory and various tests were conducted until cracking was observed in the restrained shrinkage test set-up or to a maximum duration of 91 days in cases where no cracking was observed.

Out of the sixteen mixes tested, eleven were observed to crack under restrained shrinkage. To identify the causes of cracking as well as the effects of the many variables that contribute to shrinkage cracking, various comparisons were made. These comparisons include, correlation of restrained shrinkage cracking with the coarse aggregate to fine aggregate (CA/FA) ratio, total coarse aggregate content in a mix, total cementitious materials used in a mix, mechanical properties of a mix, and most importantly the rate and total amount of shrinkage a mix experiences.

The results show that the coarse aggregate content as well as the CA/FA ratio have the greatest effect on both free and restrained shrinkage. There was a significant reduction in free shrinkage of mixes having high CA/FA ratios and relatively high coarse aggregate contents (e.g., 1800 lbs/cy) compared to similar mixes with lower ratios and total coarse aggregate content. Also, the five mixes that did not exhibit any cracking in the restrained shrinkage test all had coarse aggregate contents of 1850 lbs/cu.yd or more and the CA/FA ratio was equal to or higher than 1.48.

The rate of free shrinkage until cracking was another primary factor which correlates directly with the restrained shrinkage rate and cracking-age for a given mix. It was also found that the ultimate amount of shrinkage observed in a mix affects the shrinkage rate which in turn affects the cracking behavior. Mixes that did not experience cracking were observed to have less than 400 microstrains in free shrinkage at 56 days and the mixes that experienced cracking at a later age, had, at 56 days, between 400 and 500 microstrains in free shrinkage. Other factors that were found to increase cracking potential were increased silica fume percentages, high cementitious material contents, and properties of the coarse aggregate sources used in mix design.

In the light of observations made in this study, to reduce the potential of restrained shrinkage cracking of an HPC mix, coarse aggregate content should be increased to give a high CA/FA ratio (preferably higher than 1.50). This would help in reducing the ultimate shrinkage and also would reduce the rate at which shrinkage takes place.

Mixes that experience more than 500 micro-strains of free shrinkage at 56 days are not recommended for use in bridge decks, since all such mixes cracked under restrained ring test shortly after initiation of drying. Also, maximum percentage of silica fume utilized in a mix should be limited to 5 percent.

Introduction

HPC became increasingly popular in the United States especially for bridge decks. HPC is used to enhance the durability of concrete [1-6] by the addition of pozzolanic materials, i.e. silica fume, fly ash, and slag. All three are used as cement replacement in combination of silica fume and fly ash or silica fume and slag, or a combination of all three. The pozzolanic material reacts with the calcium hydroxide [$Ca(OH)_2$] or the weak link between the aggregate particles and the hydrated cement paste to form calcium silicate hydrates (CSH) gel or strong cementing material. However, problems with cracking have been observed by many contractors. The cracking can be combination of many factors and one of these factors is shrinkage.

There are four main types of shrinkage cracks: 1) autogenous, 2) drying, 3) carbonation, and 4) plastic shrinkage. Autogenous shrinkage is associated with the loss of water during the hydration process of concrete at early-age and is considered relatively small comparing to drying shrinkage. However, for HPC, autogenous shrinkage contributes quite significantly to the total shrinkage and in some cases (HPC with high volume silica fume) it could be as high as drying shrinkage[7-10]. Thus, the autogenous shrinkage could no longer be disregarded for HPC. Drying shrinkage is the volume change in concrete due to drying and it occurs as soon as the concrete is exposed to air. Drying shrinkage is unavoidable but the amount of drying shrinkage could be controlled by reducing the amount of cementitious material in the mix. Carbonation shrinkage occurs when the cement hydrate reacts with carbon dioxide present in air. Carbonation shrinkage is very small and only occurs at early-age of fresh concrete. It could be controlled by covering the fresh concrete with protective plastic so that the cement hydrate would not react with carbon dioxide. Plastic shrinkage occurs when the rate of evaporation exceeds the bleeding rate or when the concrete dries too fast due to the environmental conditions. Plastic shrinkage is more critical for HPC because HPC has a very low bleeding rate. However, it could be controlled by applying the proper curing practice, i.e. moist curing[10].

The shrinkage cracks observed in bridge decks are combinations of these types of shrinkage, (i.e., early-age (autogenous, plastic, and carbonation) and long-term drying shrinkage), and can be measured under either restrained or unrestrained conditions. The unrestrained (or free) shrinkage is an easy measurement where the concrete specimen is cast in a prism mold and the shrinkage is obtained by measuring the change in length between the top and the bottom of the specimen using any measuring device. On the other hand, restrained shrinkage requires secondary component to

restrain the concrete specimen. There are many methods that are developed to restrain the concrete[11-19], but only the ring method is adopted by AASHTO (PP 34-99) because of its simplicity. However, this test is not as simple in comparison with the free shrinkage test because it does not describe the properties of concrete quantitatively. It is an indicator of the age at which the concrete will crack but not the cracking strain to compare with the cracking capacity of the concrete. Thus, an attempt is made in this project to quantify the strain and stress development in the restrained concrete ring as well as determining the relationship between the unrestrained (free) and restrained shrinkage. If such a relationship is established, the unrestrained strain shrinkage can be used thereafter for quality control. The Rutgers Team has been successful in developing instrumentation techniques for this testing method. The instrumentation allows accurate prediction of the strain prior to and at cracking, age of cracking, and a correlation with the other mechanical properties of the concrete such as splitting tensile strength, elastic modulus, and compressive strength.

OBJECTIVES

The primary objectives of this research project are: 1) evaluate the restrained shrinkage properties of HPC mixes currently used for bridge deck applications in New Jersey using the AASHTO PP34-99 test method and 2) provide a comparison of their relative cracking potential.

LITERATURE SEARCH

Literature search indicated that there are several published papers that investigated and used the restrained ring test to evaluate the cracking potential of conventional concrete, HPC, fiber reinforced concrete, and latex modified concrete[11-20]. The effect of pozzolanic materials on the cracking potential of HPC was investigated by Li et. al. (1999)[11], Wiegrink et. al. (1996)[15], and Collins and Snjayan (2000)[19]. From their observations, it was concluded that concrete containing pozzolanic materials, i.e., silica fume, fly ash, and slag, exhibit higher crack widths than conventional concrete. Moreover, concrete containing corrosion inhibitors also exhibit higher crack widths than conventional concrete[11]. The effect of aggregate on cracking potential was studied by Mokarem et al (2003)[16]. They concluded that concrete mixtures with limestone exhibited the greatest cracking potential followed by gravel and diabase.

In order to study the behavior of concrete under restrained conditions, one has to understand the reasons behind volume changes of concrete. Volume change is simply defined as an increase or decrease in volume. The volume changes in concrete are generally expressed in a linear direction. This is due to the fact that in majority of exposed concrete elements one or two dimensions are much smaller than the third, and the effect of volume change is greatest in the third dimension. Most commonly, the volume change in concrete is contraction as a result of temperature and moisture

changes and this is called shrinkage of concrete. Shrinkage in concrete begins shortly after it is cast and could continue for a number of years. Chronologically types of shrinkage can be listed as plastic shrinkage, thermal shrinkage, autogenous shrinkage, and drying shrinkage.

Types of Shrinkage

Shrinkage of concrete begins shortly after it is cast. Depending on the characteristics and proportions of the mix design, different types of shrinkage will have varying effects. The types of shrinkage and their effects are discussed below.

Plastic Shrinkage

Plastic shrinkage refers to change in length that occurs while the concrete is still fresh, before hardening. The driving force behind this is rapid evaporation of water from the exposed surface of concrete due to environmental agents, such as wind, relative humidity and temperature. The critical condition is when the rate of evaporation is greater than the rate of bleeding. Wind speeds in excess on 5 mph, low relative humidity and high ambient temperatures increase the rate of evaporation and therefore the probability of having plastic shrinkage cracks.

Concrete mixtures with a reduced rate of bleeding, like HPC, are more susceptible to plastic shrinkage than regular concrete mixes. Any factor that delays the setting of concrete also increases the possibility of shrinkage cracking. Fogging and wet burlap curing (protected by plastic sheets) eliminate plastic shrinkage.

Thermal Shrinkage

Hydration of cement is accompanied by a generation of heat which results in an increase in the temperature of concrete. Soon after setting, when final dimensions of a concrete element or mass become fixed, this temperature starts to decrease causing an overall shrinkage in the concrete element. The amount of shrinkage depends on many factors such as, size and volume of concrete, type of cement, thermal properties of the aggregates used, ambient temperature and the placement temperature of concrete. For elements that are relatively thin in one dimension, such as bridge decks, the generated heat is dissipated easily and the rise in concrete temperature is negligible. Therefore, the shrinkage resulting form this temperature change is also negligible.

Autogenous Shrinkage

Visible dimensional change of cement paste, mortar, or concrete caused by hydration of cement is called autogenous shrinkage. As cement hydrates a very fine pore network is formed within the hydrated cement as a result of an absolute volume change. This network starts to drain water from the coarse capillaries created during mixing of concrete. If there is no external water supply, from curing or bleeding, the drying outer capillaries are emptied as if the concrete were drying. This is referred to as self-desiccation. This is different from drying in the sense that all the water actually remains in the concrete, but it migrates to the very fine pores created as a result of hydration.

In case of high-performance concrete (HPC) with low water to cementitious materials ratios (w/c), there is significantly more cement and less water. As a result the pore network is composed of very fine capillaries (Aitcin 1998). As soon as hydration begins self-desiccation starts, and the menisci rapidly develops within the fine capillary system in the absence of external water supply. When most of the cement particles start to hydrate simultaneously, the drying of the capillaries result in high tensile stresses which in turn results in shrinkage of the cement paste. This is basically the driving force behind autogenous shrinkage. If an external water source is present during significant portion of the hydration process, the external capillaries will not dry out which means that no menisci will develop. As a result, the tensile stresses that result in shrinkage will not exist, eliminating autogenous shrinkage. This is true as long as the pores are interconnected to the external water source. Autogenous shrinkage continues as long as the cement hydrates. Autogenous shrinkage increases with a decrease in w/c and an increase in cement content. It is mostly observed in concrete with w/c ratios less than 0.42 (Holt 2001)

Drying Shrinkage

Hardened concrete will change volume due to the moisture changes within its capillary pore system. The driving source of drying shrinkage is the evaporation of free water from this capillary pore system. Drying takes place from the surface that is exposed to the air and it only continues if the relative humidity of air is less than the humidity within the capillary pores. The loss of water due to evaporation is progressive, from outside to inside, and proceeds at a decreasing rate depending on the properties of the concrete considered. Some of these properties include porosity of the concrete, size and shape of the pores and their continuity, surface to volume ratio of the element considered and ambient relative humidity. Drying shrinkage may continue for a number of years depending on these properties. Large volume elements will experience lower shrinkage over a longer period of time where as elements with large surface areas will tend to shrink more in a shorter period of time. This is particularly important for bridges since the surface exposed to drying is much larger and this can cause significant drying shrinkage.

Drying shrinkage alone would not be of any concern if the concrete was allowed to shrink freely. However, restraints imposed on elements subject to drying shrinkage will cause internal tensile stresses to be developed. The magnitude of these stresses increases with the amount of restraint, and if the stresses exceed the tensile capacity of a particular mix, cracks will develop. When no cracking is present, stresses that are developed are locked inside the element and this will reduce the effectiveness of the element under service loads. Therefore, it is very important to select and design mixes that are less likely to shrink.

Factors Affecting Shrinkage

Major parameters that influence the shrinkage of concrete are aggregate type and volume, cement content and type, and water to binder ratio. Other parameters that can affect shrinkage include types of cementitious materials, various admixtures, environmental conditions, and curing history of concrete.

Aggregate type and volume in a concrete mix greatly affects the shrinkage behavior. Coarse aggregate physically restrains the shrinkage of hydrating cement paste. Hard, rigid aggregates are difficult to compress and provide more restraint to shrinkage than softer, less rigid aggregates. Avoiding aggregates that have high drying shrinkage properties and aggregates that contain excessive amounts of clay can also reduce the shrinkage of concrete. Quartz, granite, feldspar, limestone, and dolomite aggregates generally produce concretes with low drying shrinkage (ACI Committee 224). Volume of coarse aggregate in a mix also effects shrinkage significantly. As the amount of coarse aggregate is increased the restraint on the shrinking cement paste is also increased. This reduces the overall shrinkage of a given concrete mix. In a study by Hansen and Almudaiheem (1987) an increase of aggregate volume from 65% to 70% resulted in a decrease of 18% in drying shrinkage. Pickett (1956) also reported a 20% decrease in drying shrinkage (for mixes with the same water to binder ratio) caused by an increase in aggregate volume from 71% to 74%.

The other major factor affecting the shrinkage behavior of concrete is the cement paste itself. Controlling the cement and water content, thus the water to binder ratio, can have a significant effect on early and total shrinkage. Increasing the cement content at a constant water to binder ratio will increase the drying shrinkage since amount of paste that hydrates is increased. Increase in water content also increases drying shrinkage since amount of evaporable water in unit volume increases. Therefore, lowering the water to binder ratio, while keeping the amount of cement low, can help lower total shrinkage.

Cement type and fineness also have an effect on shrinkage. Over the past years chemistry and fineness of cements has changed. Due to improved techniques and

competition within the industry cements are blended finer (Krauss and Rogalla 1996). Finer cement particles react much more quickly and therefore can increase autogenous shrinkage considerably. Also, finer cement particles mean a finer pore structure in the concrete, which causes higher capillary stresses that increases the shrinkage (Chariton and Weiss 2002). On the other hand larger cement particles do not undergo full hydration and the reaction takes place much more slowly. This reduces the hydration temperatures as well as the autogenous shrinkage. Unhydrated cement particles act as restraints to the shrinking paste, just like coarse aggregates, which reduces shrinkage even more. Krauss and Rogalla (1996) point out that many researches have found coarse ground Type II cement to reduce shrinkage.

Modern concrete mixes, especially HPC, contain cementitious materials such as fly ash, slag and silica fume as a replacement for cement to increase cost efficiency and to achieve standards that are related to durability. The addition of these materials has effects on early and total shrinkage of concrete. Silica fume which is a highly reactive pozzolan increases the rate of hydration, temperatures during hydration and also the autogenous shrinkage of concrete. Paillere, A.M., Buil, M. and Serrano (1989) report that concrete with silica fume does not swell during hydration and shrinkage is immediate on the contrary to regular concrete. This greatly increases the susceptibility of concrete to plastic shrinkage if curing is not adequate. McDonald (1992) also claimed that silica fume increases early age shrinkage and shrinkage related cracking. Another supplementary cementitious material is fly ash. Fly ash reacts much more slowly compared to cement and this reduces the hydration temperatures as well as the strength gain of concrete. There are conflicting results in literature about the performance of fly ash concretes under shrinkage. Gebler and Klieger (1986) compare the drying shrinkage of class C and F type fly ashes to a control mix and conclude that within normal dosages fly ash has no significant effect on drying shrinkage. The dosage used in the study was 25% of the total cementing material. Nasser and Al-Manaseer (1986) studied the shrinkage and creep of concrete containing 50 percent fly ash. The shrinkage results show about 11 percent increase compared to ordinary Portland cement concrete. Sivasundaram, Carette, and Malhotra (1989) study the properties of concrete with high volume Class F fly ash of low water-cement ratio (0.31). The properties in this study are characterized by strength, modulus of elasticity, drying shrinkage, freezing and thawing durability, carbonation, and permeability to chloride ions. The drying shrinkage performance was equally good and in some cases better than control specimens.

Ground granulated blast furnace slag, also called cement slag, is the third most common supplementary material available. Average blaine fineness of slag particles is around 45 microns and compared to fly ash slag is slightly more reactive. Three grades, namely Grade 80, 100, 120, are classified by their reactivity. Shrinkage behavior of concrete that constitutes slag changes depending on the amount of cement replacement. Just as in the case of fly ash, there are conflicting reports about the effects of slag on total shrinkage in literature. However, there is an agreement that slag

significantly increases early age autogenous shrinkage. Saric-Coric and Aitcin (2003) studied the effects of curing conditions on shrinkage for concrete specimens containing 20, 30, 50, and 80% slag replacements. They reported that when under sealed conditions, concrete containing slag presented a much higher autogenous shrinkage than pure Portland cement concretes. The magnitude of shrinkage increased with increasing slag percentages. At the same time they found out that 7 day moist cured samples containing slag presented a smaller total shrinkage (autogenous and drying) than samples from pure Portland cement. Another study conducted by Collins and Sanjayan (2000) reported that concrete containing slag has 1.6 to 2.1 times greater drying shrinkage than regular concrete. This study was composed of four mixes each having a water/binder ratio of 0.5. A control mix which had only ordinary Portland cement was used to compare the unrestrained and restrained shrinkage behavior of slag concretes.

The amount and type of curing can affect the rate and ultimate amount of shrinkage. HPC must be cured quite differently from regular concrete. If HPC is not water cured immediately after placement it can be subject to severe plastic shrinkage, and later it also develops excessive autogenous shrinkage due to its rapid hydration reaction (Aitcin 1997). The critical curing period to prevent or minimize autogenous shrinkage is 12 to 36 hours after casting. If there is continuous water supply during this period autogenous shrinkage can be eliminated. However, when the pore structure of the concrete used is very fine surface water can not reach the inner parts of the concrete. Thus some autogenous shrinkage may develop. Saric-Coric and Aitcin (2003) studied the effect of curing conditions on shrinkage of concrete containing various amounts of slag. Saric-Coric and Aitcin report that total shrinkage of all mixes were reduced when 7 days moist curing was applied. The difference was due to the elimination of autogenous shrinkage in the presence of constant water supply. Although curing does not affect the magnitude of drying shrinkage it slows the rate at which it takes place. After several days of moist curing most of the cement particles at the surface reaches full hydration. Therefore the concrete develops its compact microstructure which slows down the process of evaporation of water.

Most chemical admixtures have little effect on shrinkage. Air entrainment has little or no effect on drying shrinkage (Neville 1996). Water reducing admixtures can increase shrinkage; especially the ones that contain an accelerator to counteract the retarding behavior of the admixture. Superplasticizers also have little effect on shrinkage. A study conducted by Whiting and Dziedzic (1992) compared three different concrete mixtures with different superplasticizers against a control mix with no admixtures. All four mixes had very close drying shrinkage amounts at the end of 32 weeks. However, the dosage of these admixtures can have an effect. A study conducted by Bisonnette et al. (2002) showed that melamine and naphthalene-base superplasticizers had an effect on early volume changes of concrete. As their addition rate was increased, shrinkage rate and ultimate shrinkage was also observed to increase.

Although environmental conditions do not affect the ultimate shrinkage of concrete, they play an important role on the rate at which evaporation takes place. This affects the rate at which shrinkage takes place. As relative humidity decreases it is common knowledge that it increases the rate of drying. Higher temperatures have the same effect. The importance of ambient conditions come into play while casting and curing period of concrete. If adequate curing is not provided, high temperatures coupled with low relative humidity and wind can cause excessive plastic shrinkage.

Ring Test

Many methods have been developed to test the performance of cement mortar and concrete under restrained conditions. These include flat panel test, linear restrained shrinkage test, and restrained shrinkage ring test. Restrained shrinkage ring test has been the most popular due to its simplicity and relatively low cost.

Background

In the restrained shrinkage test, concrete is cast around an inner steel ring, such that as the concrete shrinks, a compressive stress is developed in the steel ring. This is balanced by a tensile stress in the concrete ring. If this tensile stress is greater than the allowable tensile stress of the concrete, it cracks. The steel ring can be instrumented with strain gages to signal the time of cracking accurately and monitor the strain development in the steel ring.

The first ring tests were performed by Carlson and Reading (1988) between 1939 and 1942. For many years no standardized testing procedure existed to test for restrained shrinkage behavior of concrete mixes. Starting in the early 90s extensive research projects were undertaken to assess and identify the causes of transverse bridge deck cracking. One of most important factors was identified as shrinkage of concrete and cracking under restrained conditions. There was a need to evaluate the cracking tendency of different concrete mixes to choose the concrete design that was least likely to crack under restrained conditions. As a result, the restrained shrinkage ring test which was utilized as a part of NCHRP Project C12-37 was proposed for adoption by The American Association of State Highway and Transportation Officials (AASHTO) in NCHRP Report 380. In this report Krauss and Rogalla (1996) discussed the usefulness of the proposed test. The major advantage of the ring test is that it accounts for all of the material factors that influence shrinkage cracking from the time of casting. It simultaneously considers stress development, dimensional changes and creep at early ages therefore it does not require complex calculations or assumptions of early concrete behavior. Also, the test is simple to execute and the apparatus is inexpensive. Most importantly, stresses developed in the restrained test samples closely simulate those developed by real structures. The amount of restraint can be modified by changing the

dimensions of the test to simulate effects of different degrees of restraint depending on the structures under consideration. For bridge deck applications Weiss and Shah (2002) stated that the concrete ring simulates an infinitely long deck which is partially restrained from shrinking.

In 1998 AASHTO proposed the ring test as a provisional standard as "AASHTO PP34-98: Standard Practice for Estimating the Cracking Tendency of Concrete." In 2006 AASHTO has balloted this test to make it a full standards. In 2004, The American Society for Testing and Materials (ASTM) approved "C 1581 – 04: Standard Test Method for Determining the Age at Cracking and Induced Tensile Stress characteristics of Mortar and Concrete under Restrained Shrinkage"

AASHTO Ring Test

This test covers the determination of the cracking tendency of restrained concrete specimens. It is used to determine the effects of variations in the properties of concrete as related to the time-of-cracking of concrete when restrained. These variations might include aggregate type and gradation, cement type, cement content, water content, mineral and chemical admixtures. Actual cracking in service depends on many factors and therefore this method is only used for comparative analysis of concrete mixtures and to aid in the selection of mixes that are less likely to crack. The test can be modified to evaluate other factors such as curing time and methods, evaporation rate and temperature.

The procedure consists of casting a 76 mm (3 in.) thick concrete annulus around a steel ring with a wall thickness of 12.7 mm $\pm$ 0.4 mm ($1/2$ in $\pm$ $1/64$), an outside diameter of 305 mm (12 in.), and a height of 152 mm (6 in.). The inner and outer surfaces of the ring should be machined smooth, round and true, and polished. The outer mold has a 457 mm (18 in.) diameter which produces the required 3 in wall thickness. Four foil strain gages (FSG) are instrumented at mid-height of the inner surface of the steel ring so that abrupt changes in the steel strain can signal the age of cracking. The strain readings are recorded by using a data acquisition system (DAS) which is capable of recording strains every 30 minutes. The outer mold is removed from the concrete ring at 24 $\pm$ 1 h and after curing period the top and bottom surfaces of the concrete ring is sealed to allow for drying to place from the circumferential surface. The specimens are stored and monitored in a controlled-environment room with a constant air temperature of 23 ^{0}C $\pm$ 1.7 ^{0}C (73.4 ^{0}F $\pm$ 3 ^{0}F) and a relative humidity of 50 $\pm$ 4 percent. The strain measurements are started in the rings as soon after casting as possible. Every 2 to 3 days, the strain profile is reviewed and the rings are visually inspected. Concrete is considered cracked when a strain decrease of 30 microstrains or more is observed. After cracking, time to cracking is recorded and the rings are monitored for two more weeks. Within this period crack widths are recorded and cracking pattern is characterized.

ASTM Ring Test

This test is very similar to the AASHTO test although it has some differences in size and geometry of the setup. The steel ring used has a wall thickness of 13 ± 0.12 mm (0.5 ± 0.05 in), an outside diameter of 330 ± 3.3 mm (13.0 ± 0.12 in), and a height of 152 ± 6 mm (6.0 ± 0.25 in). The inner and outer surfaces of the ring are machined to produce a smooth surface with a texture of 1.6 micrometers (63 micro inches). The outer mold should have a diameter of 406 ± 3 mm (16.0 ± 0.12 in) to produce a concrete ring with a wall thickness of 38 mm (1.5 in). The size of the steel ring was increased and the thickness of the concrete was decreased to produce higher restraint in a thinner element to reduce to time to cracking. This way results can be obtained much more quickly compared to the AASHTO setup. One drawback of this change in dimensions is that it limits the maximum coarse aggregate size that can be used to 13 mm (0.5 in). The test covers the laboratory determination of the age at cracking and induced tensile stress characteristics of mortar and concrete specimens under restrained shrinkage. The procedure can be used to determine the effects of variations in the proportions and material properties of mortar or concrete on cracking due to both drying and deformations caused by autogenous shrinkage and heat of hydration. These variations can include the source of aggregate, aggregate gradation, cement type and content, water content, supplementary cementitious materials and mineral admixtures. The test is carried out by casting at least three concrete rings with the given dimensions. The inner steel ring should have at minimum 2 strain gages to record the strain development. The strain should be measured by a DAS that is capable of recording at every 30 minutes or less. After samples are cast they are moved into the testing environment within 10 minutes. The testing environment should have a constant air temperature of 23.0 ^{0}C ± 2.0 ^{0}C (73.5 ± 3.5 ^{0}F) and a relative humidity of 50 ± 4%. The specimens are cured with burlap and covered with polyethylene sheets for the first 24 h, after which the molds are removed and the top and bottom of the ring is sealed to allow circumferential drying only. The rings are monitored for at least 28 days under drying, unless cracking is observed earlier. The strain is plotted against time and monitored every 2 to 3 days to check for cracking. If the rings do not crack within 28 days, the test can be stopped and the rate of shrinkage at the termination of the test can be used to determine the cracking potential of the sample.

Previous Work

First ring tests were performed by R. W. Carlson and T.J. Reading from 1939 to 1942. They discussed these tests in a study that investigated the cracking of concrete building walls (Carlson and Reading 1998). The tests were used to explain the influence of resistance of concrete mixtures to cracking on shrinkage cracking in walls. Restrained ring specimens consisted of concrete rings with a radial thickness of 25 mm (1 in.) and a width of 38 mm (1.5 in) cast around steel rings which had an internal diameter of 125 mm (5 in.) and an external diameter of 175 mm (7 in.). The steel was coated with an incompressible paraffin wax layer to eliminate friction between concrete and the steel ring. After casting and initial moist curing, bottom and top sides of the rings were sealed

to permit drying from the outer circumference. Specimens were subjected to drying in environments with relative humidity of 25, 50, and 75 percent. Time of cracking was obtained by periodical visual observation. Companion free shrinkage bars of 300 mm (12 in.) length were also cast to determine the free shrinkage strain at the time of cracking. To simulate the same drying condition as the rings, these bars were allowed to dry from one face only; either the top or the bottom of the specimen. They found that the specimens which were exposed to lowest relative humidity developed the highest stresses and the time to cracking was observed to be much faster than at higher humidity. They also found the type of aggregate had an important effect on the cracking resistance.

Until the development of standardized ring tests many studies incorporated the use of restrained ring specimens. Grzybowski and Shah (1990), while studying the effects of fiber reinforcement on shrinkage cracking made use of a restrained ring test setup. They chose this setup since it was difficult to provide sufficient restraint with linear specimens. They modified the setup used by Carlson and Reading to achieve uniform tensile stresses at the inner and outer surfaces of the concrete ring. The inner and outer diameters of the steel ring they used were 254 and 305 mm (10 and 12 in.), respectively. The concrete that was cast around the steel ring had a thickness of 35 mm (1.38 in.) and a width of 140 mm (5.5 in). They pointed out that for their setup this difference was 10% and that the radial stress in the ring was only 20% of the hoop stresses. With these values in mind they assumed that the concrete is subject to uniform uniaxial tensile stress. Also, they assumed that shrinkage was uniform along the width of the specimen since the width to thickness ratio of the specimen was four. The mix proportions were 1:2:2:0.5 by weight of cement, sand, coarse aggregate and water, respectively. The maximum aggregate size was limited to 9 mm ($3/8$ in.). Steel and polypropylene fibers were also used to test their effects. The concrete was cast around the steel ring using a cardboard tube as an outer mold. The mold was stripped off after 24 hours for regular specimens and 2.5 hours later for early age specimens. Regular specimens were cured for 4 days at 20 ^{0}C and 100% relative humidity, and after 4 days they were stored in a controlled environment with the rest of the specimens at 20 ^{0}C and 40% relative humidity. The top and bottom of the specimens were sealed using a silicon rubber sealer to allow circumferential drying only. In addition to the restrained ring specimens, free ring specimens and two companion free shrinkage blocks measuring 225 x 75 x 25 mm (9 x 3 x 1 in.) were cast for comparison purposes. For manufacturing free ring specimens, a steel inner ring with four removable pieces was used and after de-molding inner surface of the concrete ring was sealed using the same sealer. The authors used a specially designed microscope setup to check for cracking and also for measuring crack widths. Also, they mounted three equally spaced strain gages on mid-height of the concrete ring to monitor strain development. As a result of the study, they found out that addition of fibers did not affect restrained shrinkage cracking but helped in reducing crack widths. They also concluded that free-shrinkage test results of ring specimens were independent of specimen geometry.

Krauss and Rogalla (1996) performed an extensive study on transverse bridge deck cracking. One of the parameters that were investigated included the cracking tendency of typical concrete mixes used in bridge decks subject to restrained shrinkage. The effects of concrete mix design factors such as cement content, water to binder ratio, aggregate type, silica fume addition, fly ash addition, superplasticizers, certain chemical admixtures, and entrained air were studied to determine their effects on cracking. In addition, effects of the evaporation rate, temperature, curing period, casting time and insulation were also taken into account. The geometry of the ring was selected after a finite element analysis, which examined the theoretical shrinkage stresses in the inner steel ring and the restrained concrete ring. Various steel and concrete radii were tested to find the most suitable geometry which would be cheap, practical, and yield reliable results. Their analyses revealed that for steel ring wall thicknesses between 13 and 25 mm ($1/2$ and 1 in.), concrete shrinkage stresses and cracking-tendency are not significantly different, but the stresses in the steel are much greater with decreasing thicknesses. Also, they showed that concrete experiences more stresses as the diameter of the steel ring increases. As a result, they used steel rings with 305 mm (12 in.) outside diameter, 19 mm ($3/4$ in.) wall thickness, and a 152 mm (6 in.) height. The rings were custom machined for the project and were more expensive than regular steel pipe sections. The procedure followed in sample preparation and mixing was very similar to previously discussed ring test setups. Two rings, five 100 x 200 mm (4 x 8 in.) cylinders, and two 75 x 75 x 280 mm (3 x 3 x 11 in.) companion free shrinkage samples were cast for each concrete mixture. All specimens were removed from their forms at 24 hours and placed in a 22 ^{0}C and 50% relative humidity room. The evaporation rate in the controlled environment was approximately 0.15 kg/m^3/hr (0.03 lb/ft^2/hr). The ring specimens were left on the forms and sealed on top with double layer of polyethylene or rubber to allow circumferential drying only. Strain development in the steel rings was monitored using a data acquisition system that collected measurements hourly. The strains were periodically analyzed and the concrete rings were checked for cracks in the event of a sudden change in the strain profile. When a ring cracked the initial crack width was measured and it was monitored for at least one more week. The authors found that the mixes that performed the best under restrained shrinkage were the ones with low cement and water contents. However, these mixes had essentially no slump, and therefore, were not practical. For the remaining mixes cracking tendency decreased with a decrease in cement content. Increasing the water-cement ratio also decreased the cracking tendency. Although free shrinkage of mixes was directly proportional to the cement paste volume, cracking tendency was not. Krauss and Rogalla associated this fact to the complexity of the restrained shrinkage behavior, which is governed by an interaction of shrinkage, strength and moduli development, and early creep. Also, they found out that the type of aggregate has a significant effect on cracking tendency. From the four types of aggregate types, No. 56 crushed limestone performed the best. The rings cast with this material did not exhibit a single distinct crack, but instead minor surface cracks that extended 1 in. towards the steel ring were discovered. Also, a sudden decrease was not experienced in these rings. The authors also experienced earlier cracking in samples that were not cured versus samples that were wet cured. As a result of the study, the Krauss and Rogalla proposed the ring test to AASHTO as a standard method for testing the cracking tendency of concrete.

As discussed before, the proposed test was accepted as a provisional test in 1998. Although it was an affective method in measuring relative likelihood of cracking of different mixes, it did not provide any information on concrete mixes that did not crack. There was a need to quantify the stress development within the concrete. Also, the long times before a visual crack would occur made it a time consuming experiment. The stress development and the time to cracking can all be associated with the geometry of the ring test which determines the amount of restraint on the concrete ring. The geometry also has a profound effect on drying of concrete and the humidity gradient within the concrete ring.

Weiss and Shah (2002) investigated the effect of moisture gradients and specimen geometry on maximum strain development and cracking. They used various ring test arrangements while studying the effects of shrinkage reducing admixtures (SRA) on restrained shrinkage cracking. The authors performed two series of experiments which both incorporated ring specimens of different geometries and drying conditions cast around a solid cylindrical plate with a radius of 150 mm (6 in.). Three different concrete wall thicknesses were selected for the experiment, namely 25, 75, and 150 mm (1, 3, and 6 in.). In the first series of experiments, called short ring series, 30 mm (1.2 in.) high samples were cast and drying was permitted through the top and bottom of the ring by sealing the outer circumference. By doing this a uniform moisture gradient was achieved along the radial direction which would result in uniform shrinkage. Also, free shrinkage specimens of 100 x 100 x 400 mm (4 x 4 x 16 in) dimensions were cast to compare the drying shrinkage of the mixes under investigation. All samples were stored in a controlled environment with 30 ^{0}C and 40% for the duration of the tests. The authors found out that for a given mix the potential for cracking was reduced as the wall thickness of the concrete ring was increased. The difference in cracking potential was related to the geometry since surface to volume ratio and drying shrinkage was same for all samples under consideration. Taking these factors into account and assuming uniform moisture gradient and no radial displacement between the steel and concrete ring Weiss and Shah outlined a procedure to quantify the stresses in the concrete ring. The second phase of the study concentrated on effect of geometry considering moisture profiles using tall ring specimens. The concrete rings used had 150 mm (6 in.) height and they were cast with varying thicknesses to simulate slabs of different thicknesses. The top and bottom of the specimens were sealed and drying was permitted form the outer circumference. This resulted in a moisture gradient which decreased from outside surface to the inner surface in contact with the steel ring. The increasing concrete wall thickness again was shown to delay the age of cracking even in the presence of a moisture gradient. The authors also measured higher change in radius for the specimens with uniform shrinkage (short rings) than the tall specimens. They explained that this was due to the fact that the taller specimens experience most of the shrinkage on the outer radius where as the short rings shrink uniformly throughout the radius. Even though the authors outlined a procedure to determine the stresses in the concrete,

they stated that the closed form solution for non-uniform drying would be much more difficult.

See et al. (2003) performed also performed a study to determine the effects of geometry and to identify the shrinkage cracking characteristics of concrete. The test setup included an inner steel ring with a 13 mm (1/2 in.) wall thickness, 305 mm (12 in.) inner diameter, and 330 mm (13 in.) outside diameter. Also, a 405 mm (16 in.) inside diameter PVC pipe was cut to a height of 152 mm (6 in) to be used as the outer mold. The rings were allowed to dry from the outer circumference only. The authors calculated the degree of restraint R, by comparing stiffness of the steel ring to combined stiffness of steel and concrete ring,

$$R = \frac{A_{st} E_{st}}{A_{st} E_{st} + A_c E_C} \tag{1.1}$$

where A_{st} and A_c are the cross-sectional areas of the steel and concrete rings, respectively, and E_{st} and E_c are the modulii of elasticity of the steel and concrete, respectively. For their setup, the authors calculated the degree of restraint to be from 70 to 75% depending on the modulus of elasticity of concrete. Also, the average radial compressive stress was 10% of the hoop stresses. In contrast, AASHTO setup would only yield 55 to 60% restraint, which explains the longer times for a visual crack to take place. Also, the average radial compressive stresses were 25% of the hoop stresses which made analysis of this setup more difficult.

See et al. (2003) also proposed the following equation to evaluate the average tensile stress in the concrete at time t,

$$\sigma_t(t) = \frac{E_{st} r_{ic} h_{st}}{r_{is} h_c} \varepsilon_{st}(t) \tag{1.2}$$

Where E_{st} is the modulus of elasticity of steel, h_{st} and h_c are the thicknesses of the steel and concrete ring, respectively, and r_{is} and r_{ic} are the internal radii of steel and concrete, respectively. This equation compared theoretical time to cracking, to the observed time of cracking. They observed that the actual observed time to cracking was much later than the theoretical time to cracking. They concluded that tensile creep relaxation is the most likely reason for this difference. However, they also mentioned that other factors, such as shrinkage rate might play a significant role in cracking.

See et al. (2004) improved their formulation of average residual stress that they derived in 2003 by including the effects of tensile creep and rate of stress development. The experimental setup was exactly the same as the setup used by See et al. (2003). The test program included the testing of 16 concrete and 4 mortar mixtures under restrained

shrinkage. The effect of curing was also studied by using a variety of curing times. The authors' main argument was that the elastic strain rate and tensile creep play a significant role on the net time to cracking. Following the analysis in 2003 they defined the average residual stress in the concrete at time t after initiation of drying as,

$$\sigma_t(t) = G\left|\varepsilon_{st}(t)\right| = G\left|\varepsilon_{sh}(t) - \varepsilon_e(t) - \varepsilon_{cp}(t)\right| \quad (1.3)$$

Where $\varepsilon_{st}(t)$ is the absolute strain in the steel ring, and $\varepsilon_{sh}(t)$, $\varepsilon_e(t)$, and $\varepsilon_{cp}(t)$ are the free drying shrinkage strain, elastic strain, and tensile creep strain, respectively. Elastic strain is dependent on the modulus of elasticity of the concrete used in the test, and G is a constant for the ring test setup which can be calculate using the following formula.

$$G = \frac{E_{st} r_{ic} h_{st}}{r_{is} h_c} \quad (1.4)$$

Where E_{st} is the modulus of elasticity of steel, h_{st} and h_c are the thicknesses of the steel and concrete ring, respectively, and r_{is} and r_{ic} are the internal radii of steel and concrete, respectively. The authors' also developed a method to assess the potential for cracking of the mixes based on the stress rate at cracking or at the time of termination of the test. They introduced an equation which defined the stress rate at time, t, after initiation of drying as,

$$S(t) = \frac{G|\alpha|}{2\sqrt{t}} \quad (1.5)$$

where the value of α is determined from the strain readings obtained form the ring test. To do this, See at al. plotted the strains against the square root of time to obtain linear relationships in which the slope of the equation, which defines this relationship, would yield α. As a result of their experiments they concluded that lower stress rates generally meant the mix would crack at a later age, which means that it would have a lower potential for cracking. They suggested four zones of performance which were 1) a zone of "High" potential for cracking with stress rates exceeding 0.34 MPa/day (50 psi/day) and cracking occurring within 7 days after drying starts; 2) a zone of "Moderate-High" potential for cracking with stress rates between 0.17 and 0.34 MPa/day (25 and 50 psi/day) and cracking occurring between 7 and 14 days; 3) a zone of "Moderate-Low" potential for cracking with stress rates between 0.10 and 0.17 MPa/day (15 and 25 psi/day) and cracking occurring between 14 and 28 days; and 4) a zone of "Low" potential for cracking with stress rates lower than 0.10 MPa/day (15 psi/day) and cracking occurring beyond 28 days or no cracking occurring at all. For mixes that do not crack they suggested the comparison to be made based on the stress rate at the termination time of the test.

In 2004, ASTM adopted the restrained shrinkage setup used by See at al. (2004) as a standard test to measure the cracking potential of concrete and mortar. The test setup was identical to the one used by See at al. (2004), and used the same criteria to define the potential for cracking of mixes. Since a 28 day limit for maximum test duration was specified it became a quick and reliable method to measure the cracking potential of mixes with aggregate sizes less than 0.5 in. However, concrete mixes used in bridge decks commonly incorporate 0.75 in (or larger) aggregates, which means that ASTM ring test can not be used for these mixes. AASHTO setup still is being used for that purpose. Recently, several studies focused on the cracking behavior and residual stress build up in the AASHTO ring test.

Hossain and Weiss (2006) studied the effects of boundary conditions and geometry on stress development in the concrete ring. The study compared the effects of curing from top and bottom to drying from the outer circumference. Also, effects of using different steel and concrete ring thicknesses were investigated. The authors used three different test methods to compare the effects of geometry and drying conditions. First they used two different free shrinkage tests in which they measured the free shrinkage of unrestrained rings specimens and standard linear free shrinkage specimens that are used by ASTM C-157 test. Restrained shrinkage test samples were separated into three different groups to study the various effects under consideration. In the first group, where the degree of restraint was studied, concrete wall thickness was fixed to 450 mm (18 in), and the steel ring thicknesses were varied by using rings with 3.1 mm (1/8 in.), 9.5 mm (3/8 in.), and 19 mm (3/4 in.) wall thicknesses. In the second group, the steel ring thickness was fixed 9.5 mm (3/8 in.), however, the concrete ring thicknesses were varied to include rings with wall thicknesses of 37.5 mm (1.5 in.), 75 mm (3.0 in), 112.5 mm (4.5 in.), and 150 mm (6.0 in). Finally, in the last group rings similar to the first two groups were used but the drying conditions were changed. The rings were sealed with aluminum tape to obtain two different boundary conditions, such as drying from the outer circumference, and drying from top and bottom. In all groups the height of the ring specimens were limited to 75 mm (3.0 in), and the inner diameter of the concrete rings were 300 mm (12 in.). All steel rings were instrumented with four strain gages at mid-height and they were monitored continuously for the duration of the test. The authors also used acoustic emission sensors to detect crack development, and compare the cracking behavior of rings with different boundary conditions. One of the important conclusions of the study was the significant difference in cracking behavior of rings which had different boundary conditions. On the specimens which had circumferential drying (top and bottom sealed) visual cracks were observed earlier even though the interface pressures on the steel rings were lower. On the other hand, the rings which were allowed to dry from top and bottom (sides sealed) experienced higher ring pressures, but cracked at a later age. The authors explained this by comparing the moisture profiles of the two boundary conditions. When concrete is allowed to dry from the outer circumference, the outer surface looses moisture much more quickly due to the large surface area that is exposed to drying. This creates a moisture gradient in the ring, which results in cracking starting from the outer circumference moving towards the inner steel ring. In the case where the top and bottom drying is allowed moisture is lost

more uniformly along the radius and therefore a more uniform moisture profile is attained. Hossain and Weiss supported this theory by comparing the acoustic emission measurements from both setups. The acoustic sensors showed that the cracks developed on the outside surface and moved inwards for the samples that dried from the circumference. The cracking for the top and bottom drying was exactly the opposite. The effects of using various steel and concrete thicknesses were as expected. Thicker steel rings would lead to higher restraints and therefore earlier cracking. Where as thicker concrete rings would lead to higher resistance to cracking which would delay the age of cracking.

Summary of Previous Work

Restrained ring test is being used widely due to its simplicity, cost, and the ease with which the data can be analyzed and interpreted. Currently one standard ASTM test and a provisional AASHTO test are being used to test restrained shrinkage behavior of concrete and mortar of various proportions. Although much work has been done on quantifying the stresses that are developed in the ring test due to effects of drying conditions and ring geometry, there is still room for improvement. Currently the only standard test, which is the ASTM C-1581, has some limitations due to the maximum coarse aggregate size that can be used in the test. This is a major limitation for many common and realistic mixes that are being used in the industry. Most of the mixes used in bridge decks, pavements or other structures use aggregate sizes greater than 1/2 inch. In consequence, AASHTO restrained shrinkage test is being used to evaluate such mixes. Recent studies that focus on quantifying the stress profiles in the AASHTO test all face the same challenge, which is the non-uniform stress development due to the moisture gradients that are present in thicker rings which are subjected to drying from the outer circumference. Although analytical solutions have been proposed for this case, they have not been fully tested or confirmed by other researchers. It should also be noted that all of the studies derive the stress profile in the concrete ring based on the strains that are experienced in the inner steel ring, using certain assumptions, and applying basic laws of engineering mechanics. Although these formulas are useful in interpreting the results of restrained shrinkage ring tests, they should be verified and tested thoroughly before they can be used confidently. Moreover, many assumptions were made on the strain compatibility which may or may not be true. Thus, a better method would be to directly know the stress development in the concrete.

This report provides a new modified approach for measuring the concrete stress under restrained condition directly such that the cracking potential could be quantified for concrete mixture that does not exhibit any cracking.

EXPERIMENTAL SETUP

The experimental setup consists of mixing and testing of 16 HPC mixes using the designs that are given by NJDOT, which are common bridge deck mixes in The State of New Jersey. The materials used in the study are from local sources throughout the state (except for fly ash, which is supplied from Maryland). The mixes utilize various combinations of slag and silica fume to enhance the durability of concrete. Silica fume replacement is within 4-7.5% and slag replacement is within the range of 30-40%. Fly ash is also utilized in one of the mixes. Although the majority of the mixes use a water-to-cement (w/c) ratio of 0.40, there are few mixes with 0.34 and 0.37 w/c ratios.

A broad range of tests are performed on each mix to determine their mechanical properties to assist in determining the cracking potential. Table 1 illustrates all the tests that are performed for each mix. In addition to the tests in Table 1, gradation of coarse and fine aggregates was also tested. The specific gravities for those materials are also determined to better understand the differences caused by various sources and quarries.

Table 1 - Summary of Laboratory Tests for HPC Performed on Each Mix

Test	Number of Specimens	Applicable ASTM Standard	Curing Conditions	Age of Concrete at Test, days
1. **Slump**	1 per batch	C143	None	0, fresh
2. **Fresh Air Content**	1 per batch	C231	None	0, fresh
3. **Free Shrinkage**	3 per mix	C157	7 day wet	1 to 90 days
4. **Restrained Shrinkage**	2 per mix	AASHTO PP34	7 day wet	1 to age of crack (max 90 days)
5. **Compressive Strength**	15 per mix (4 × 8 in)	C39	7 day wet	3, 7, 14, 28 days, and crack age
6. **Splitting Tensile Strength**	15 per mix (4 × 8 in)	C496	7 day wet	3, 7, 14, 28 days, and crack age
7. **Modulus of Elasticity**	15 per mix (4 × 8 in)	C469	7 day wet	3, 7, 14, 28 days, and crack age

Material Properties

The raw materials are obtained from various sources in New Jersey with the exception of fly ash. Fly ash is obtained from Pennsylvania since it is the only source in this region. The project involves the use of two different cement types (Type I and II) from four suppliers, silica fume from three suppliers, slag from three suppliers, and fly ash from a single source as far as the cementitious materials are concerned. In addition,

coarse aggregates utilized are from nine different local quarries and sand is supplied from seven different sources. The admixtures used in mixing HPC are also from various sources. All of the materials and the respective suppliers can be seen in Table 2 through Table 4.

Table 2 - Cementitious Materials and Suppliers

	Material	Supplier
Portland Cement	Portland Type I/II	Essroc
		LaFarge
		Lehigh
		Riverside Cement
Slag	Slag Grade 120	Essroc
	Newcem	Lafarge
	Grancem	St. Lawrence
Silica Fume	Euclide MSA	Euclide Chemical
	Rheomac SF100	Master Builder
	Sikacrete 950DP	Sika
Fly Ash	Type F Fly Ash	Seperation Tech

Table 3 - Aggregates and Suppliers

	Material	Supplier
Coarse Aggregate	No. 57 Coarse Aggregate	Tilcon Quarries
		Trap Rock Industries
		Plumstead Material
		Fanwood Crushed Stone
		Independence Materials #57 Devault
		Better Materials Penns Park
		Stavola Construction Materials
		Mt. Hope Rock Products
		Oxford Quarry
Fine Aggregate	C33 Fine Aggregate	Sahara Sand
		Clayton Sand
		Tuckahoe Sand &Gravel
		RE Pierson
		Dunrite Sand
		Amboy Aggregates
		County Concrete

Table 4 - Chemical Admixtures and Suppliers

	Material	Supplier
AEA	Daravair 1000	W.R. Grace
	Euclid Air	Euclide Chemical
	Euclide AEA-92	Euclide Chemical
	MB AE-90	Master Builder
	MB VR	Master Builder
	Setcon 6A	Great Eastern
	Sika AEA-15	Sika
Water Reducer	Chemstrong A	Great Eastern
	Euclide WR 89	Euclide Chemical
	WRDA/HYCOL	W.R. Grace
HRWR	Chemstrong SP	Great Eastern
	Daracem 19	W.R. Grace
	Eucon 37	Euclide Chemical
	MB Glenium 3030	Master Builder
	MB Rheobuild 1000	Master Builder
	Sika Sikament 86	Sika
Retarder	Eucon 75	Euclide Chemical
	MB Pozz 100xr	Master Builder
	Sika Plastiment	Sika

Mix Proportions

Mix design proportions are obtained from NJDOT and most of them are common bridge deck mixes used within the state. The original designations for the mixes were kept, but new designations were also given by Rutgers according to comparison parameters to make the process of analysis easier. The majority of the mixes include slag as a cementitious replacement in high percentages (such as 30 or 40%). There are two mixes which have only silica fume in their composition, which is currently not allowed in NJDOT specifications due to problems encountered with cracking on bridge projects. There is only one mix with fly ash replacement. All mix proportions are shown in Table 7 through Table 9. NJDOT designations are followed by Rutgers designations. Mixes have been grouped into 4 groups and the group properties are defined in Table 5.

Table 5 - Mix Group Definitions

Group	Definition
1	40% Slag replacement
2	4% Silica fume and 30% Slag replacement
3	Only Silica fume replacement
4	Various percentages of silica fume, slag, and fly ash

Abbreviations were also used to identify properties of each mix and they are summarized below.

Table 6 – Abbreviations

Abbreviation	Definition
SF	Silica Fume
SL	Slag
F. Ash	Fly Ash
CA	Coarse Aggregate
FA	Fine Aggregate

Table 7 - Group 1 Mix Design Proportions

(lb/cyd)	R311266	R408847	R200578S	R309494*
Mix Designation	G1M1	G1M2	G1M3	G1M4
Portland Cement	480	395	396	394
Type	1	1	1	1
Silica Fume	0	0	0	0
Fly Ash Class F	0	0	0	0
Slag	320	263	264	263
	40%	40%	40%	40%
Total Cementitious Content	800	658	660	657
Course Agg. No. 57	1650	1700	1875	1850
Fine Agg.	1240	1199	1195	1250
Course Agg./Fine Agg.	1.33	1.42	1.57	1.48
Water (gal)	38.3	31.2	31.7	31.5
W/(C+P)	0.4	0.4	0.4	0.4
Water Reducer (oz/cwt)	2.3		3.5	3
Retarder				
Superplasticizer (oz/cwt)	19.9	8.4	13.4	12
AEA (oz/cwt)	1.0	0.7	1.0	0.8
Slump (in)	6	5.5	8	-
Air Content (%)	6.4	7.5	4.0	-

* This mix was not mixed due to the wrong size aggregate that was delivered to the laboratory.

Table 8 - Group 2 Mix Design Proportions

(lb/cyd)	R408850	R409239	R309497	R310682	R200626S	R200633S
Mix No.	1	2	3	4	5	6
Mix Designation	G2M1	G2M2	G2M3	G2M4	G2M5	G2M6
Portland Cement	436	436	435	436	436	461
Type	1	1	1	1	2	2
Silica Fume	25	25	25	25	25	25
	4%	4%	4%	4%	4%	4%
Class F Fly Ash	0	0	0	0	0	0
Slag	197	197	197	197	200	197
	30%	30%	30%	30%	30%	30%
Total Cementitious Content	658	658	657	658	661	683
Course Agg. No. 57	1700	1700	1850	1850	1825	1811
Fine Agg.	1196	1196	1247	1230	1170	1156
Course Agg./Fine Agg.	1.42	1.42	1.48	1.50	1.56	1.57
Water (gal)	31.1	31.1	31.5	31.5	30.5	32.8
W/(C+P)	0.4	0.4	0.4	0.4	0.4	0.4
Water Reducer			3	3	3	
Retarder		1.0				2.0
Superplasticizer (oz/cwt)	7.6	8.0	12.0	12.0	8.0	4.0
AEA (oz/cwt)	0.7	0.9	0.6	1	1.3	0.36
Slump (in)	5.25	6	5.5	5.25	6.5	5
Air Content (%)	7.00%	7.75%	3.75%	5.70%	7.50%	4.50%

Table 9 - Group 3 Mix Design Proportions

(lb/cyd)	R308163	R308278
Mix Designation	G3M1	G3M2
Portland Cement	700	655
Type	1	2
Silica Fume	35	50
	5%	7%
Class F Fly Ash	0	0
Slag	0	0
Total Cementitious Content	735	705
Course Agg. No. 57	1725	1750
Fine Agg.	1190	1280
Course Agg./Fine Agg.	1.45	1.37
Water (gal)	35.2	33.8
W/(C+P)	0.4	0.4
Water Reducer (oz/cwt)		
Retarder (oz/cwt)	1.5	2.0
Superplasticizer (oz/cwt)	8.0	10.0
AEA (oz/cwt)	0.5	0.8
Slump (in)	5.5	5
Air Content (%)	6.5	6.0

Table 10 - Group 4 Mix Design Proportions

(lb/cyd)	R309495	R408844	R309496	R408694
Mix Designation	G4M1	G4M2	G4M3	G4M4
Portland Cement	435	411	394	571
Type	1	1	1	1
Silica Fume	35	50	50	50
	5%	7.5%	7%	7%
Class F Fly Ash	0	0	0	69
				10%
Slag	197	197	263	0
	30%	30%	37%	
Total Cementitious Content	667	658	707	690
Course Agg. No. 57	1850	1700	1850	1800
Fine Agg.	1247	1187	1250	1232
Course Agg./Fine Agg.	1.48	1.43	1.48	1.46
Water (gal)	29.5	31.1	31.5	28.4
W/(C+P)	0.37	0.4	0.37	0.34
Water Reducer (oz/cwt)	3		3	
Retarder (oz/cwt)				
Superplasticizer (oz/cwt)	12.0	7.3	12.0	18.0
AEA (oz/cwt)	1	0.7	0.6	1.7
Slump (in)	6.75	4	7	6.75
Air Content (%)	5.0	6.5	4.0	7.0

Mixing and Fresh Sampling

Mixing (ASTM C - 192 - 06)

The mixing starts with adding coarse and fine aggregates to the mixer. While the mixer is running, 1/3 of the water is added, followed by air entraining agent. The mixer is allowed to run for 30 seconds and then the cement is added with the rest of the water, and the cementitious materials. The concrete is mixed with all ingredients in the mixer for at least three to four more minutes. After three or four minutes of mixing, the batch is allowed to hydrate by resting for three to four minutes. During the waiting period the

concrete mixer is covered to avoid the loss of moisture. Then the Superplasticizer is added to the mix while the mixer is spinning. Finally the mixer is allowed to run for three more minutes or until the Superplasticizer reacts with the concrete such that there is uniformity in the concrete.
Figure 1 shows the concrete mixer that is used for mixing in the laboratory.

Figure 1. Concrete Mixer

Slump Test (ASTM C - 143 - 05a)

The slump of each batch of concrete is measured immediately after mixing in accordance with ASTM C-143. The slump cone is filled in three layers, with each layer approximately one-third the volume of the mold. Each layer is rodded with 25 strokes using the tamping rod. The strokes are uniformly spread over the cross section of each layer. Each layer is rodded throughout its depth, so that the strokes just penetrate into the underlying layer. In filling and rodding the top layer, the concrete is heaped above the mold before rodding is started. If the concrete level falls below the top edge of the mold after rodding, additional concrete is added to keep an excess of concrete above the top of the mold. The surface of the concrete is struck off by rolling motion of the tamping rod. The mold is immediately removed from the concrete by raising it in a vertical direction avoiding lateral or tensional motion. The slump is immediately measured by determining the vertical difference between the top of the mold and the displaced original center of the top surface of the specimen. Illustration of the slump test can be seen in
.

Figure 2. Slump Test

Air Content (ASTM C - 231 - 04)

Concrete air content is measured using a Type – B Pressuremeter (
Figure 3) according to ASTM C – 231. After dampening the insides of the meter bowl, it is filled in three layers of equal volume. Each layer is rodded with 25 strokes using the tamping rod. The bottom layer is rodded throughout its depth without the rod forcibly striking the bottom of the bowl. The second and top layers are rodded throughout their depth so that the strokes penetrate about 1in. into the underlying layer. The bowl is tapped smartly 10 to 15 times with a rubber mallet after each layer is rodded. The top surface struck is off with plate or bar and finished smooth after rodding and tapping the last layer. The flanges of bowl and cover assembly are thoroughly cleaned, and air meter is assembled to obtain a pressure tight seal. The air valve between air chamber and bowl is closed, and both petcocks are opened. Using a rubber syringe, water is injected through one petcock until water emerges from the opposite petcock. The meter is jarred gently until all air is expelled from this same petcock. The air bleeder valve on the air chamber is closed and air is then pumped into the air chamber until the gage hand is on the initial pressure line. A few seconds should be allowed for compressed air to cool after which the gage hand at the initial pressure line is stabilized by pumping or bleeding-off air as necessary while tapping the gage lightly. Both petcocks are then closed, and the air valve between air chamber and measuring bowl is opened. The sides of measuring bowl are tapped with mallet to relieve local restraints. The pressure gage is tapped lightly with hand to stabilize the reading while air valve is open and percentage of air on the dial of pressure gage is read and recorded.

Figure 3. Type - B Pressuremeter for determining concrete air content

Sampling of Specimens and Consolidation

A total of 45 cylindrical specimens with a diameter of 4 inches and a height of 8 inches are taken for standard ASTM tests. In addition 2 ring specimens are cast for testing restrained shrinkage. Companion the free shrinkage blocks are also cast to determine the free shrinkage of all mixes and correlate the results with those from restrained shrinkage tests. All specimens are cast using a vibrating table. Consolidation requirements of AASHTO are used while casting the test specimens. Figures 4 and 5 show free shrinkage molds and the vibrating table.

Figure 4. Shrinkage Blocks and Cylinder Molds

Figure 5. Vibrating Table

Curing

The NJDOT Specifications in the field require 7 day moist curing of concrete using wet burlap covered with polyethylene sheets. The same curing procedure is applied to all samples under study. After demolding at 18-24 hours, all samples are covered with wet burlap and polyethylene sheets and placed in an environmental chamber with a constant temperature of 74^0F. After the end of curing period, the burlap is removed and the specimens are left in the environmental chamber. The relative humidity in the chamber is kept constant at $50 \pm 4\%$.

Figure 6. Restrained shrinkage specimen covered with wet burlap

Figure 7. All Specimens Under Burlap and Polyethylene Sheet

Laboratory Testing Procedures

Sieve Analysis of Fine and Coarse Aggregates (AASHTO T 27 - 06)

Gradation of sand and stone is important in evaluating shrinkage characteristics of a concrete mix. A more uniform gradation prevents formation of gaps between the aggregates and improves the pore structure of concrete. The sieve analysis determines the gradation (the distribution of aggregate particles, by size, within a given sample) in order to determine compliance with design, production control requirements, and verification specifications. The gradation data can be used to calculate relationships between various aggregate or aggregate blends, to check compliance with such blends, and to predict trends during production by plotting gradation curves graphically.

To perform the test, a known amount weight of material (the amount being determined by the largest size of aggregate) is placed upon the top of a group of nested sieves (the top sieve has the largest screen openings and the screen opening sizes decrease with

each sieve down to the bottom sieve which has the smallest opening size screen for the type of material specified) and shaken by mechanical means (Figure 8) for a period of time. After shaking the material through the nested sieves, the material retained on each of the sieves is weighed using one of two methods. The cumulative method requires that each sieve beginning at the top be placed in a previously weighed pan (known as the tare weight), weighed, the next sieve's contents added to the pan, and the total weighed. This is repeated until all sieves and the bottom pan have been added and weighed. The second method requires the contents of each sieve and the bottom pan to be weighed individually. Either method is satisfactory to use and should result in the same answer. The amount passing each sieve is then calculated.

Figure 8. Mechanical Sieve Shaker

Specific Gravity and Absorption of Fine Aggregate (AASHTO T 84 – 00(2004))

In concrete mix design, the specific gravity of the aggregate is employed in calculating the percentage of voids and the solid volume of aggregates in computations of yield values. On the other hand, the absorption is important in determining the net water-cement ratio in the concrete mix. The test requires the use of a scale, pycnometer (a flask or a container which the sand sample will be introduced), metal mold, and a tamper. After a sand sample is obtained by the procedures in AASHTO T 248, it is dried to constant mass. Immediately after it cools to handling temperature, the sand sample is soaked in water for 15 to 19 hours. Next, the excess water is removed and the sand is slowly dried to saturated surface dry (SSD) condition. Cone test is done by using the tamper and the metal mold to ensure that the sand has reached the SSD condition. Immediately after SSD is reached, the pycnometer is filled with water and the sand is introduced. After all air bubbles are removed by gently agitating the pycnometer total mass of the pycnometer is recorded. Than, the pycnometer is cleaned and weighed one more time with only water in it filled to its calibration capacity. The

obtained measurements are used to calculate the absorption and bulk specific gravity of the sand sample.

Specific Gravity and Absorption of Coarse Aggregate (AASHTO T 85-91(2004))

This test is very similar to the T 84 test and the determinations that may be made from this procedure are identical to those made from AASHTO T 84. To briefly summarize, an oven dried sample of coarse aggregate is submerged in water for approximately 15 hours. Next it is dried to SSD condition and weighed and than it is dried completely and weighed one last time. These measurements are used in determining of absorption and bulk specific gravity.

Compressive Strength of Cylindrical Concrete Specimens (ASTM C - 39 - 05)

Two 4 X 8 in. cylinders are tested at 3, 7, 14, 28, and cracking day of restrained ring specimens using the Forney-1 million pound- compression machine (Figure 9) that complies with ASTM C-39. The loading rate of the Forney compression machine is kept constant throughout the test. The specimens are either capped with high strength sulfur capping compound or covered with steel caps. When steel caps are used, the rubber pads are replaced after 60 tests or according to the manufacturer recommendation. The maximum strength is recorded for each specimen.

Figure 9. Forney 1-Million Pound Compression Machine

Standard Test Method for Splitting Tensile Strength of Cylindrical Concrete Specimens (C – 496 – 04$^{\varepsilon 1}$)

Splitting tensile strength is determined by splitting a 4 X 8 in. cylinder in accordance with ASTM C496 using the 400-kip Tinius Olsen Compression machine. The Tinius Olsen Compression machine is used because it has longer head extension than the Forney 1-million pound compression machine. Likewise in order to automate and to minimize human error, a 250-kip digital load cell is also used in this test. Figure 10 shows the setup for the splitting tensile strength test.

Figure 10. Splitting Tensile Strength Test Setup

Modulus of Elasticity (ASTM C-469-02$^{\varepsilon 1}$)

The modulus of elasticity is measured according to ASTM C-469. At least two specimens are capped with sulfur compound to be tested in compression using a compressometer shown in Figure 11. The sulfur compound eliminates the creeping of the rubber pad in the steel cap. The specimens are loaded at least twice. During the first loading, which is primarily for the seating of the gages, the performance of the gage is observed. The load is applied at constant rate within the range of 30-40 psi/sec, and the load is applied up to approximately 40 percent of the ultimate compressive strength. The load and deformation are recorded manually at regular intervals. In order to determine the modulus of elasticity, the strains are plotted against the stresses where the slope represents the modulus of elasticity. Figure 12 shows the modulus of elasticity test setup.

Figure 11. Compressometer used for modulus tests

Figure 12. Modulus of Elasticity Test Setup

Free Shrinkage Test

The free shrinkage test is performed according to ASTM C157 - 06. Three 3x3x10-in prism concrete specimens are cast with gage studs placed at each end. The gage studs are screwed into the plates at each end of the mold using a hex screw. The length between the two gage studs is measured as well as the length of the reference bar using a length comparator (Figure 13). When using the comparator, the specimen is slowly rotated such that the minimum reading is recorded. The length change at various ages is recorded. In addition, embedded VWSG can be installed to capture autogenous shrinkage of concrete. This was done for several mixes to see the contribution of autogenous shrinkage on total shrinkage using the setup shown in Figure 14.

Figure 13. Length Comparator

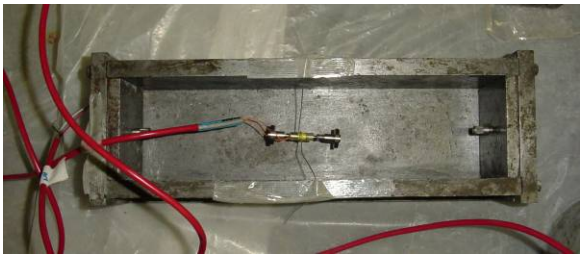

Figure 14. Shrinkage Molds with VWSG (Autogenous Shrinkage).

Restrained Shrinkage Test

Ring Test Setup with Four VWSG's

To measure restrained shrinkage, concrete is cast around a steel ring in accordance to the test method of AASHTO PP34 as shown in Figure 15. The concrete is cast around a steel ring, such that, as the concrete shrinks, a compressive stress is developed in the steel ring and balanced by a tensile stress in the concrete ring. If this tensile stress is greater than the allowable tensile stress of the concrete, it cracks. The cracks in the ring are monitored daily using a crack microscope. However, as mentioned earlier, to obtain more refined results, the ring test has been instrumented as shown in Figures 15a and 15b. Four foil strain gages (FSG) are instrumented at mid-height on the inner circumference of the steel ring so that abrupt changes (due to the release in concrete stress after cracking) in the steel strain can be observed indicating the exact age of cracking. The strain readings are recorded by using a data acquisition system (DAS). The data collected by the DAS is verified using a portable strain readout unit. Moreover, four vibrating wire strain gages (VWSG) are installed at the top surface of the concrete ring using threaded bolts. The VWSG sensors are used to signal the crack location as well as to measure the exact strain in concrete. The advantage of using VWSG sensors is that the actual strain in the concrete is monitored and therefore, if the concrete does not crack the stress development can be quantified. This leads to better understanding of the test results and allows for a more refined comparison between mixes.

Two specimens were cast per mix in an environmental chamber with constant ambient temperature and relative humidity of 74°F ± 3°F and 50% ± 5%, respectively. The concrete specimens were placed in the molds in three equal lifts and consolidated using a vibrating table. Immediately after casting the specimens, they were covered with wet burlap. After 24 hours, each specimen was striped from its molds and covered with wet burlap for 14 days. Typical sample preparation is summarized in Figure 16 below. It consists of 3 stages.

1. Molds are prepared and placed on a plastic sheet inside the environmental chamber. (Figure 16a)
2. Concrete is cast, consolidated, and sensors are embedded carefully in their positions. (Figure 16b)
3. Samples are covered immediately with burlap and then sealed with plastic cover to prevent loss of moisture. (Figure 16c and Figure 16d)

After curing period is over, the plastic sheet and burlap is removed and the rings are monitored up to 91 days. During this period checks for cracks are made everyday both by naked eye and also with the help of microscopes. Data collected from the samples are examined to help determine possible crack locations. At the end of the 91 day test period the ring specimens are carefully mapped for cracks and crack width measurements are taken.

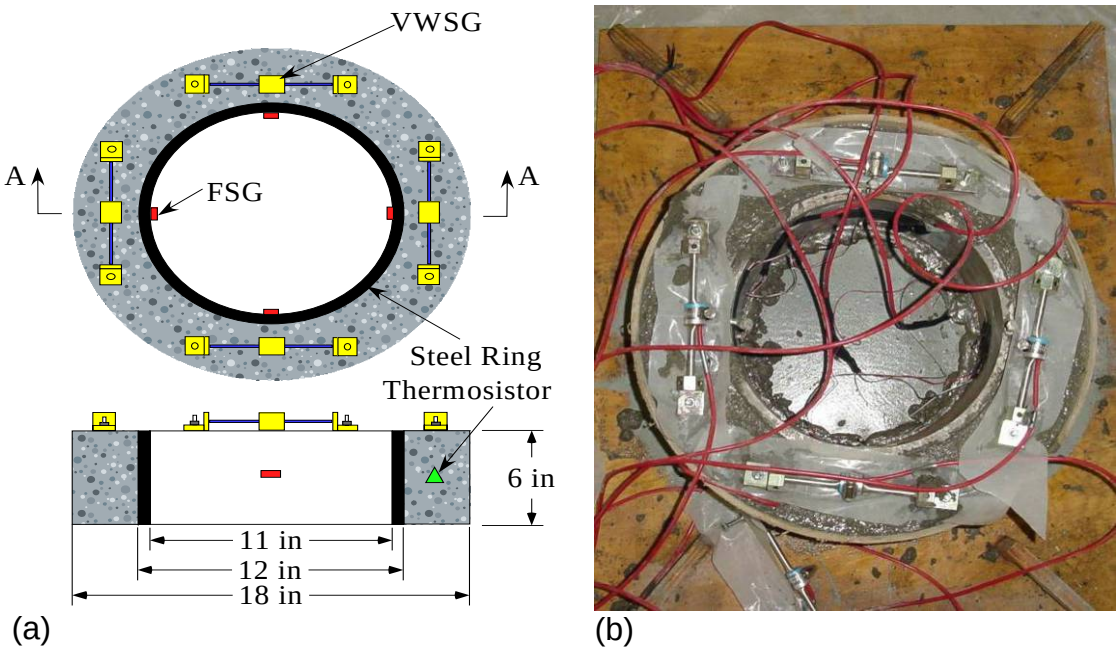

Figure 15. a) Schematic Diagram and b) picture of the 4 VWSG Restrained Shrinkage Test Setup

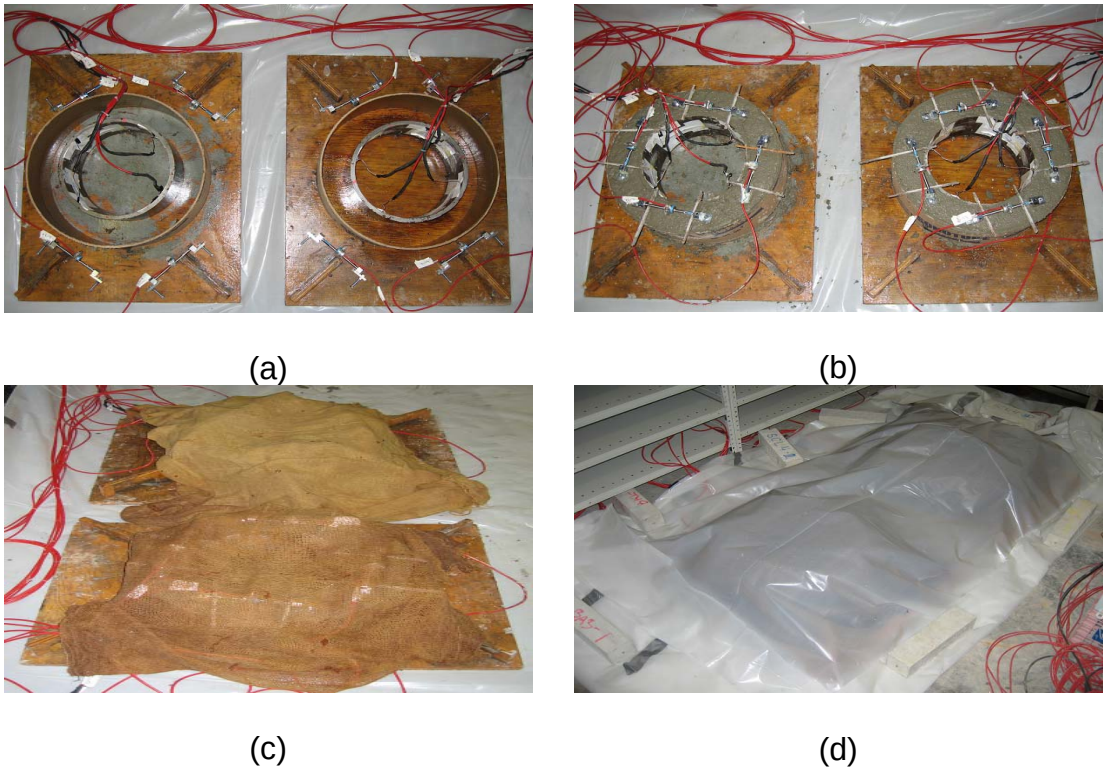

Figure 16. Preparation of Restrained Ring Specimens

Ring Test Setup with Six VWSG's

During the course of the study, another arrangement of strain gages were developed by the authors to better monitor the strain profile in the restrained rings for the duration of the test. This setup includes six VWSG sensors instead of four. These sensors are connected to each other to form a closed loop in the centerline of the concrete ring. This way, strain in any portion of the ring can be monitored and cracking locations can be identified much easier. A schematic and picture of this setup can be seen in Figure 17a and
Figure 17b respectively.

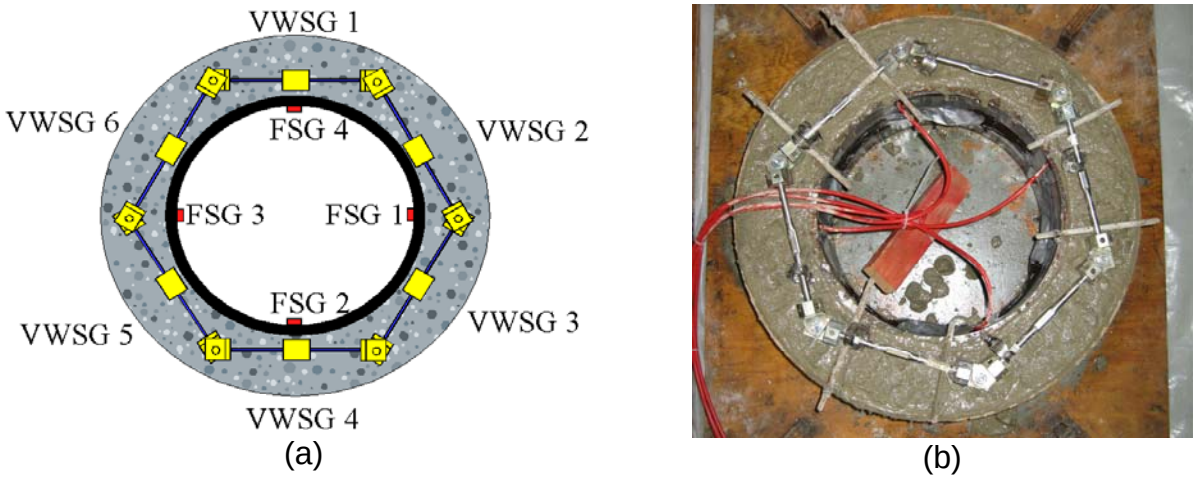

Figure 17. a) Schematic Diagram of Six VWSGs, and b) picture of the Six VWSG Restrained Shrinkage Test Setup.

Data Collection and Analysis

Data collection is done with the help of a data acquisition system (DAS) manufactured by Campbell Scientific, Inc. The DAS (Figure 18) is installed permanently into the environmental chamber. It is equipped with strain gage modules that are able to monitor 12 rings simultaneously. For the specified mixes DAS was programmed to collect data at an interval of 5 minutes and to download the data daily to a permanent computer every 24 hours.

The recorded data is monitored and plotted everyday to check for sudden jumps in strain readings (which may signal cracking). In addition to the data collected from the rings, ASTM tests such as compressive strength, tensile splitting strength, and elastic modulus tests are done at various ages (Day 3, 7, 14, 28 and 56). Also, gradual increase in strain is monitored and plotted against the cracking strain to quantify the cracking potential of each mix. Cracking strain of each mix is obtained from the results of standard cylinder tests as follows.

$$\varepsilon_t = \frac{f_t}{E}$$

f_t : Tensile splitting strength

E : Modulus of elasticity

ε_t : CRACKING STRAIN

Figure 18**.** Data Acquisition System

After 91 day period ends, an evaluation is made whether to continue collecting readings from the rings or not. If the strain values in the foil gages and VWSG have stabilized it means that shrinkage has come to a stop and the test can be finalized. This can also be checked my examining the length comparator readings from the free shrinkage blocks. If the free shrinkage has ended and the concrete has not cracked after 91 days it is concluded that it will not crack. However, if the readings are changing and increasing strains are observed in the rings, the tests are extended beyond 91 days.

Figure 19 below summarizes the restrained shrinkage test and data analysis procedure. Readings are obtained from DAS and graphed every 2 to 3 days. Any sensor which shows close to or higher than cracking strain signals a crack (In the case below VWSG 4 exceeds cracking strain first and the picture shows the observed crack). The first 7 days, where there is no tensile strain development, is the curing duration and when analyzing results strain measurements are started from initiation of drying.

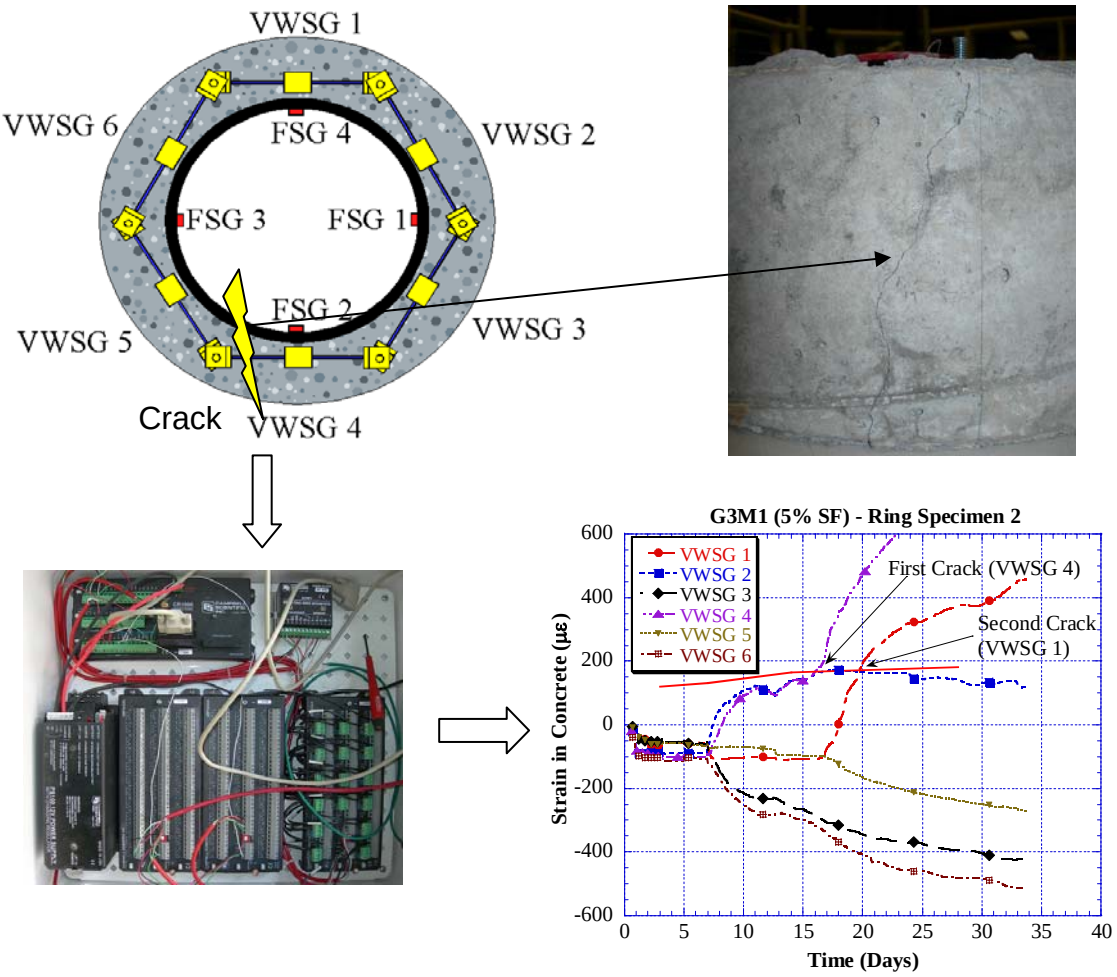

Figure 19. Schematic of the restrained shrinkage test setup, data collection schemes, and test results.

Environmental Chamber

Shrinkage is very sensitive to surrounding environment; therefore the shrinkage specimens need to be stored in an environmental chamber. The environmental chamber is a 24 × 16 × 8 ft room (Figure 20) that is made of insulated aluminum wall. The temperature and humidity of the room is controlled by a digital control unit located outside the chamber. The digital control unit acquires temperature and humidity readout from an environmental sensor inside the chamber. The sensor is positioned such that the overall temperature and humidity is at the set point. The range of temperature and humidity that the chamber could be set are between 39 – 104 degrees Fahrenheit and 40 – 70 percent, respectively. Inside the chamber, the temperature is adjusted through the heater and freezer units that are placed on one side of the wall. The unit is shielded with aluminum sheets with blowers to circulate the air in the chamber. The humidity is controlled by means of a steam generator that is located

underneath the blowers. Dehumidification is done using an air conditioning unit to dry the air.

Figure 20. Inside View of the Environmental Chamber

Figure 21. Close Up View of Rings in the Environmental Chamber

RESULTS

Mechanical Properties

Compressive Strength

Analyzing Table 7, it can be seen that mix G1M1 has the highest amount of cementitious materials. Mixes G1M2 and G1M3 have slightly less but equal amount of cement content. The difference in their compressive strength is due to the higher aggregate content of G1M3. Strength of G1M1 is the highest as expected. It was observed that all the mixes attained 80% or more of their strength by day 14. After day 28, strength did not increase by more than 5%. This is typical for slag mixes since it is more reactive than ordinary cement at early ages. Figure 22 and Table 11 show the variation of compressive strength with time for Group 1 mixes.

Table 11 - Compressive Strength of Group 1 (40% Slag) Mixes (psi)

Day	G1M1	G1M2	G1M3
3	4189	3154	5569
7	5860	4853	6285
14	6934	5648	7186
28	7769	6126	7239
56	-	6433	7677
91	-	6245	7518

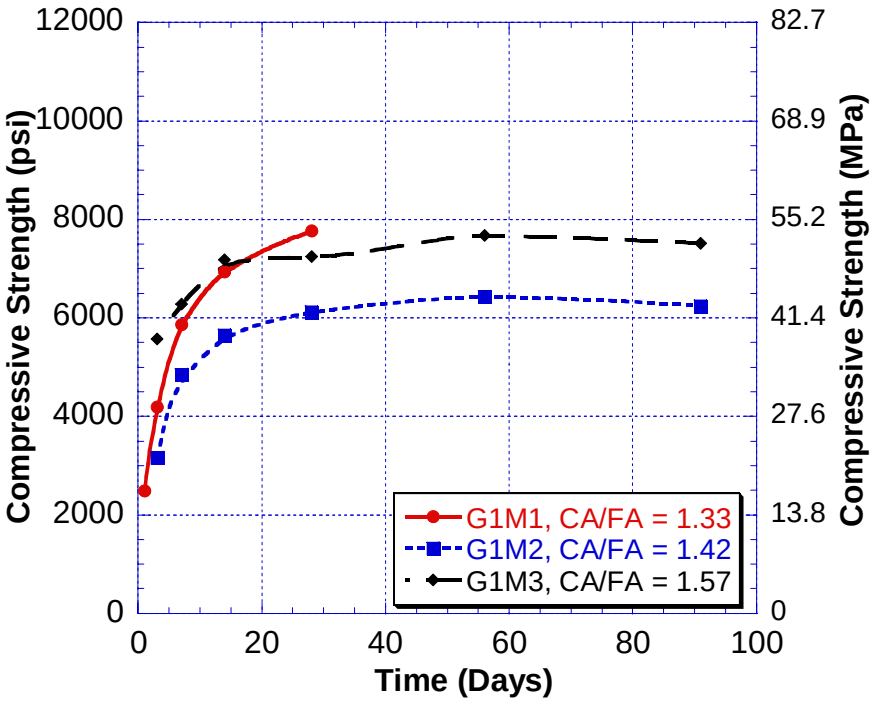

Figure 22. Compressive Strength of Group 1 (40% Slag) Mixes

Table 12 - Compressive Strength of Group 2 (5% Silica Fume and 30% Slag) Mixes (psi)

Day	G2M1	G2M2	G2M3	G2M4	G2M5	G2M6
1	-	1087	-	2247	-	1114
3	3779	3142	5927	4853	3699	4269
7	5569	4415	7133	6298	5290	6497
14	6086	5145	7969	7173	6311	8022
28	6762	5111	8393	7823	6815	8612
56	7001	5357	8930	8115	7100	8791
91	7021	5290	9175	8207	7359	8811

Although total cementitious material is approximately same for all Group 2 mixes, there is tremendous variance in terms of compressive strength. This difference can be correlated to the amount of coarse aggregate used in mix design and the CA/FA ratio. The mixes that attained the highest strengths have the highest coarse aggregate content (1825 lbs/cu.yd or higher). The difference could also be the result of different fine and coarse aggregate sources and their respective properties. This is much harder to correlate since the number of variables is too many to make a reasonable comparison. In comparison to Group 1 mixes with same proportions, higher strengths were achieved in Group 2. Also, Group 2 mixes continued to gain strength after day 14 as illustrated in Table 12 and Figure 23.

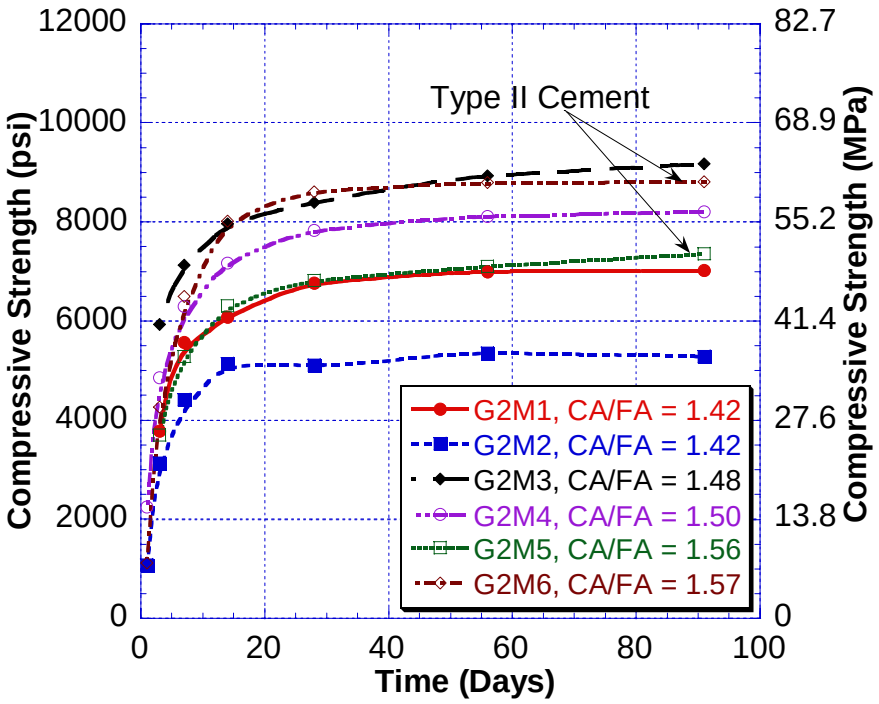

Figure 23. Compressive Strength of Group 2 (5% Silica Fume and 30% Slag) Mixes

The results illustrated in Table 13 and Figure 24 show that the lower strength was observed in G3M1 which is the 5% silica fume only mix. It should be noted that G3M2 uses Type II cement where as G3M1 uses Type I. Some of the difference in strength can be attributed to the percentage of silica fume that was used but the main difference was due to the structure of the aggregate source that was used in G3M1 (Plumstead #57 Rock). The rock type from this source was argillite, which was contaminated with mud stones. This could dramatically reduce the strength of any concrete mix and also affect other properties such as modulus of elasticity and shrinkage.

Table 13 - Compressive Strength of Group 3 (Silica Fume Only) Mixes (psi)

Day	G3M1	G3M2
1	-	2586
3	3660	5914
7	4322	7120
14	4912	8731
28	5449	8930
56	5065	9308
91	4972	-

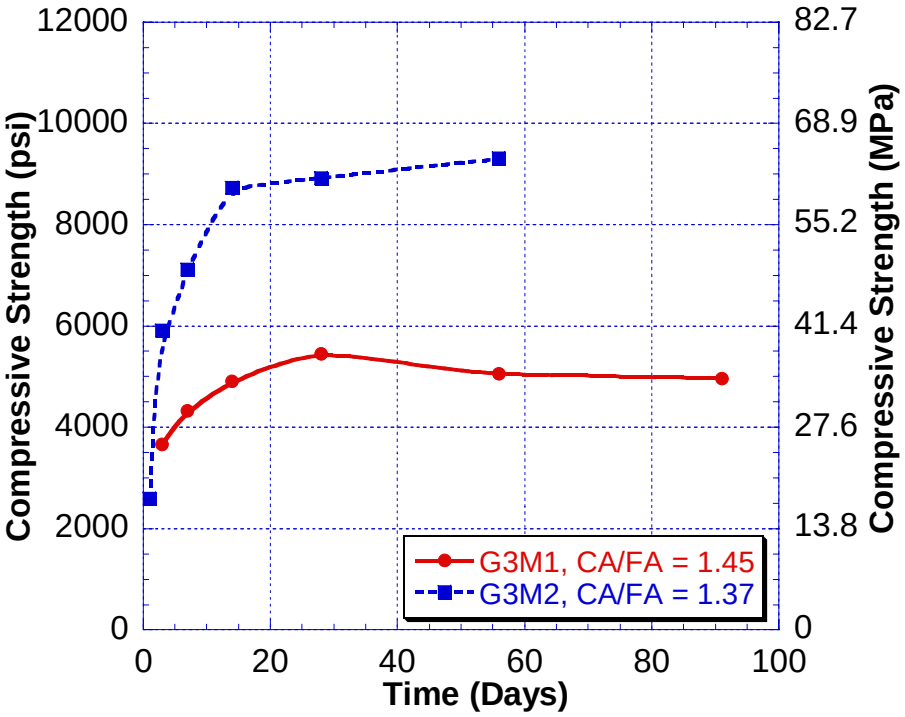

Figure 24. Compressive Strength of Group 3 Mixes

The variation of compressive strength of the various mixes in Group 4 versus time is shown in Table 14 and Figure 25. The highest strength was again achieved by mixes that have the highest CA/FA ratio. It should also be noted that all mixes, except G4M2 have coarse aggregate contents of 1800 lbs/cu.yd or more. Where as G4M2 has only 1700 lbs/cu.yd of coarse aggregate on top of the low CA/FA ratio. The effect of increasing the silica fume and slag amounts can also be analyzed when G4M1 and G4M3 are compared. Clearly increasing the percentages increased the ultimate strength of G4M3.

Table 14 - Compressive Strength of Group 4 Mixes (psi)

Day	G4M1	G4M2	G4M3	G4M4
1	-	-	-	-
3	5728	4018	5728	5231
7	6683	5370	7299	6828
14	7558	6126	8353	8115
28	8539	6563	8910	8221
56	8791	6683	9626	8313
91	9414	6702	10223	8764

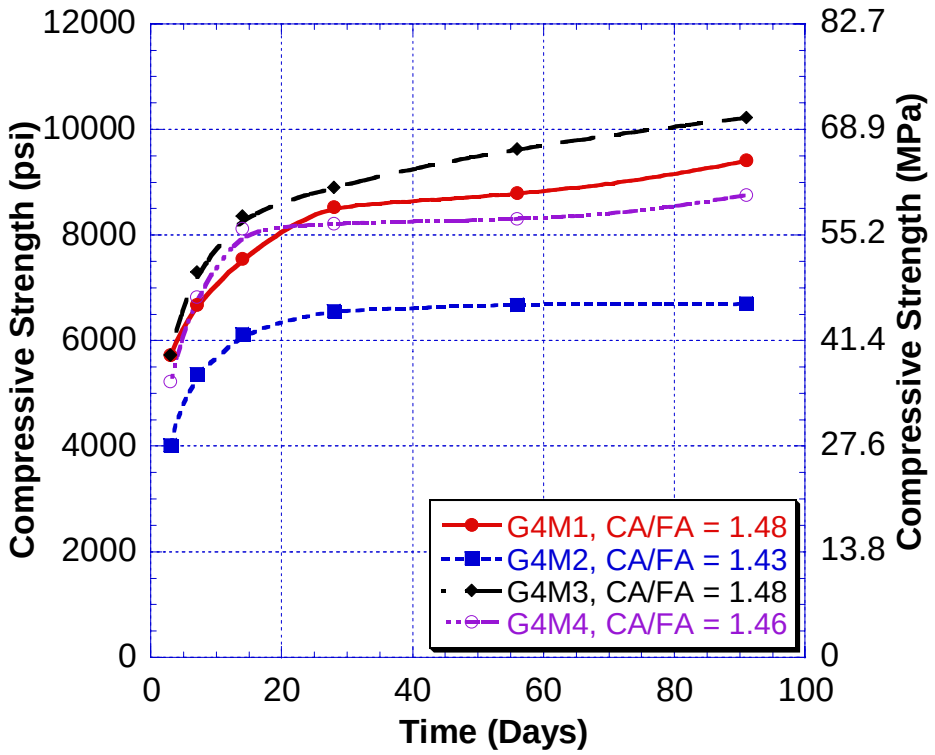

Figure 25. Compressive Strength of Group 4 Mixes

Splitting Tensile Strength

Tensile strength of all mixes closely resembled the trend obtained from compressive strength tests. Table 15 through Table 18 show the splitting tensile strengths with time for Group 1, 2, 3, and 4 mixes, respectively. Again, as in the case of compressive strengths, those mixes with high CA/FA ratio in every Group showed higher splitting tensile strength. Splitting tensile strength is known to depend primarily on the total amount of coarse aggregate in the mix and the lower values obtained from G1M1 are expected.

Table 15 - Splitting Tensile Strength Group 1 (40% Slag) Mixes (psi)

Day	G1M1	G1M2	G1M3
3	507	592	371
7	643	647	557
14	703	796	617
28	789	817	627
56	-	824	629
91	-	-	659

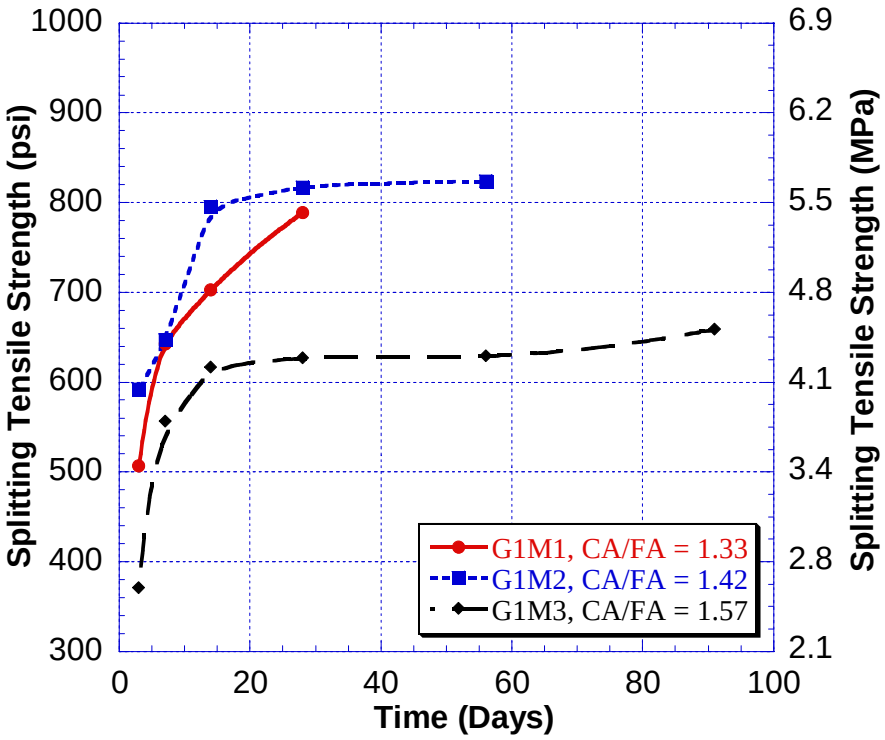

Figure 26. Splitting Tensile Strength of Group 1 (40% Slag) Mixes

The effects of coarse aggregate content, type, and the CA/FA ratio on tensile strength are shown in Figure 26 through Figure 29 for Groups 1, 2, 3, and 4 respectively.

Table 16 - Splitting Tensile Strength of Group 2 (5% Silica Fume and 30% Slag) Mixes (psi)

Day	G2M1	G2M2	G2M3	G2M4	G2M5	G2M6
3	453	329	656	521	446	478
7	517	405	713	643	473	625
14	555	527	766	770	621	691
28	574	576	882	770	674	795
56	594	598	891	781	731	876
91	629	571	901	782	741	872

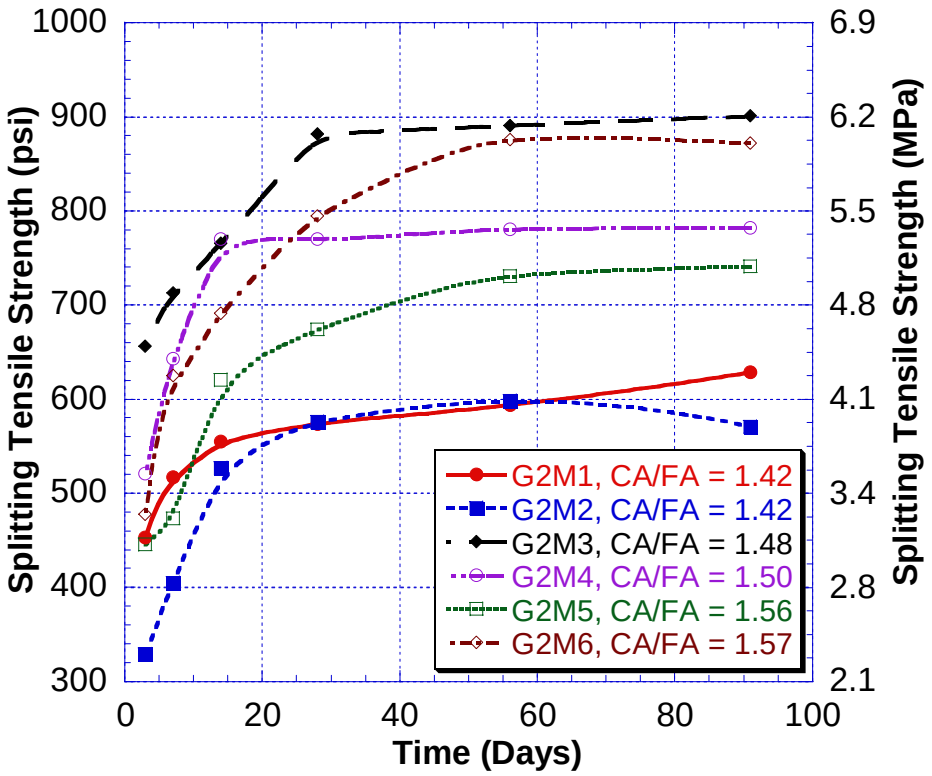

Figure 27. Splitting Tensile Strength of Group 2 (5% Silica Fume and 30% Slag) Mixes

Table 17 - Splitting Tensile Strength of Group 3 (Silica Fume Only) Mixes (psi)

Day	G3M1	G3M2
3	384	508
7	428	686
14	553	730
28	639	848
56	603	838
91	534	-

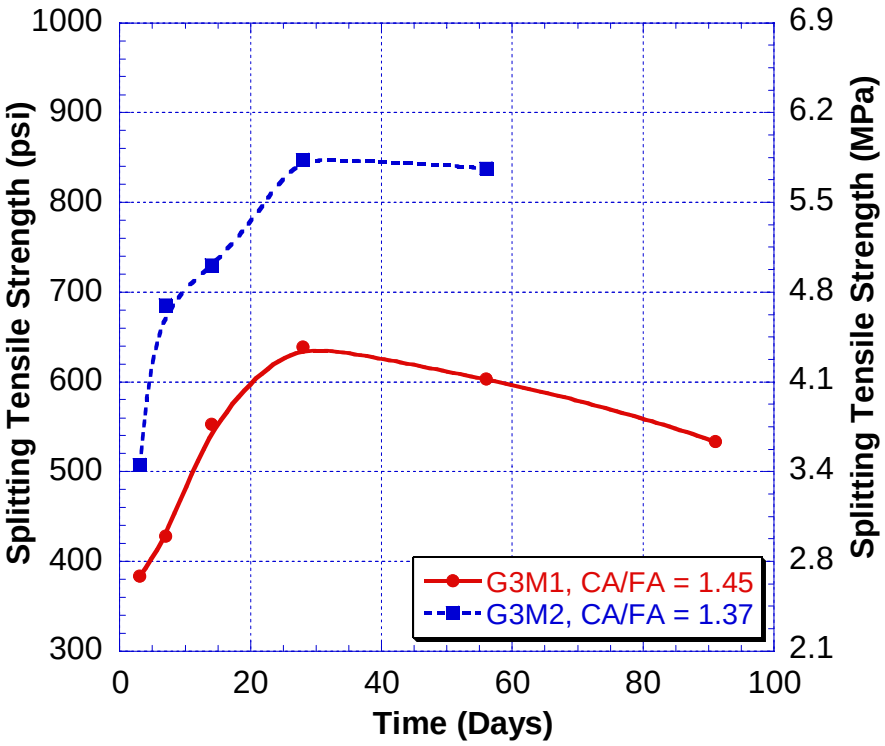

Figure 28. Splitting Tensile Strength of Group 3 (Silica Fume Only) Mixes

Note that G3M1 has decreasing tensile strength after day 28. This is most probably due to the argillite deposits as mentioned earlier. Test results had too much variation and the average of 3 samples were low on day 56 and day 91 compared to day 28.

Table 18 - Splitting Tensile Strength of Group 4 Mixes (psi)

Day	G4M1	G4M2	G4M3	G4M4
3	621	464	678	544
7	733	564	749	637
14	775	-	789	781
28	814	617	856	823
56	848	657	906	840
91	860	670	943	808

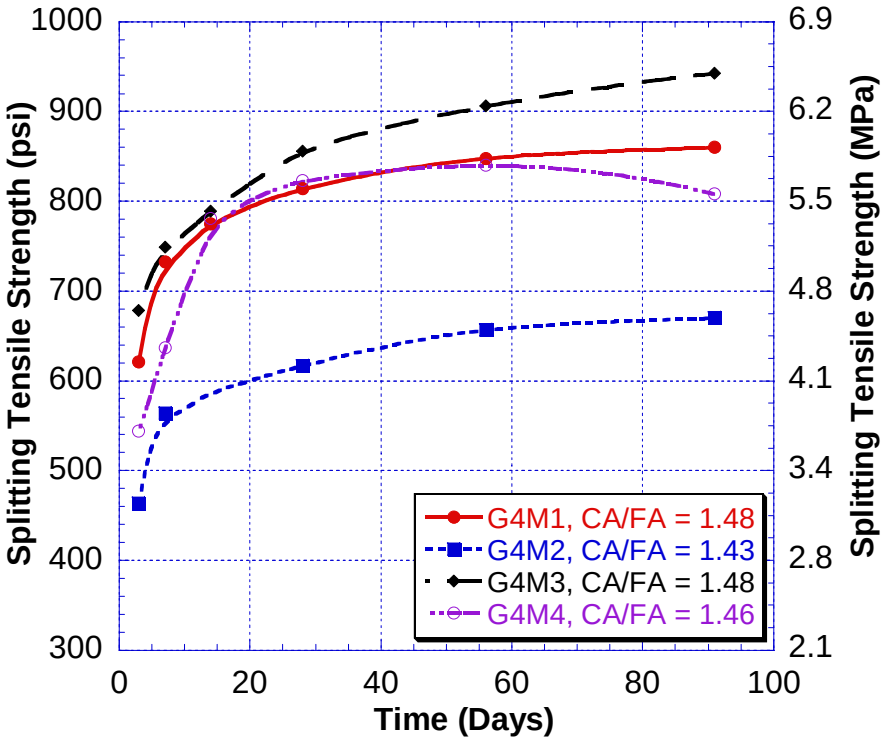

Figure 29. Splitting Tensile Strength of Group 4 Mixes

Free Shrinkage

The major factors that affect shrinkage are cementitious content, percentage of cementitious materials, w/c ratio, coarse aggregate content, and C/F ratio. Considering all these variables it is logical to see that mix G1M2 has experienced more shrinkage than G1M3 since the total aggregate content in its composition is lower. Results from mix G1M1 also support the argument that using low CA/FA ratio in a mix will increase the free shrinkage. These results are shown in Table 19 at various ages of concrete and also shown graphically in Figure 30. It can be seen that mix G1M2, which cracked at day 9, would be rejected if the proposed limit for shrinkage was used. Current specifications however, permit the use of this mix which might lead to shrinkage cracking due to its high cracking potential.

Table 19 - Free Shrinkage of Group 1 (40% Slag) Mixes (με)

Day	G1M1	G1M2	G1M3
7	0	0	0
8	-112	-170	-90
10	-233	-249	-163
14	-323	-374	-237
21	-413	-471	-307
28	-483	-513	-367
42	-557	-577	-408
56	-	-614	-440
91	-	-663	-477
154	-	-716	-509
187	-	-	-543

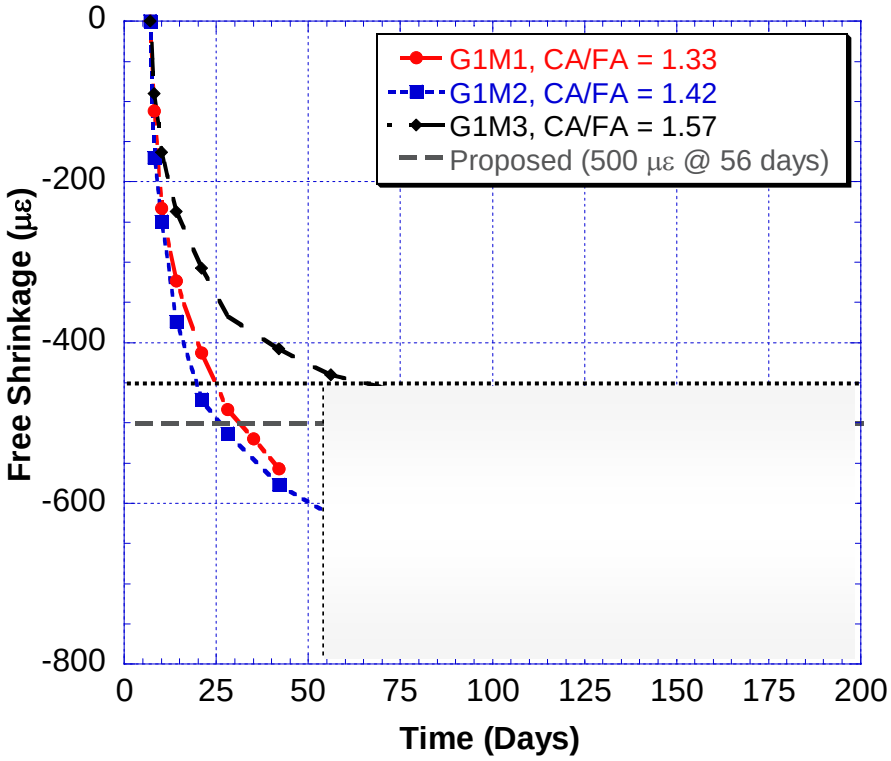

Figure 30. Free Shrinkage of Group (40% Slag) 1 Mixes

Figure 31 and Table 20 illustrate the free shrinkage results from Group 2 mixes. The highest shrinkage was observed in mixes with the lowest CA/FA ratio. The lowest shrinkage was in mix G2M3 which has the highest aggregate content. Using Type II cement also reduced the free shrinkage considerably (G2M5 and G2M6). Again, if the

proposed free shrinkage limit is used two mixes with the highest free shrinkage are eliminated.

Table 20 - Free Shrinkage of Group 2 (5% Silica Fume and 30% Slag) Mixes (με)

Day	G2M1	G2M2	G2M3	G2M4	G2M5	G2M6
7	0	0	0	0	0	0
8	-123	-136	-63	-136	-83	-116
10	-216	-240	-129	-230	-156	-196
14	-323	-336	-176	-313	-213	-253
21	-397	-419	-217	-353	-266	-310
28	-493	-470	-250	-386	-306	-346
42	-536	-529	-298	-434	-343	-393
56	-563	-570	-340	-460	-366	-426
91	-605	-633	-360	-506	-406	-463
154	-660	-	-420	-	-	-
187	-660	-	-480	-	-	-

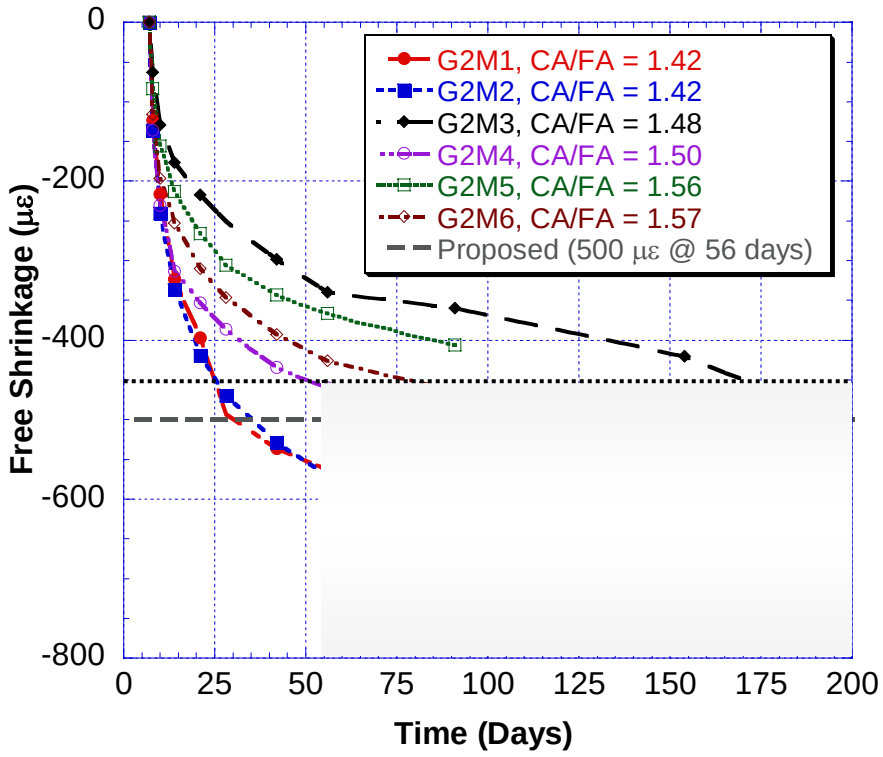

Figure 31. Free Shrinkage of Group 2 (5% Silica Fume and 30% Slag) Mixes

Figure 32 and Table 21 illustrate the free shrinkage results for Group 3 mixes. Although the CA/FA ratio of G3M2 is lower than G3M1, the total amount of coarse aggregate is slightly higher. Also, G3M2 uses Type II cement. However, as mentioned earlier, the main reason for the difference between the two mixes is the source of the aggregate. G3M1 utilizes aggregates with argillites deposits which are known to have high shrinkage characteristics. Once again, if the current specifications are considered both mixes would be acceptable. However, it can be seen in Figure 32 that based on the new proposed limit mix G3M1, which cracked on day 9 would be rejected and G3M2 which did not crack would be accepted.

Table 21 - Free Shrinkage of Group 3 (Silica Fume only) Mixes (με)

Day	G3M1	G3M2
7	0	0
8	-113	-80
10	-217	-147
14	-310	-213
21	-430	-286
28	-490	-323
42	-542	-358
56	-570	-383
91	-610	-426

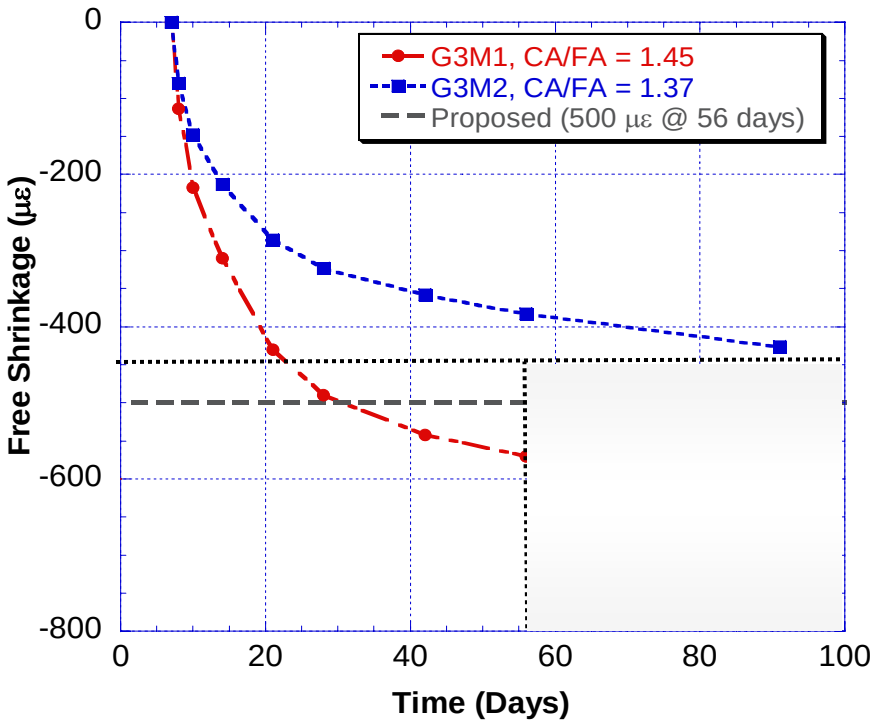

Figure 32. Free Shrinkage of Group (Silica Fume only) 3 Mixes

The free shrinkage results for Group 4 mixes are shown in Table 22 and Figure 33. Highest free shrinkage was observed in mix G4M2 which has the lowest CA/FA ratio and low aggregate content of 1700lbs/cu.yd. Remaining mixes have aggregate contents of 1800 lbs/cu.yd or more and experienced considerably less free shrinkage. Even though mix G4M2 experienced cracking at early age and is susceptible to restrained shrinkage cracking, the current specifications allow it to be used. The new proposed limit at 56 days would eliminate that mix while keeping the remaining mixes which had comparatively much lower cracking potentials.

Table 22 - Free Shrinkage of Group 4 Mixes (με)

Day	G4M1	G4M2	G4M3	G4M4
7	0	0	0	0
8	-70	-75	-70	-73
10	-130	-174	-130	-120
14	-190	-310	-176	-193
21	-249	366	-220	-246
28	-290	-426	-226	-270
42	-334	-467	-265	-312
56	-365	-506	-303	-336
91	-410	-603	-340	-366
154	-	-663	-399	-
187	-		-426	-

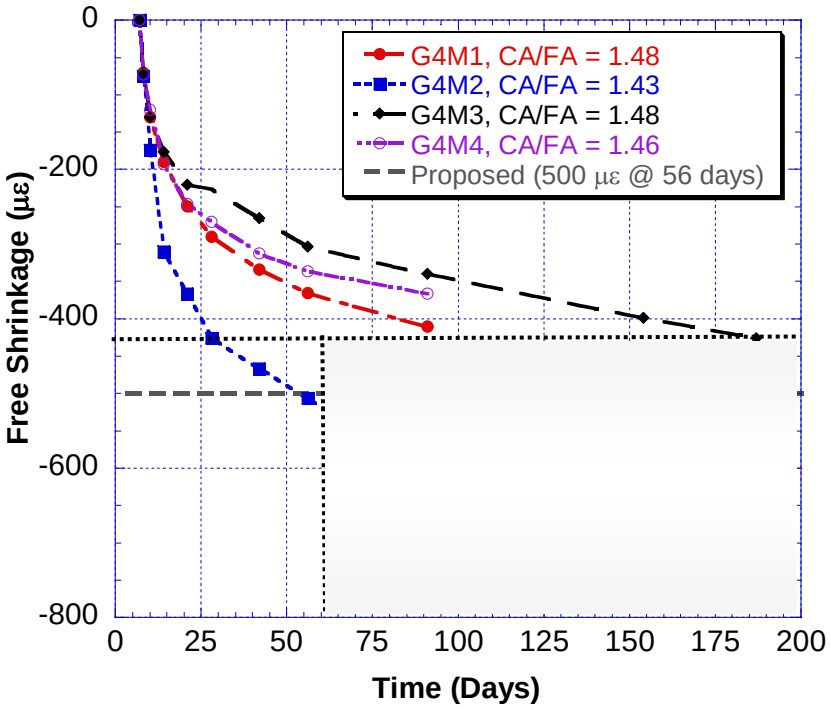

Figure 33. Free Shrinkage of Group 4 Mixes

Autogenous Shrinkage

Autogenous shrinkage is generally not significant if the initial water in a concrete mix design is enough to fully hydrate the cement particles. Therefore, this type of shrinkage is not expected to be significant for w/c ratios of 0.36 or higher. To test this, 3 mixes in Group 2 were tested using the setup in Figure 14. The strains obtained are shown in Figure 34 and the temperature profile is illustrated in Figure 35. It can be seen that only mix G2M6 has experienced shrinkage, but this value is negligible compared to ultimate shrinkage. Remaining mixes showed expansion during hydration which is an indication that the initial water was enough to fully hydrate the cement particles. This is also supported by the temperature profile within the specimens. Strain values peak when the temperatures peak and later they start decreasing due to decreasing temperature. It should also be noted that these samples were completely sealed and no curing water was available for the duration of the test. Autogenous shrinkage is known to decrease or even eliminated in the presence of an outside water source. Since curing was started immediately following casting of specimens, effects of autogenous shrinkage can be neglected for unrestrained and restrained shrinkage tests.

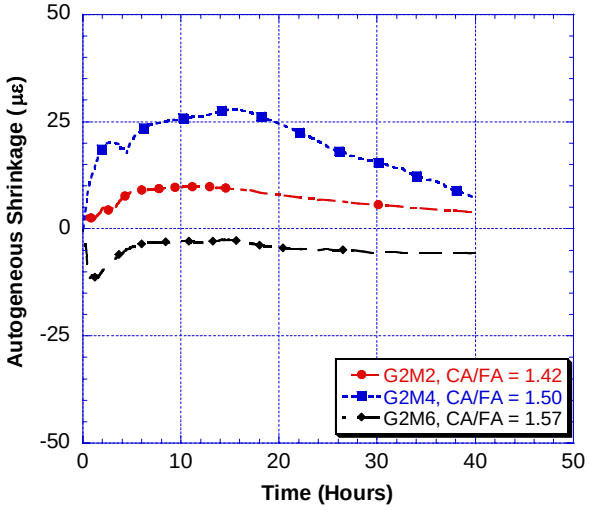

Figure 34. Autogenous Shrinkage of Various Mixes in Group 2

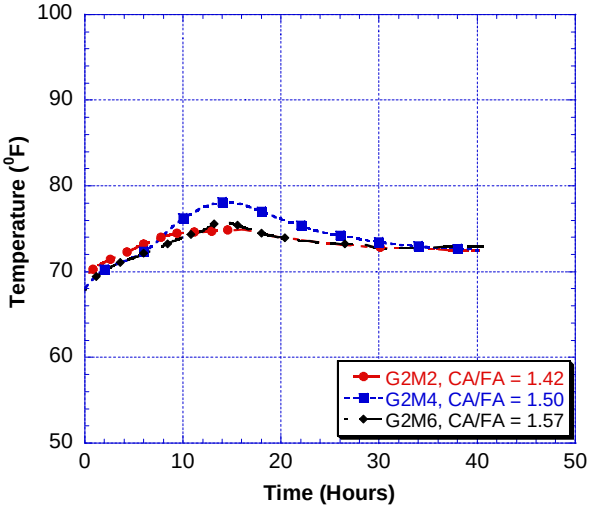

Figure 35. Temperature Profile of Autogenous Shrinkage Specimens

Modulus of Elasticity

All mixes have similar behavior in terms of elastic modulus development. During the first 7 day wet curing period, the elastic modulus is observed to increase rapidly. After the curing period modulus values peak at 14 days, and at later ages the elastic modulus remains constant or in some cases shows a slight decrease. This is due to the curing history of the test specimens. For the first seven days the samples are wet cured and the pore network within the concrete is filled with water. After removal of curing the

specimens begin to dry and the water in the pores is replaced by air. As a result the modulus of elasticity does not increase much or even decreases in some cases.

Test results for Group 1 mixes are summarized in Table 23 and graphically represented in Figure 36. As with all mechanical properties the higher values are obtained in mixes with high coarse aggregate contents or high CA/FA ratios. Also, the increase of elastic modulus with time is not significant. This is most likely due to the reactive nature of slag. Since it reacts much faster than cement at an early age elastic modulus is high for all mixes.

Table 23 - Modulus of Elasticity of Group 1 (40% Slag) Mixes (ksi)

Day	G1M1	G1M2	G1M3
3	4205	3577	4943
7	5087	3876	5156
14	5083	4052	5317
28	5128	4072	5341
56	-	3851	5328
91	-	3672	5493

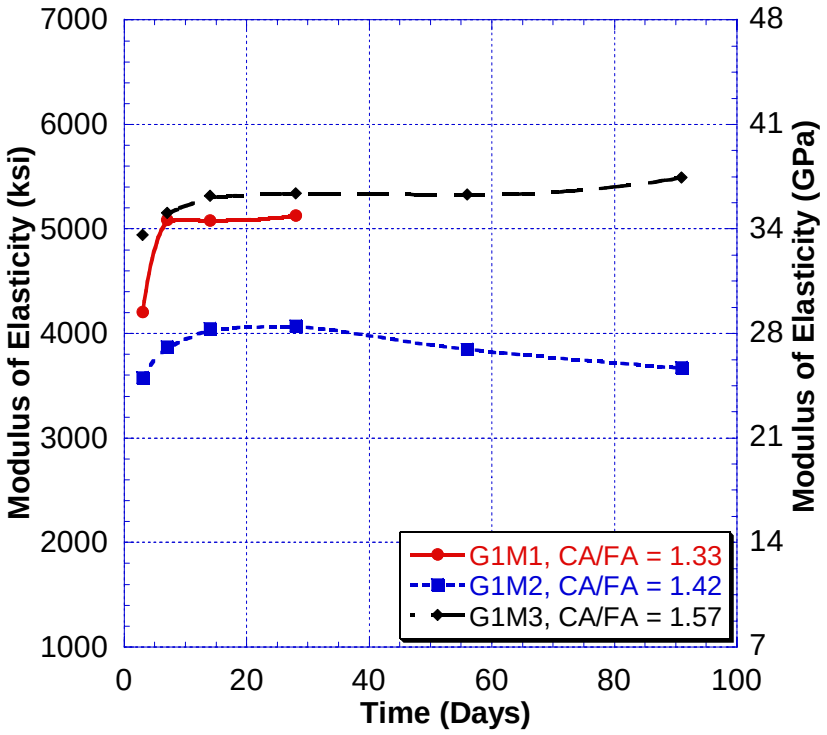

Figure 36. Modulus of Elasticity of Group (40% Slag) 1 Mixes

Figure 37 and Table 24 illustrate the modulus of elasticity of Group 2 mixes. The results are similar to Group 1 results with highest modulus observed in mixes with of a CA/FA ratio greater than 1.48.

Table 24 - Modulus of Elasticity of Group 2 (5% Silica Fume and 30% Slag) Mixes (ksi)

Day	G2M1	G2M2	G2M3	G2M4	G2M5	G2M6
3	3501	3389	5522	4829	3800	3739
7	4289	3959	5838	5076	4026	4465
14	4094	3650	5898	5126	4093	4657
28	3991	3493	5820	4829	4181	4552
56	4019	3484	-	4710	4091	4727
91	3823	3344	5773	4387	3890	4600

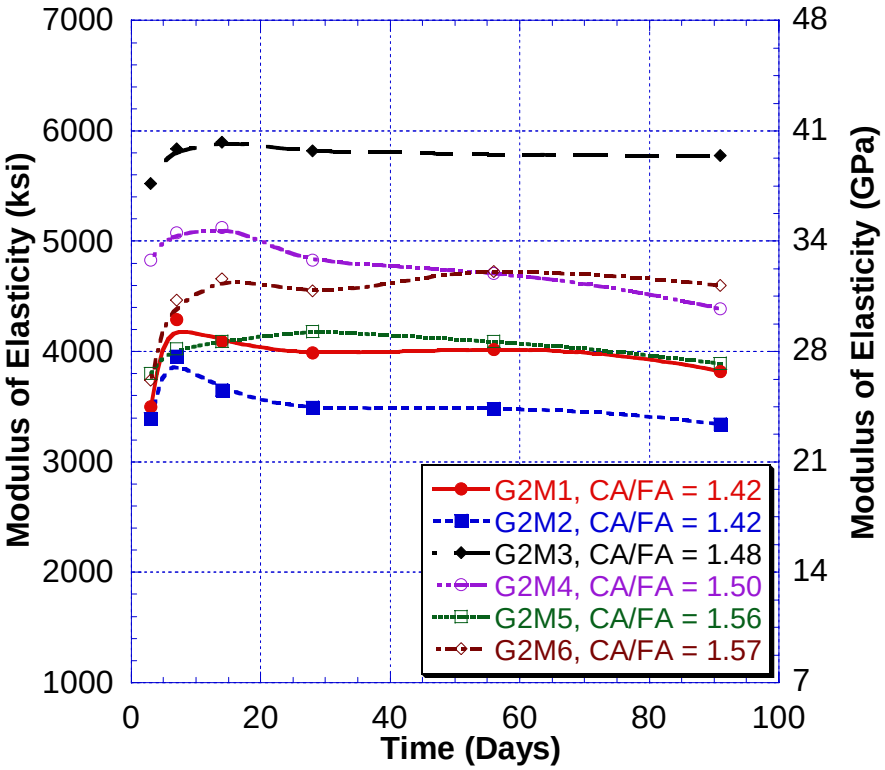

Figure 37. Modulus of Elasticity of Group 2 (5% Silica Fume and 30% Slag) Mixes

Results for Group 3 and Group 4 are illustrated in Table 25, Table 26, Figure 38, and Figure 39.

Table 25 - Modulus of Elasticity of Group 3 (Silica Fume only) Mixes (ksi)

Day	G3M1	G3M2
3	3168	4290
7	3276	4615
14	3376	4563
28	3533	4543
56	3712	4620
91	3416	-

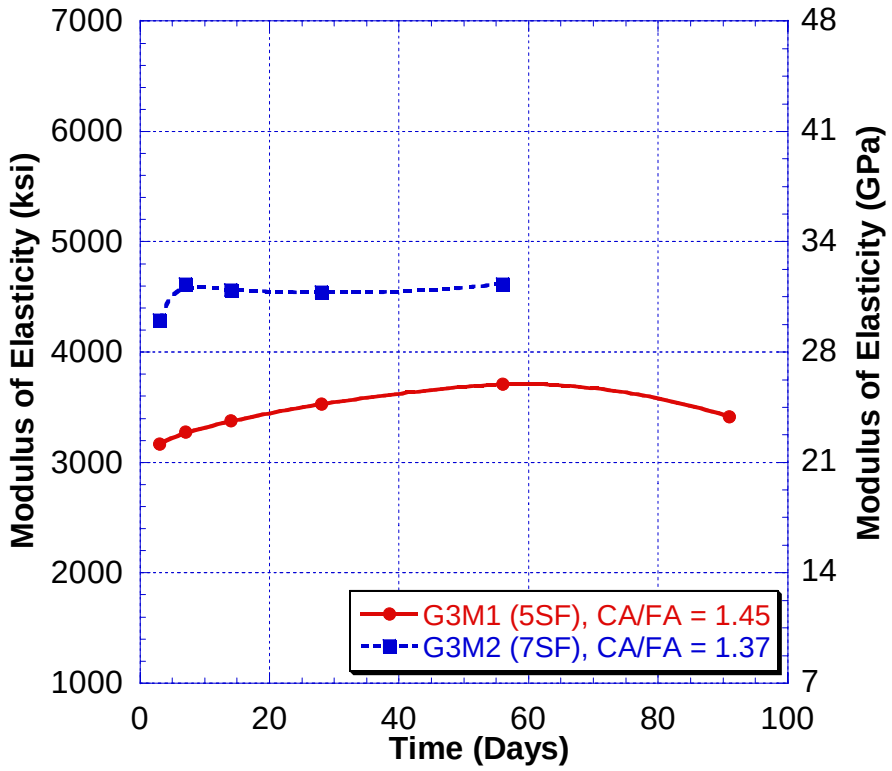

Figure 38. Modulus of Elasticity of Group 3 (Silica Fume only) Mixes

Table 26 - Modulus of Elasticity of Group 4 Mixes (ksi)

Day	G4M1	G4M2	G4M3	G4M4
3	5189	3540	5449	4853
7	5348	4202	5572	5259
14	5463	4260	5578	5655
28	5783	4218	5596	5252
56	5885	-	5655	5278
91	5962	3977	5559	5133

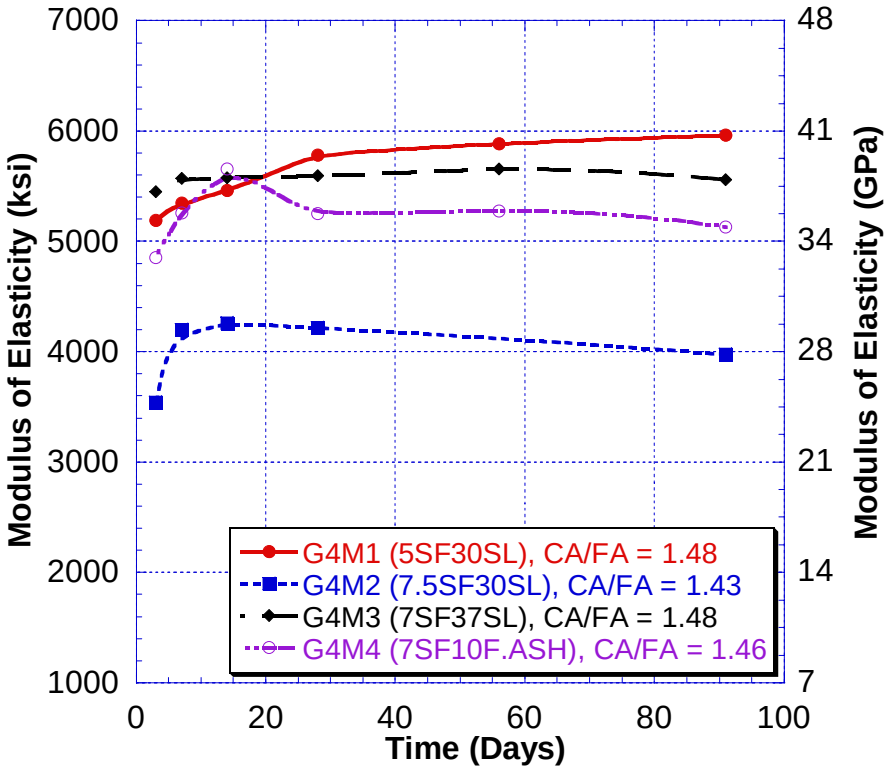

Figure 39. Modulus of Elasticity of Group 4 Mixes

Correlation of Cracking Potential under Restrained Shrinkage Conditions with Free Shrinkage Performance

Although restrained shrinkage is dependant on a combination of free shrinkage and other mechanical properties of a given mix, the mechanism involving both are the same. Therefore, the magnitude and rate of free shrinkage could be a good indication of the performance of a concrete mixture in restrained shrinkage.

From literature, it is known that for thin concrete rings drying is directly proportional to the square root of time. In the AASHTO setup, which is considered a thick ring, the drying relationship was found to be proportional to the logarithm of time. When observed strains in free and restrained shrinkage are plotted against the logarithm of time, linear relationships are obtained. If a mix has cracked within 56-days, the rate at cracking age is used but if the mix did not crack before 56 days, the 56-day rate is used.

To understand the relationship between both rates, each group was analyzed separately, and the free as well as restrained shrinkage rates were compared. Figure 40 and Figure 41 illustrate the free and restrained shrinkage rates in Group 1 mixes, respectively. It can be seen that G1M1 mix having higher free shrinkage rate also has higher restrained shrinkage rate. The reason for this high rate and early cracking is the high cementitious content and the low CA/FA ratio of this mix. It should be also noted that G1M3 mix, which has not cracked has less than 500 microstrains of free shrinkage at 56 days.

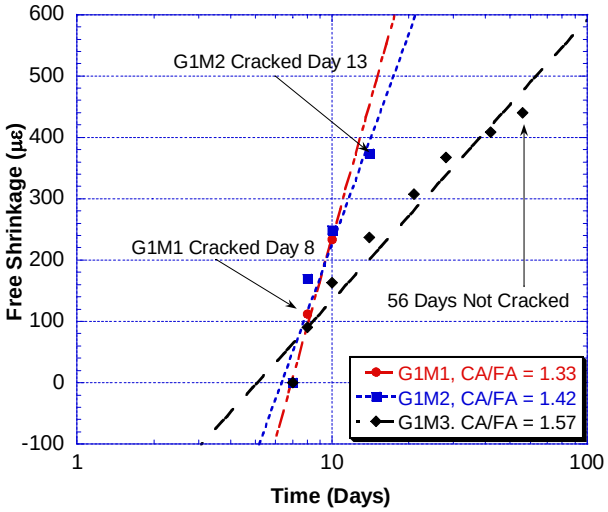

Figure 40. Rate of Free Shrinkage for Group 1 Mixes

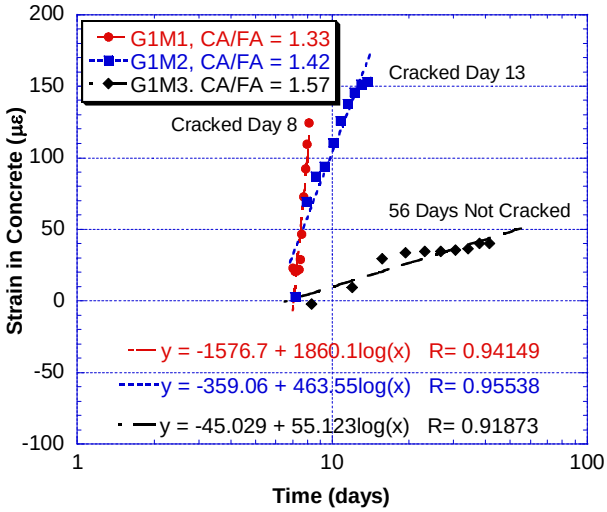

Figure 41. Rate of Restrained Shrinkage for Group 1 Mixes

Figure 42 and Figure 43 show that for Group 2 mixes the free and restrained shrinkage are highly correlated. The only mix which has not cracked within Group 2 is mix G2M3 and it has the lowest free shrinkage as well as restrained shrinkage rates. The two mixes G2M1 and G2M5, which both cracked around day 44, have the lowest free and restrained shrinkage rates after G2M3. The other mixes have very high shrinkage rates since the mixes cracked within the first 7 days after initiation of drying confirming their high potential for cracking.

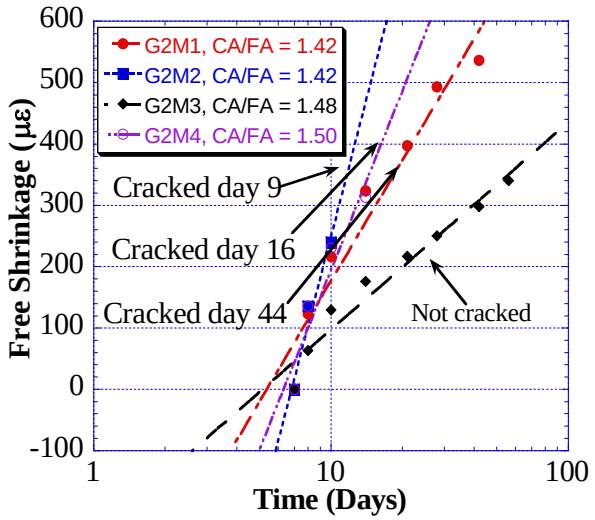

Figure 42. Rate of Free Shrinkage for Group 2 Mixes

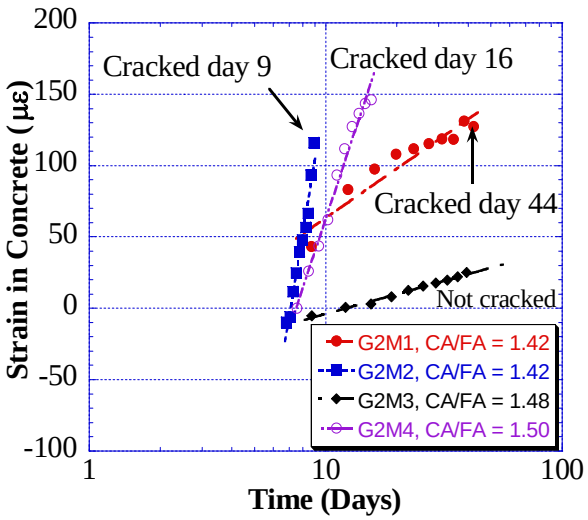

Figure 43. Rate of Restrained Shrinkage for Group 2 Mixes

Figure 44 and Figure 45 illustrate the same relationship for Group 3 mixes. Again the mix with the higher free shrinkage rate has a much higher restrained shrinkage rate. It can be observed that although mix G3M2 has a lower CA/FA ratio it also has a lower strain rate. It is also observed that mix G3M2 has lower than 500 microstrains at 56 days where as mix G3M1 has higher than 500 microstrains. This is due to the total amount of coarse aggregate used in these mixes. If the mix design tables are analyzed it can be seen that G3M2 actually has more total coarse aggregate in its design. Also, the presence of argillite deposits in the coarse aggregate source of mix G3M1 greatly reduces its performance in terms of free and restrained shrinkage.

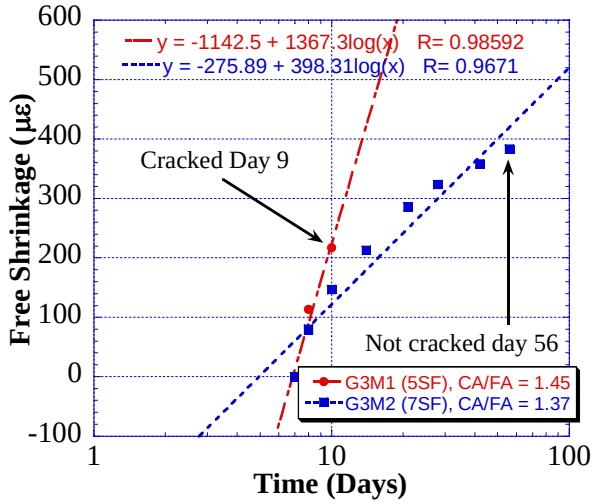

Figure 44. Rate of Free Shrinkage for Group 3 Mixes

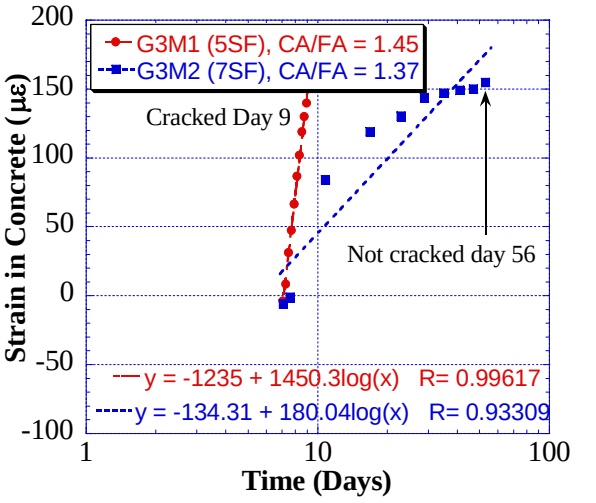

Figure 45. Rate of Restrained Shrinkage for Group 3 Mixes

Finally, Group 4 mixes also follow the same trend. Figure 46 and Figure 47 show that the rate of free shrinkage correlates directly with the restrained shrinkage rate. G4M2 mix has the highest rate and it cracked at 11 days. Mix G4M4 has the second highest rate and it cracked at day 60. The remaining two mixes have the lowest restrained shrinkage rates and they did not experience any cracking for the period of testing.

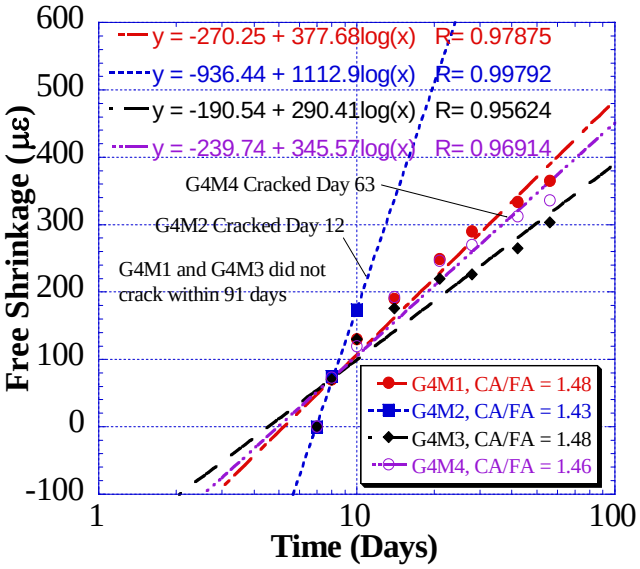

Figure 46. Rate of Free Shrinkage for Group 4 Mixes

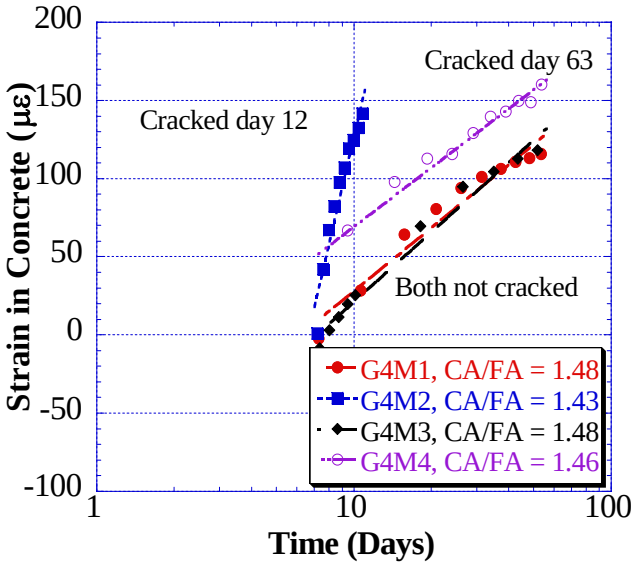

Figure 47. Rate of Restrained Shrinkage for Group 4 Mixes

Figure 48 illustrates the correlation of restrained shrinkage rates from all mixes against the free shrinkage rates. It can be seen that mixes that have low free shrinkage rates also have low restrained shrinkage rates. As the free shrinkage rate increases, the restrained shrinkage rate increases. This means that if there is an increase in free shrinkage rate, the increase in restrained shrinkage rate will be higher. Therefore, it is very important to keep free shrinkage rates as low as possible. The mixes that have been circled in the graphs were observed to have the lowest free shrinkage rates. Moreover, all of these mixes have at 56 days free shrinkage values of less than 500 microstrains. This means that keeping 56-day free shrinkage values low will lower both free and restrained shrinkage rates. It should also be noted that five of the seven mixes that are in the low zone (represented by full rectangles) have not cracked for the duration of the test. The remaining two mixes cracked the latest compared to the rest of the mixes in the study.

Table 27 - Mixes with Lowest Free and Restrained Shrinkage Rates

	G1M3	G2M3	G3M2	G4M1	G4M3	G4M4
Cracking Day	N/A	N/A	N/A	N/A	N/A	60
56 day Free Shrinkage (με)	-440	-340	-383	-365	-303	-336

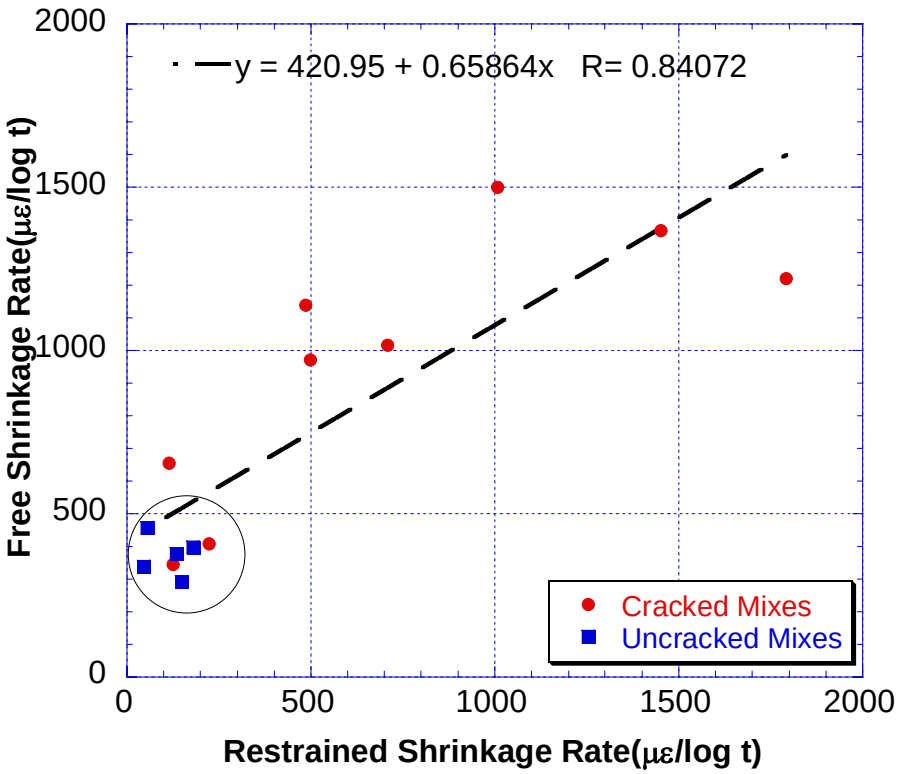

Figure 48. Free Shrinkage Rate vs. Restrained Shrinkage Rate

Correlation of Cracking Potential with Aggregate Content and CA/FA Ratio

Using all mixes in the study correlation of restrained and free shrinkage rates with CA/FA ratio was investigated. Also, a comparison was made between cracked and uncracked mixes to determine the affect of coarse aggregate content and CA/FA ratio on cracking behavior of the mixes. Table 28 below illustrates this comparison. It can be seen that four out of the five mixes that did not crack have coarse aggregate content of 1850 lbs/cu.yd or more. Also, the CA/FA ratio for these four mixes is in the range of 1.48 to 1.57. Majority of the cracked mixes, however, have coarse aggregate contents of 1725 lbs/cu.yd or less, and the CA/FA ratio for those mixes are all below 1.48. It is observed that mix G1M1, which has the lowest coarse aggregate content, lowest CA/FA ratio, and the highest cementitious content cracked earliest. The results from mixes G2M5 and G2M6 are inconclusive since one ring specimen cracked while the other specimen did not. Therefore, these mixes were not included in the correlations.

Table 29 illustrates the percentages of cracked and uncracked mixes with respect to the amount of coarse aggregate used in their design and the CA/FA ratios. Seven out of the eight cracked mixes have CA/FA ratios lower than 1.48. Also, six of these mixes have less than 1725 lbs/cu.yd of coarse aggregate content in their design. This result is numerically presented in Figure 49. By comparing these results it can concluded that

the majority of the mixes that cracked have low aggregate content and the majority of the mixes that did not crack have high coarse aggregate contents.

Table 28 - Comparison of Cracked and Uncracked Mixes with Respect to Coarse Aggregate Content and CA/FA Ratio

Group	MIX	Cracking Day		CA/FA	CA Content (lbs/cu.yd)	Cement Content (lbs/cu.yd)
		Ring 1	Ring 2			
1	G1M1	8	10	1.33	1650	800
	G1M2	13	13	1.42	1700	658
	G1M3	Not Cracked	Not Cracked	1.57	1875	660
2	G2M1	47	44	1.42	1700	658
	G2M2	9	10	1.42	1700	658
	G2M3	Not Cracked	Not Cracked	1.48	1850	657
	G2M4	16	20	1.5	1850	658
	G2M5	43	53	1.56	1825	661
	G2M6	Not Cracked	Not Cracked	1.57	1811	683
3	G3M1	10	9	1.45	1725	735
	G3M2	Not Cracked	Not Cracked	1.37	1750	705
4	G4M1	Not Cracked	Not Cracked	1.48	1850	667
	G4M2	13	11	1.43	1700	658
	G4M3	Not Cracked	Not Cracked	1.48	1850	707
	G4M4	65	60	1.46	1800	690

Table 29 - Percentage of Cracked or Uncracked Mixes with respect to Coarse Aggregate Content and CA/FA Ratio

	Number of Mixes	CA/FA Ratio	CA Content
Total Uncracked	5	80% equal to or greater than 1.48	80% equal to or higher than 1850 lbs/cu.yd
Total Cracked	8	88% less than 1.48	75% Less than 1725 lbs/cu.yd

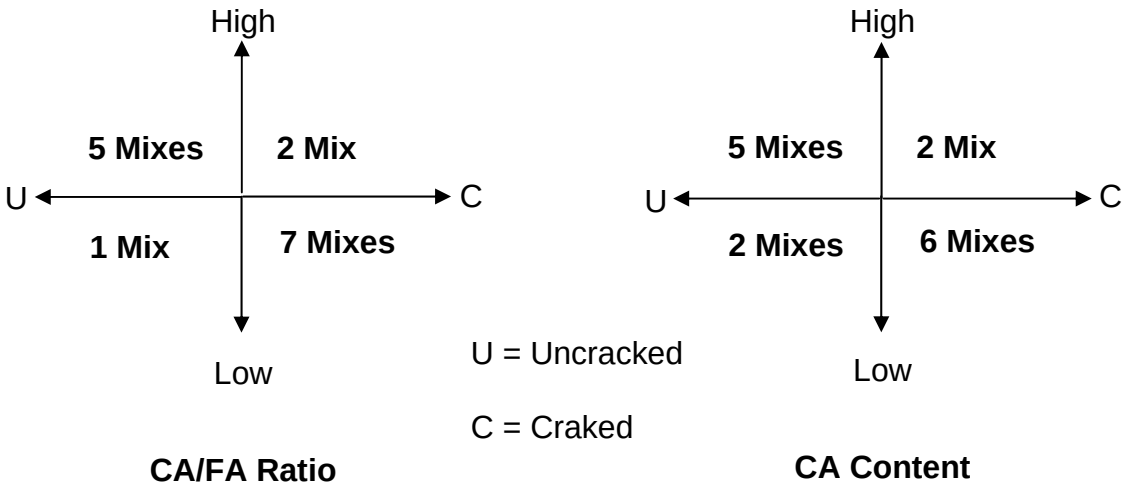

Figure 49. Number of Cracked or Uncracked Mixes with Respect to Coarse Aggregate Content and CA/FA Ratio

If on the other hand two mixes having almost the same mix proportions, except with different CA/FA ratios, are compared the influence of this parameter is much clearer as shown in Figure 52 and Figure 53. Mixes G1M2 and G1M3 are 40% slag mixes and their mix proportions are shown in Table 7. The only difference between the two mixes is the amount of coarse aggregate used (therefore the CA/FA aggregate ratio). Figure 50 through Figure 53 compare the free shrinkage, average steel strain, free shrinkage rate, and restrained shrinkage rate that was observed in the two mixes. Although the steel strains observed are similar, the strain observed in concrete is much different for the two mixes. Mix G1M3 only used 37% of its capacity in tension where as mix G1M2 cracked at day 14 and strains continued to increase which means that the crack was expanding. This difference is also noticed in free shrinkage, free shrinkage rate, and restrained shrinkage rate. At the end of 150 days free shrinkage of G1M3 is considerably less than free shrinkage of G1M2. Also, free and restrained shrinkage rates of mix G1M2 were much greater than mix G1M3. The effect of CA/FA ratio is therefore clear. For a given cementitious content and w/c ratio, increasing the total amount of coarse aggregate, and therefore the CA/FA ratio, will decrease the cracking

potential of a concrete mix considerably. Another important point is that using the new proposed limit for free shrinkage at 56 days would result in rejecting mix G1M2.

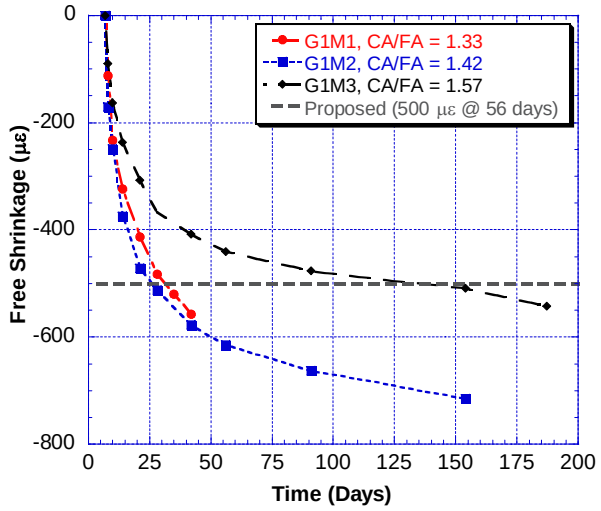

Figure 50. Free Shrinkage Comparison of 40% Slag Mixes

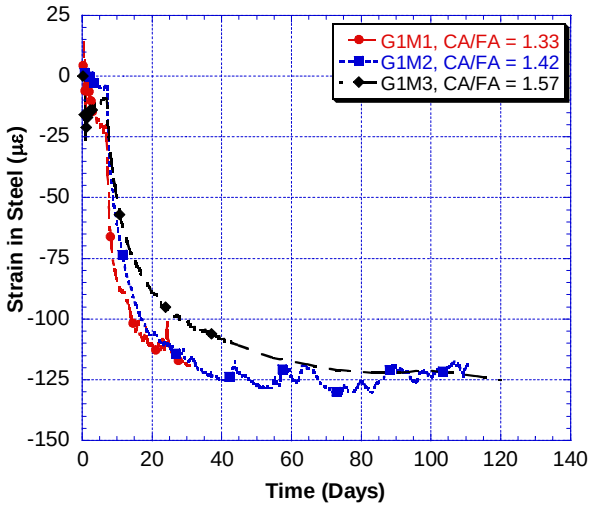

Figure 51. Steel Strain Comparison of 40% Slag Mixes

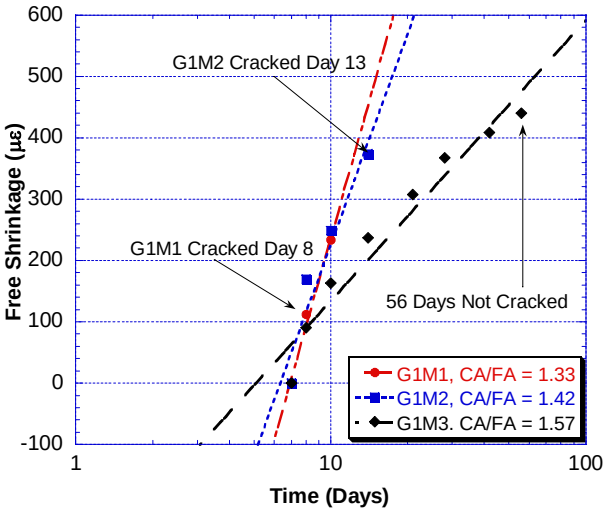

Figure 52. Comparison of Free Shrinkage Rate for 40% Slag Mixes

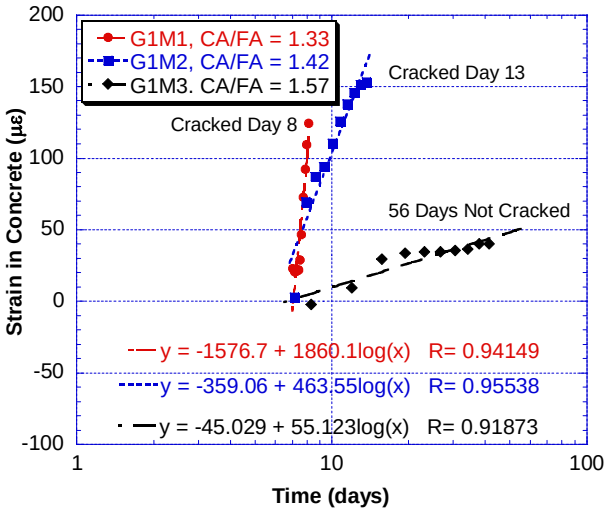

Figure 53. Comparison of Restrained Shrinkage Rate for 40% Slag Mixes

The results obtained from mix G1M1 also strengthens the conclusion drawn. This mix has more cementitious content and has the lowest CA/FA ratio of all the mixes. Figure 52 shows that this mix cracked at day 8, which is considerably earlier than the other two mixes. The strains observed in the steel ring and the free shrinkage experienced also supports this point.

Table 8 illustrates the mix proportions for Group 2 mixes. If G2M2 and G2M4 are analyzed the difference is in the coarse and fine aggregate amounts used. Mix G2M4 has a CA/FA ratio of 1.50 with a high coarse and fine aggregate content (1850 lbs/cu.yd coarse aggregate and 1230 lbs/cu.yd sand). On the other hand, mix G2M2 has a slightly lower CA/FA ratio of 1.42 (1700 lbs/cu.yd coarse aggregate and 1190 lbs/cu/yd sand). Figure 54 through Figure 57 illustrate the difference in shrinkage behavior of these mixes. As before, the mix with the higher CA/FA ratio experiences less free shrinkage and both free and restrained shrinkage rates are lower. Although both mixes cracked, the mix with the higher CA/FA ratio cracked 7 days later than the other mix.

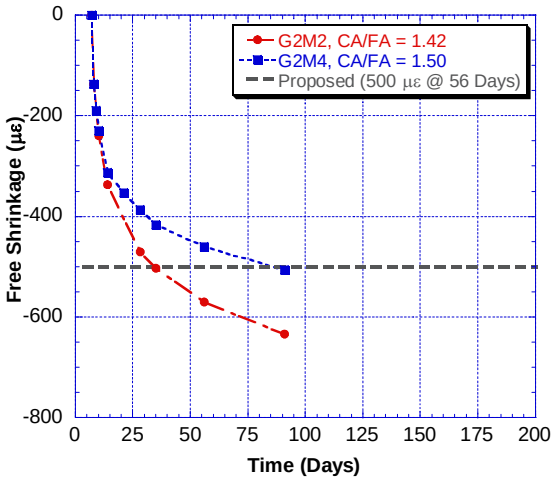

Figure 54. Free Shrinkage Comparison of G2M2 and G2M4

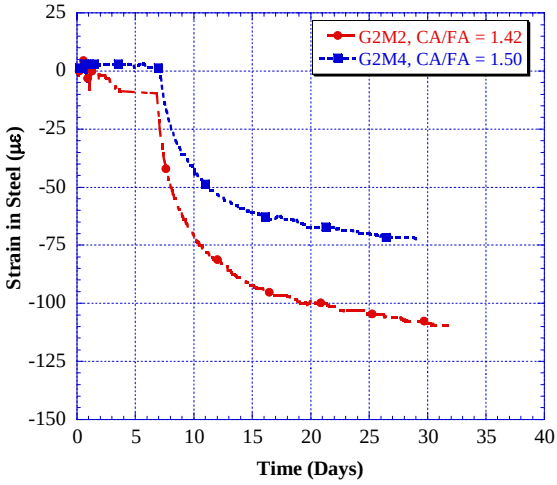

Figure 55. Steel Strain Comparison of G2M2 and G2M4

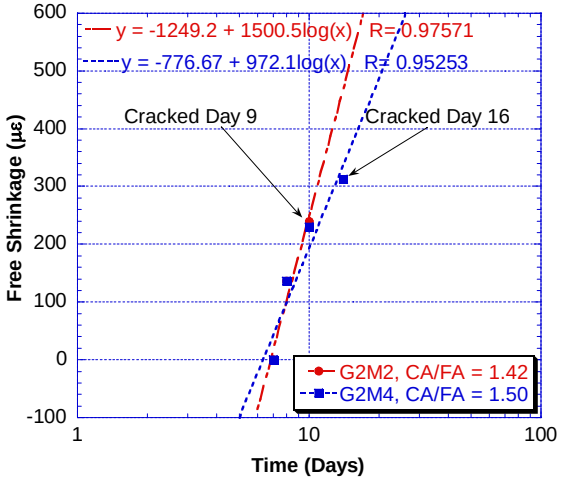

Figure 56. Comparison of Free Shrinkage Rate for G2M2 and G2M4

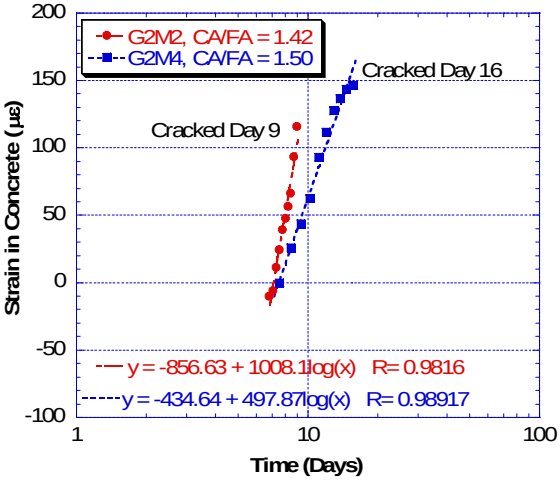

Figure 57. Comparison of Restrained Shrinkage Rate for G2M2 and G2M4

As discussed before the CA/FA has a significant effect on reducing free shrinkage and cracking potential. Generally higher CA/FA ratios are associated with high coarse aggregate contents. Figure 58 and Figure 59 correlate restrained shrinkage rate and free shrinkage rate to coarse aggregate content for all mixes. There is no clear relationship for restrained shrinkage rate and the relationship with free shrinkage is rather weak. This is expected since these rates are dependent on many parameters. However, it should be noted that mixes that did not experience cracking had coarse aggregate contents of 1800 lbs/cu.yd or more. Also, mixes containing 1700 lbs/cu.yd coarse aggregate in their design all experienced cracking.

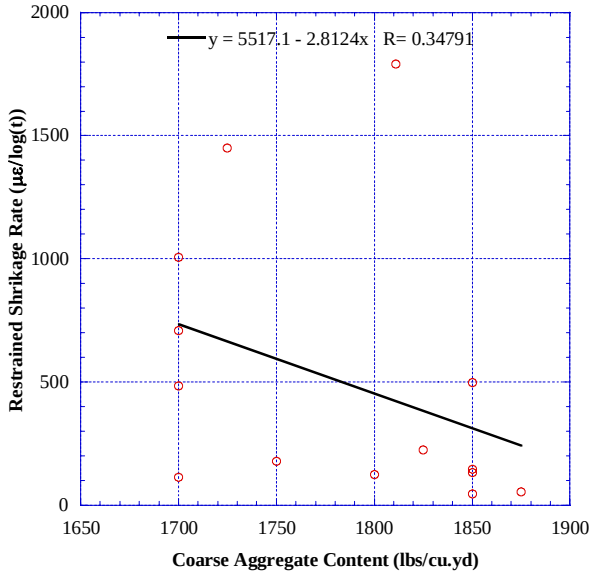

Figure 58. Coarse Aggregate Content vs. Restrained Shrinkage Rate for All Mixes

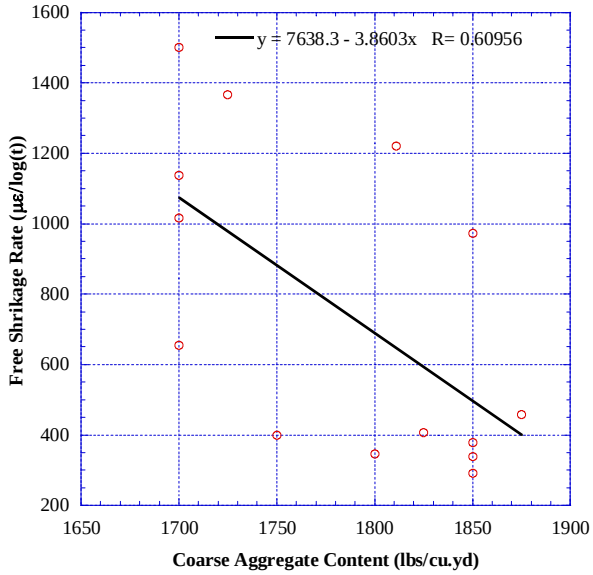

Figure 59. Coarse Aggregate Content vs. Free Shrinkage Rate for All Mixes

It can be seen in Figure 58 that majority of the mixes that have low restrained shrinkage rates have coarse aggregate contents of 1850lbs/cu.yd or more**.**

Correlation of Cracking Potential with Cementitious Content

When all mixes were used to study the relationship between cracking potential and cementitious content no clear relationship was found. This is most probably due to the small range of this variable. Except one mix (G1M1) all mixes have very similar cementitious contents (650 – 735 lbs/cu.yd). Concrete mixes with high cement contents are expected to experience higher shrinkage, and this was observed in mix G1M1 which cracked earliest among all mixes. For the remaining mixes shrinkage rate is affected by a combination of cement content, CA/FA ratio, w/c ratio, coarse aggregate content, and mechanical properties of concrete such as modulus of elasticity, and strength. This dependency is clear when shrinkage rates of mixes with 658 lbs/cu.yd cement content are analyzed. Although all of the mixes have the same cement content, the shrinkage rates vary tremendously.

Correlation of Cracking Potential with Pozzolanic Materials

The percentage of cementitious materials used and their proportions also affects the performance of the mixes. Figure 60 through Figure 63 illustrates the comparison of two very similar mixes with only difference being the silica fume percentage.

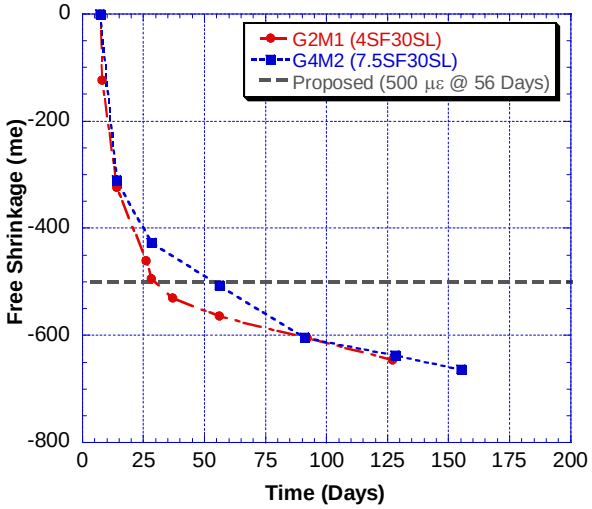

Figure 60. Free Shrinkage Comparison of G2M1 and G4M2

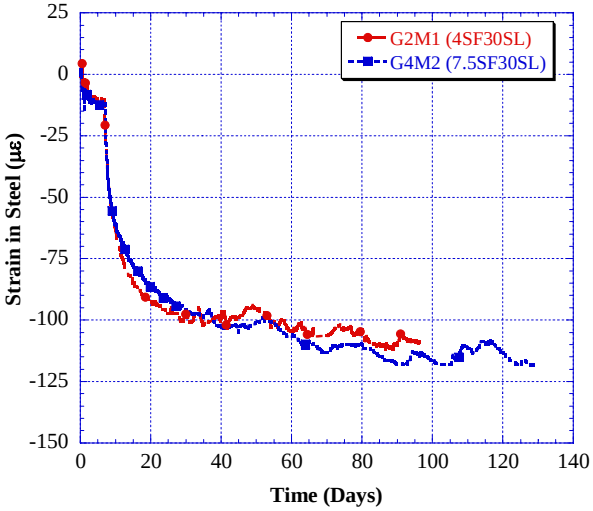

Figure 61. Steel Strain Comparison of G2M1 and G4M2

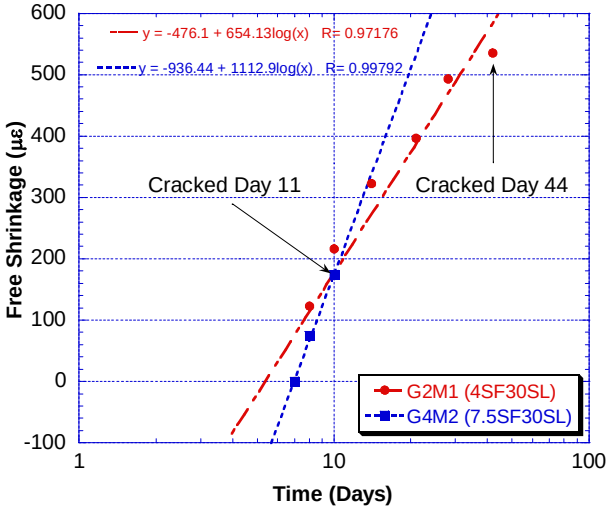

Figure 62. Comparison of Free Shrinkage Rate for G2M1 and G4M2

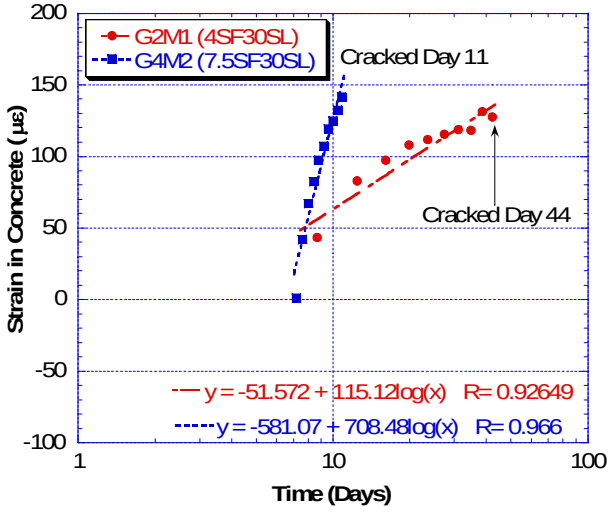

Figure 63. Comparison of Restrained Shrinkage Rate for G2M1 and G4M2

G4M2 has 7.5% silica fume where as G2M1 has only 4% silica fume. As expected compressive strength, tensile splitting strength and elastic modulus values of the mix with higher silica fume is slightly higher compared to the other mix. Free shrinkage is same for both mixes at day 128. The strain in steel rings for both mixes is similar. However, strain observed in the concrete is much higher for G4M2 which has higher

amounts of silica fume in its composition. The rate at which shrinkage takes place also is higher for this mix. Cracks for mix G4M2 was observed 5 days after drying was initiated. G2M1 on the other hand did not produce any visible cracks until around day 50.

Correlation of Cracking Potential with Mechanical Properties

Correlation of free shrinkage with restrained shrinkage was done in detail in the previous section. The two other mechanical properties of concrete that is important in terms of affecting the cracking age is the tensile strength and elastic modulus. Higher tensile strength would provide more resistance to cracking by allowing concrete to sustain more loads before cracking. Modulus of elasticity on the other hand can increase or decrease the cracking strain of a mix depending on its magnitude. The higher the elastic modulus the lower the cracking strain limit will be, and the sooner this limit will be reached by a given strain rate. When the relationship between tensile strength and elastic modulus was investigated for the mixes considered in this study, it was seen that the rate of increase in tensile strength was identical to rate of increase in elastic modulus. This provided more or less very similar cracking strains for all of the mixes. Therefore, the governing factor in cracking under restrained shrinkage was the rate at which these different mixes were shrinking. This is supported by Figure 64 and Figure 65 where the relationship of modulus of elasticity and tensile strength with restrained shrinkage rate is shown to be identical.

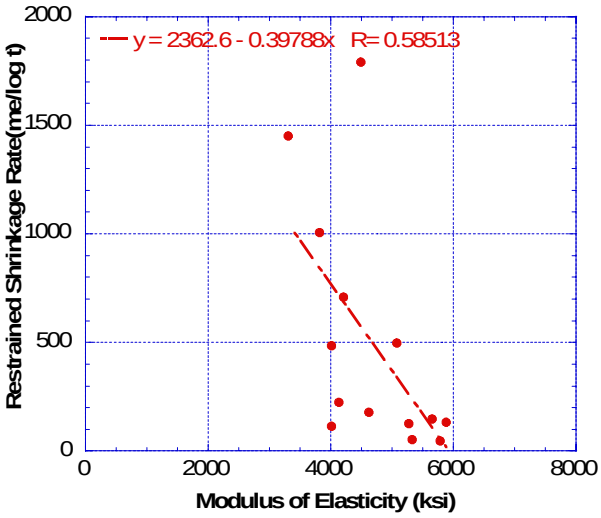

Figure 64. Restrained Shrinkage Rate versus Modulus of Elasticity

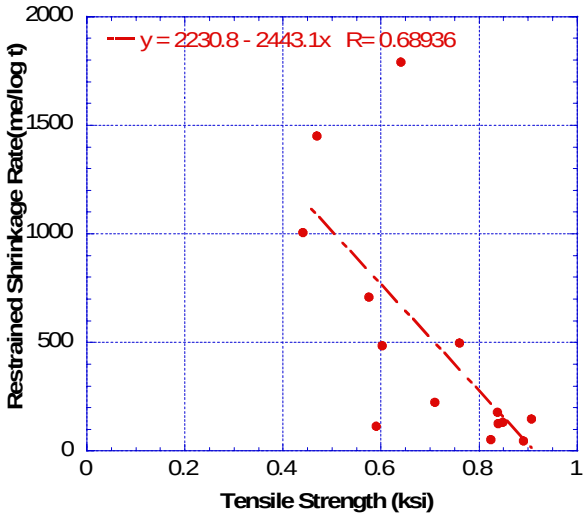

Figure 65. Restrained Shrinkage Rate versus Tensile Strength

The relationship of these mechanical properties with the free shrinkage rate was also investigated. As shown in Figure 66 and Figure 67, this relationship is stronger for free shrinkage rate.

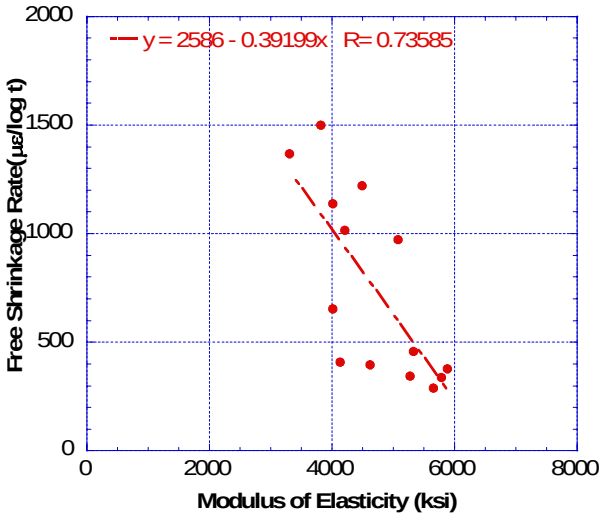

Figure 66. Free Shrinkage Rate versus Modulus of Elasticity

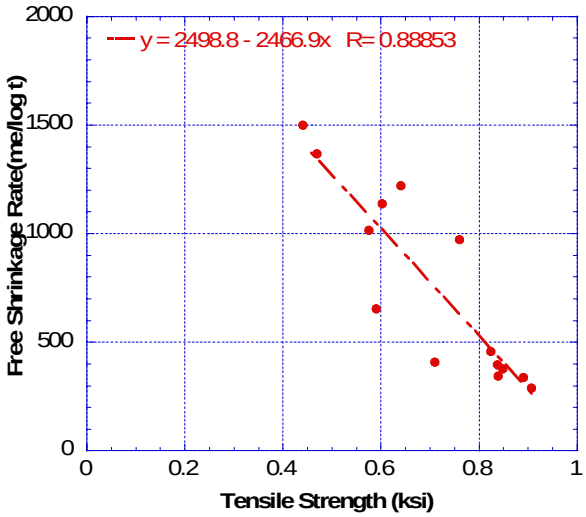

Figure 67. Free Shrinkage Rate versus Tensile Strength

Evaluation and Ranking of Mixes Based on Measured Concrete Strains

The results of the restrained shrinkage test can be used to comparatively rank mixes in terms of restrained shrinkage performance. However, it should be noted that the ranking presented does not mean that the first and best mix in the list would not crack in field applications. Cracking in a real world applications depend on many factors like construction practices, the level of restraint in the structure, loads and etc. The list presented only compares the relative performance of the mixes in this study.

Table 30 - Comparison of Restrained Shrinkage Performance

			% of Cracking Strength			Cracking Day		
Mix Rank	**Mix Name**	**Designation**	**Ring 1**	**Ring 2**	**Average**	**Ring 1**	**Ring 2**	**Average**
1	R200578S	G1M3	37%	NA	37%	NC	NC	NC
2	R309497	G2M3	58%	30%	44%	NC	NC	NC
3	R200633S	G2M6	67%	58%	63%	NC	NC	NC
4	R308278	G3M2	83%	68%	76%	NC	NC	NC
5	R309496	G4M3	86%	NA	86%	NC	NC	NC
6	R309495	G4M1	94%	NA	94%	NC	NC	NC
7	R408694	G4M4	100%	100%	100%	60	65	62.5
8	R200626S	G2M5	100%	100%	100%	43	53	48
9	R408850	G2M1	100%	100%	100%	44	47	45.5
10	R310682	G2M4	100%	100%	100%	16	20	18
11	R408847	G1M2	100%	100%	100%	13	13	13
12	R408844	G4M2	100%	100%	100%	11	13	12
13	R409239	G2M2	100%	100%	100%	9	10	9.5
14	R308163	G3M1	100%	100%	100%	9	10	9.5
15	R311266	G1M1	100%	100%	100%	8	10	9
16		G1M4*	NA					

Unable to re-produce this mix with proportions as provided.

CONCLUSIONS AND RECOMMENDATIONS

The modified AASHTO T34 restrained shrinkage test was used successfully to determine the relative performance of the given 16 high performance concrete (HPC) mixes used by NJDOT. A ranking was given to each mix based on cracking day after casting.

The results show that total coarse aggregate content and the CA/FA ratio has the greatest effect on both free and restrained shrinkage. There was a significant reduction in free shrinkage of mixes with high CA/FA ratios and coarse aggregate contents compared to similar mixes with lower ratios and lower total coarse aggregate content. The five mixes that did not exhibit any cracking in the restrained shrinkage test all had coarse aggregate contents of 1850 lbs/cu.yd or more and their CA/FA ratio was equal to or higher than 1.48. Moreover, seven out of eight mixes which cracked under restrained shrinkage had a CA/FA ratio of less than 1.48 and six of these mixes were observed to have low coarse aggregate content (less than 1725 lbs/cu.yd).

Free shrinkage rate prior to cracking was found to correlate directly with the restrained shrinkage rate prior to cracking and time to cracking for a given mix. There was also a relationship between free shrinkage rate and ultimate amount of free shrinkage observed in a mix at the end of testing period. Mixes which had lower ultimate shrinkage values experienced lower shrinkage rates overall. All five mixes that did not experience cracking were observed to have less than 400 microstrains of free shrinkage at 56 days. The two mixes that experienced cracking after 28 days were observed to have a free shrinkage value in between 400 and 500 microstrains at 56 days. Five out of the six remaining mixes, which experienced cracking before 28 days, had more than 500 microstrains of free shrinkage at 56 days.

Other factors that were found to increase cracking potential were high cementitious material contents (two mixes with the highest cementitious content were observed to crack earliest), and the properties of the coarse aggregate used in mix design (Mix G3M1 has deposits of argillites within its coarse aggregate source which significantly affected its performance).

As observed in this study, to reduce the potential of restrained shrinkage cracking of an HPC mix, the coarse aggregate content should be increased (preferably higher than 1800 lbs/cu.yd) to give a high CA/FA ratio (minimum of 1.48). This would help in reducing the ultimate shrinkage and also would reduce the rate at which shrinkage takes place. Mixes that experience more than 450 microstrains free shrinkage at 56 days are not recommended, since such mixes cracked under restrained ring test shortly after initiation of drying. Moreover, it is recommended that the amount of cementitious material be limited to 700 lb/cu yd. Also, maximum percentage of silica fume utilized in a mix should be limited to 5 percent.

BIBLIOGRAPHY

1. Ozyildirim, C., “HPC Bridge Decks in Virginia,” *Concrete International*, February 1999, pp. 59-60.
2. Waszczuk, C., and Juliano, M., “Application of HPC in a New Hampshire Bridge,” *Concrete International*, February 1999, pp. 61-62.
3. Ralls, M.L., “Texas HPC Bridge Decks,” *Concrete International*, February 1999, pp. 63-65.
4. Beacham, M., “HPC Bridge Deck in Nebraska,” *Concrete International*, February 1999, pp. 66-68.
5. Streeter, D. A., “Developing High-Performance Concrete Mix for New York State Bridge Decks,” *Transportation Research Record, Journal of the Transportation Research Board,* No. 1532, TRB, National Research Council, Washington, D.C., 1996. pp. 60-65.
6. Nassif, H. H., and Suksawang, N., “Development of High-Performance Concrete for Transportation Structures in New Jersey,” FHWA NJ 2003-06, Final Report Submitted to NJDOT Research Bureau, August 2003, p. 123.
7. Kanstad, T., Bjøntegaard, Ø., Sellevold, E. J., Hammer, T. A., and Fidjestøl, P. “Effect of Silica Fume on early age crack sensitivity of High Performance Concrete,” Proceedings of the International RILEM Workshop, Paris, France, October 2000.
8. Tazawa, E., and Miyazawa, S., “Influence of Cement and Admixture on Autogenous Shrinkage of Cement Paste,” *Cement and Concrete Research*, Vol. 25, No. 2, 1995, pp. 281-287.
9. Igarashi, S., Bentur, A., Kovler, K., “Autogenous Shrinkage and Induced Restraining Stress in High-Strength Concretes,” *Cement and Concrete Research*, Vol. 30, No. 11, 2001, pp. 1701-1707.
10. Nassif, H. H., Suksawang, N., Mohammed, M., “Effect of Curing Methods on Early-Age and Drying Shrinkage of High-Performance Concrete,” *Transportation Research Record: Journal of the Transportation Research Board*, No. 1834, TRB, National Research Council, Washington, D.C., 2003, pp. 48-58.
11. Li, Z., Qi, M., Li, Z., and Ma, B., “Crack Width of High-Performance Concrete Due to Restrained Shrinkage,” *Journal of Materials in Civil Engineering,* Vol. 11, No. 3, August, 1999, pp. 214-233.
12. Weiss, J. W., Yang, W., and Shah, S. P., “Shrinkage Cracking of Restrained Concrete Slabs,” *Journal of Engineering Mechanics*, Vol. 124, No. 7, July. 1998, pp. 765-774.
13. Grzybowski, M., and Shah, S. P., “Model to Predict Cracking in Fiber Reinforced Concrete due to Restrained Shrinkage,” *Magazine of Concrete Research,* Vol. 41, No. 148, September, 1989, pp. 125-135.
14. Kraai, P.P., “A Proposed Test to Determine the Cracking Potential due to Drying Shrinkage of Concrete,” *Concrete Construction*, Vol. 30, September 1985, pp. 775-778.
15. Wiegrink, K., Marikunte, S., Shah, S. P., “Shrinkage Cracking of High Strength Concrete,” *ACI Material Journal*, Vol. 93, No. 5, Sep.-Oct., 1996, pp. 409-415.

16. Mokarem, D.W., Weyers, R.E., and Lane, S. "Development of Performance Specification for Shrinkage of Portland Cement Concrete," *Transportation Research Record: Journal of the Transportation Research Board*, No. 1834, TRB, National Research Council, Washington, D.C., 2003, pp. 40-47.
17. Hossain, A. B., and Weiss, J., "Assessing Residual Stress Development and Stress Relaxation in Restrained Concrete ring Specimens," *Cement and Concrete Composite*, Vol. 26, No. 5, July, 2004, pp. 531-540.
18. Hossain, A. B., Pease, B., Weiss, J., "Quantifying Early-Age Stress Development and Cracking in Low Water-to-Cement Concrete," *Transportation Research Record: Journal of the Transportation Research Board*, No. 1834, TRB, National Research Council, Washington, D.C., 2003, pp. 24-32.
19. Collins, F., and Sanjayan, J. G., "Cracking Tendency of Alkali Activated Slag Concrete Subjected to Restrained Shrinkage," *Cement and Concrete Research*, Vol. 30, 2000, pp. 791-798.
20. Suksawang, N., Nassif, H.H., Mohammed, A. "Properties of Latex-Modified Concrete under Different Curing Conditions," *Transportation Research Board, Proceedings of the 84th Annual Meetings*, Washington, D.C., 2005, January 9-13 (on CD).
21. Czarnecki, B. and Kroman, J., "Evaluation of Cracking Tendency and Unrestrained Shrinkage of High-Performance Concrete Mixes in Cast-in-Place and Precast Bridge Applications," *ACI Seventh International Symposium on Utilization of High Strength/High Performance Concrete*, ACI, SP-228, Vol. 2, Farmington Hills, M.I., pp. 1315-1328.
22. Attiogbe, E.K., See, H.T., and Miltenberger, M.A., "Cracking Potential of Concrete Under Restrained Shrinkage", *Proceedings, Advances in Cement and Concrete: Volume Changes, Cracking, and Durability,* Engineering Conferences International, Copper Mountain, CO, 10-14 August 2003, pp. 191-200
23. Krauss P., E. A. Rogalla, "Transverse Cracking in Newly Constructed Bridge Decks", NCHRP Report 380, 1996
24. Chariton, T. and Weiss, W. J., "Using Acoustic Emission to Monitor Damage Development in Mortars Restrained from Volumetric Changes", Concrete: Material Science to Application, A Tribute to Surendra P. Shah, ACI SP-206, 2002, pp. 205-218.
25. Paillere, A. M., Buil, M., Serrano, J. J., "Effect of Fibre Addition on the Autogenous Shrinkage of Silica Fume Concrete", ACI Materials Journal, Vol. 86 No. 2, March-April 1989, pp. 139-144
26. McDonald, J.E., "The Potential for Cracking of Silica-Fume Concrete.", Concrete Construction, 1992
27. Gebler, S. H., Klieger, P., "Effect of Fly Ash on Physical Properties of Concrete," ACI, SP-91, 1986, pp. 1 – 50.
28. Nasser, K. W., and Al-Manaseer, A. A., "Shrinkage and Creep of Concrete Containing 50 Percent Lignite Fly Ash at Different Stress-Strength Ratios," ACI, SP-91, 1986, pp. 433 – 448.
29. Mladenka Saric-Coric, Pierre-Claude Aitcin, "Influence of Curing Conditions on Shrinkage of Blended Cements Containing Various Amounts of Slag", ACI Materials Journal, Vol. 100, December-2003, pp. 477-483

30. Frank Collins, J.G. Sanjayan, “Cement and Concrete Research”, Vol. 30, 2000, pp. 791-798
31. Bisonnette B., J. Marchand, C. Martel, M. Pigeon, “Influence of Superplasticizer on the Volume Stability of Hydrating Cement Pastes at an Early Age”, Concrete: Material Science to Application, A Tribute to Surendra P. Shah, ACI SP-206, 2002, pp. 167-176
32. Neville, A. M., Properties of Concrete, Fourth Edition, 1996
33. Whiting, D., and Diezdzic, W., “Effects of Conventional and High-Range Water Reducers on Concrete Properties”, Research and Development Bulletin RD107, Portland Cement Association, 1992
34. R. W. Carlson, T. J. Reading, “Model Study of Shrinkage cracking in Concrete Building Walls”, ACI Structural Journal, Vol. 85. July-August 1988, pp. 395 – 404
35. Grzybowski M., Surendra P. Shah, “Shrinkage Cracking of Fiber Reinforced Concrete”, ACI Materials Journal, Vol. 87 March-April 1990, pp. 138 – 148
36. Wiegrink K., Marikunte S, and Surendra P. Shah, “Shrinkage Cracking of High-Strength Concrete”, ACI Materials Journal, Vol. 93 September-October 1996, pp. 409-415
37. Heather T. See, Emmanuel K. Attiogbe, and Matthew A. Miltenberger, “Shrinkage Cracking Characteristics of Concrete Using Ring Specimens”, ACI Materials Journal, Vol. 100 May-June 2003, pp. 239-245
38. Akhter B. Hossain, Jason Weiss, “Assessing Residual Stress Development and Stress Relaxation in Restrained Concrete Ring Specimens”, Cement & Concrete Composites, Vol. 26 July 2004, pp. 531 – 540
39. W. J. Weiss and S.P. Shah, “Restrained Shrinkage Cracking: the Role of Shrinkage Reducing Admixtures and Specimen Geometry”, Materials and Structures, Vol. 35 March 2002, pp. 85-91
40. Heather T. See, Emmanuel K. Attiogbe, and Matthew A. Miltenberger, “Potential for Restrained Shrinkage Cracking of Concrete and Mortar”, Cement, Concrete, and Aggregates, Vol. 26 December 2004, No. 2, pp. 123 – 130
41. Akhter B. Hossain, Jason Weiss, “The role of specimen geometry and boundary conditions on stress development and cracking in the restrained ring test”, Cement and Concrete Research, Vol. 36 2006, No. 1, pp. 189 – 199
42. Jae Heum Moon, F. Rajabipour, and W. J. Weiss, “Incorporating Moisture Diffusion in the Analysis of the Restrained Ring Test”, Presented at CONSEC (Concrete Under Severe Conditions—Environment and Loading), Seoul Korea, 2004, pp. 1973–1980
43. Jae Heum Moon, Jason Weiss, “Estimating residual stress in the restrained ring test under circumferential drying”, Cement and Concrete Composites, Vol. 28 2006, pp. 486 – 496

APPENDIX A

PROPERTIES OF AGGREGATES

Bulk Specific Gravity of Fine Aggregates as Tested in Rutgers Civil Engineering Lab and NJDOT Laboratory

Source	Bulk Specific Gravity (Rutgers)	Bulk Specific Gravity (NJDOT)	Bulk Specific Gravity (SSD) (Rutgers)	Bulk Specific Gravity (SSD) (NJDOT)
Clayton Jackson	2.54	2.64	2.56	2.65
Dunrite	2.49	2.63	2.50	2.64
Sahara	2.57	2.61	2.58	2.62
Tuckahoe	2.57	2.63	2.60	2.64
County	2.66	2.66	2.69	2.68
Amboy	2.54	2.54	2.57	2.57
Pierson	2.49	2.60	2.51	2.62

Apparent Specific Gravity and Absorption of Fine Aggregates as Tested in Rutgers Civil Engineering Lab and NJDOT Laboratory

Source	Apparent Specific Gravity (Rutgers)	Apparent Specific Gravity (NJDOT)	Absorption (%) (Rutgers)	Absorption (%) (NJDOT)
Clayton Jackson	2.61	2.66	1.03	0.3
Dunrite	2.52	2.65	0.52	0.3
Sahara	2.61	2.65	0.54	0.6
Tuckahoe	2.66	2.66	1.21	0.4
County	2.73	2.72	1.01	0.8
Amboy	2.60	2.60	0.97	0.97
Pierson	2.54	2.65	0.72	0.7

Sieve Analysis of Fine Aggregates

Source	Fineness Modulus
Clayton Jackson	2.5
Dunrite	2.78
Sahara	2.54
Tuckahoe	2.94
County	NA
Amboy	2.61
Pierson	2.69

Comparison of Specific Gravity and Absorption of Coarse Aggregates as Tested in Rutgers Civil Engineering Lab and NJDOT Laboratory

Source	Bulk Specific Gravity (SSD) (Rutgers)	Absorption (Rutgers)	Bulk Specific Gravity (SSD) (NJDOT)	Absorption (NJDOT)
Trap Rock	2.88	0.82	2.90	0.7
Tilcon Millington	2.84	1.94	2.84	1.4
Tilcon Oxford	2.89	0.61	2.84	0.3
Better Materials	2.67	1.20	2.65	0.6
Independence Materials	2.81	0.23	2.81	0.4
Fanwood	2.89	1.40	2.86	1.1
Stavola	2.90	1.34	2.90	0.9
Plumstead	2.69	0.94	2.71	0.7

APPENDIX B

RESTRAINED SHRINKAGE TEST RESULTS

GROUP 1 MIXES

G1M1 – R311266

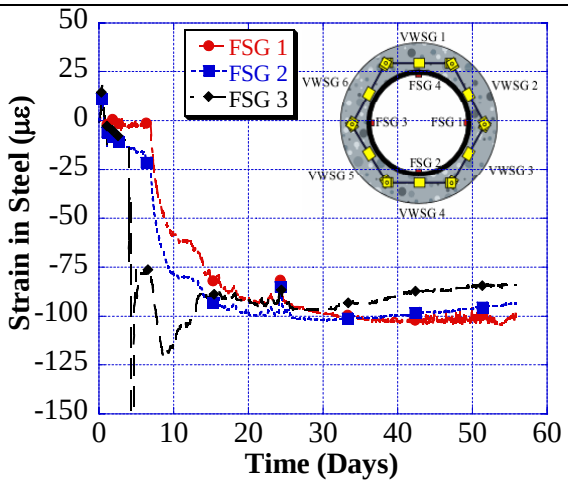

G1M1 – Specimen 1 – Steel Strains

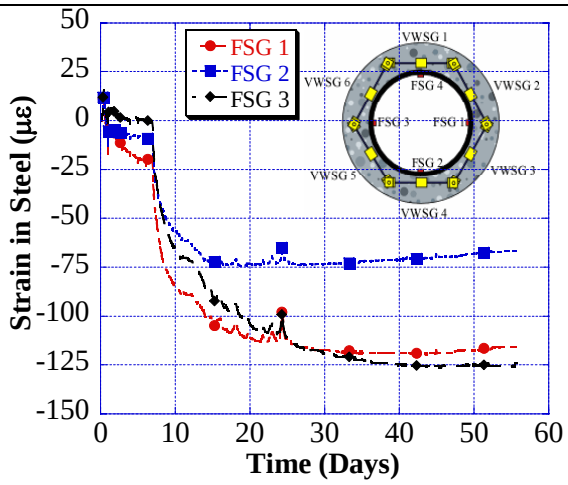

G1M1 – Specimen 2 – Steel Strains

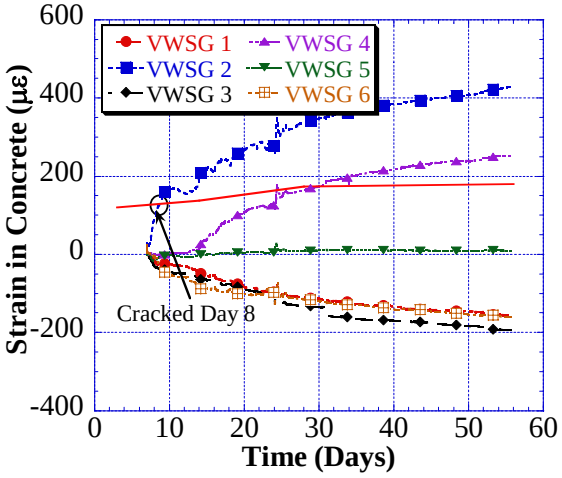

G1M1 – Specimen 1 – Concrete Strains

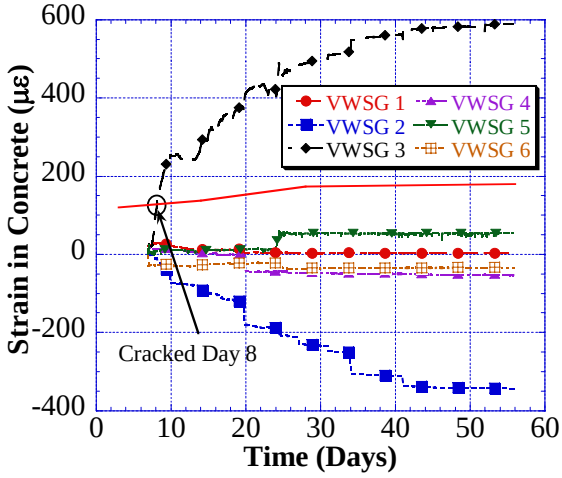

G1M1 – Specimen 2 – Concrete Strains

G1M2 – R408847

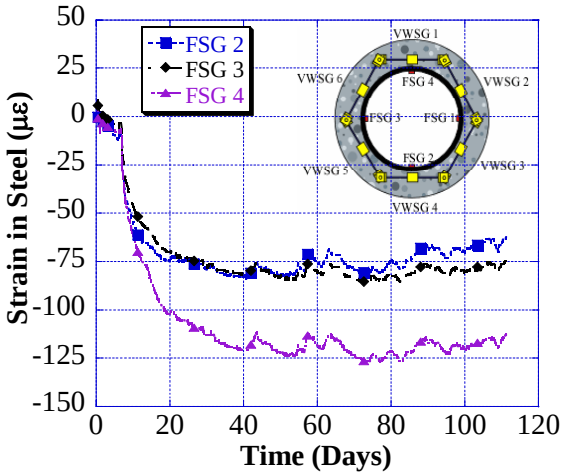

G1M2 – Specimen 1 – Steel Strains

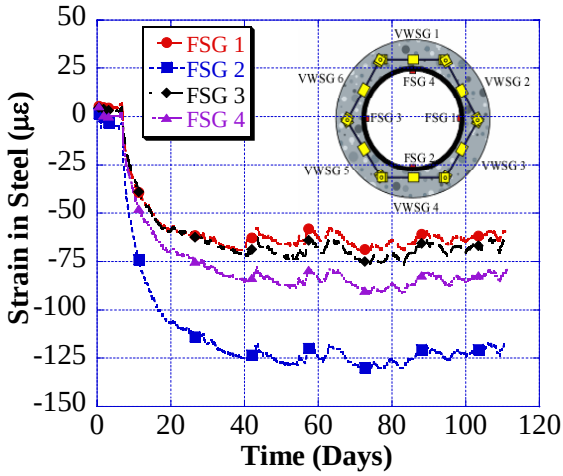

G1M2 – Specimen 2 – Steel Strains

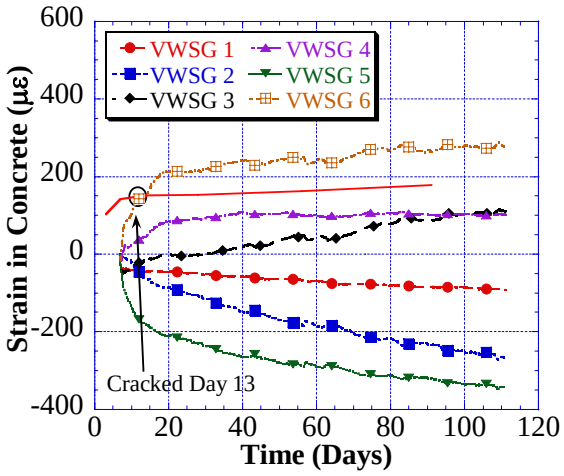

G1M2 – Specimen 1 – Concrete Strains

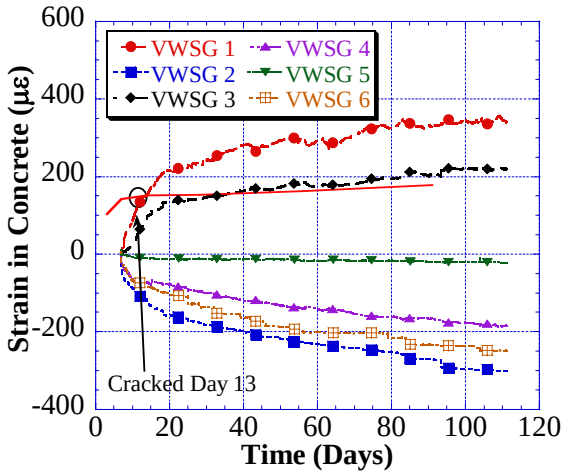

G1M2 – Specimen 2 – Concrete Strains

G1M3 – R200578S

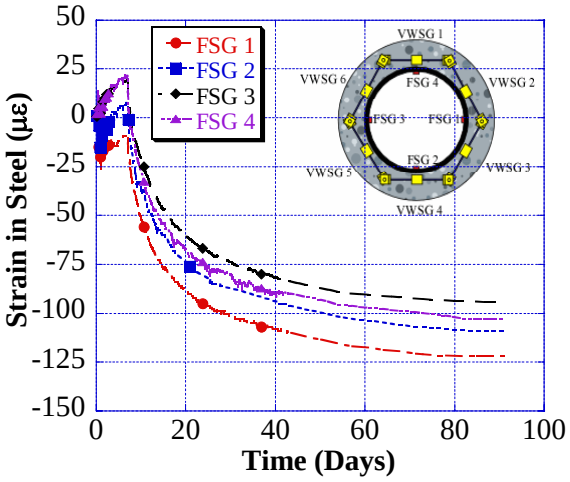

G1M3 – Specimen 1 – Steel Strains

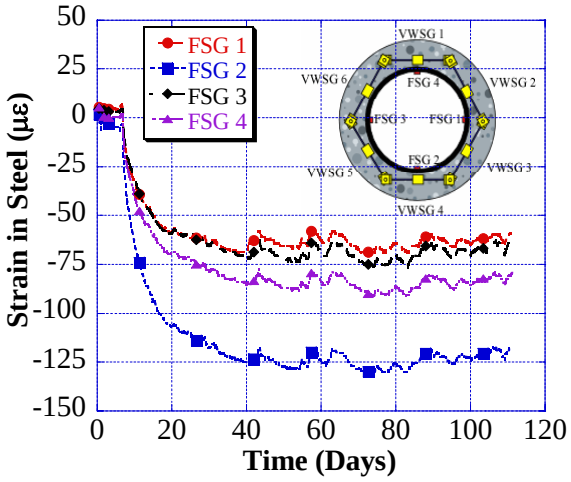

G1M3 – Specimen 2 – Steel Strains

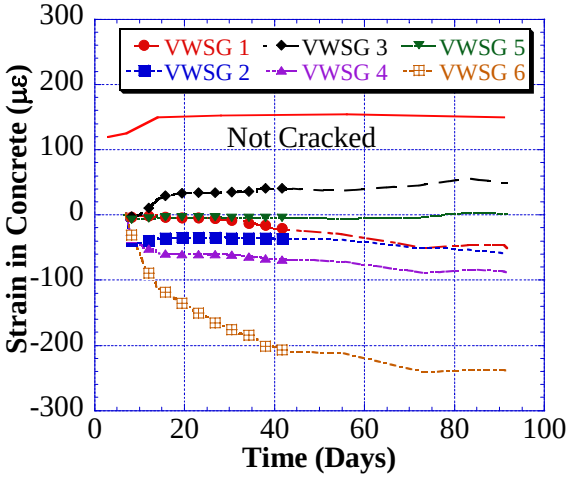

G1M3 – Specimen 1 – Concrete Strains

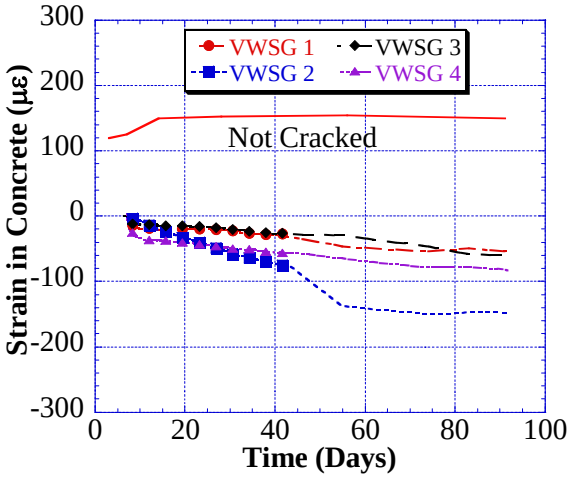

G1M3 – Specimen 2 – Concrete Strains

GROUP 2 MIXES

G2M1 – R408850

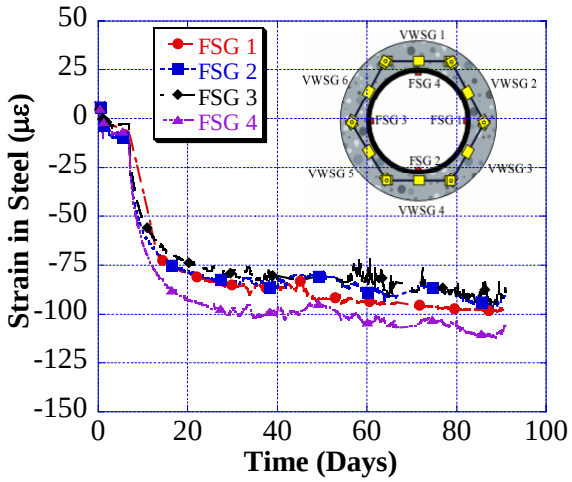

G2M1 – Specimen 1 – Steel Strains

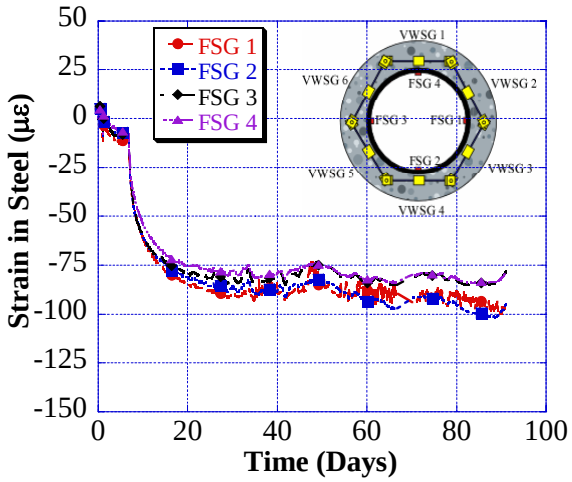

G2M1 – Specimen 2 – Steel Strains

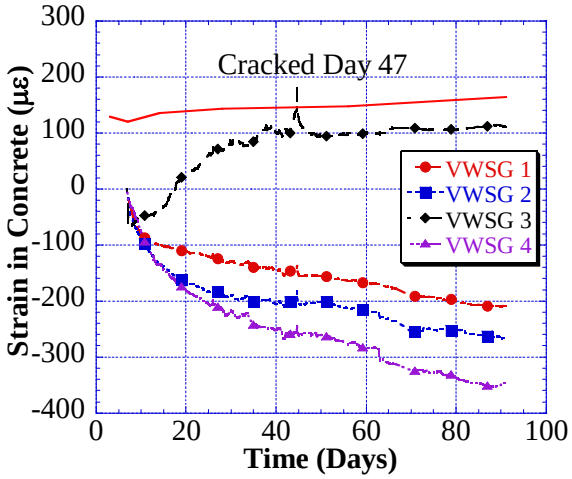

G2M1 – Specimen 1 – Concrete Strains

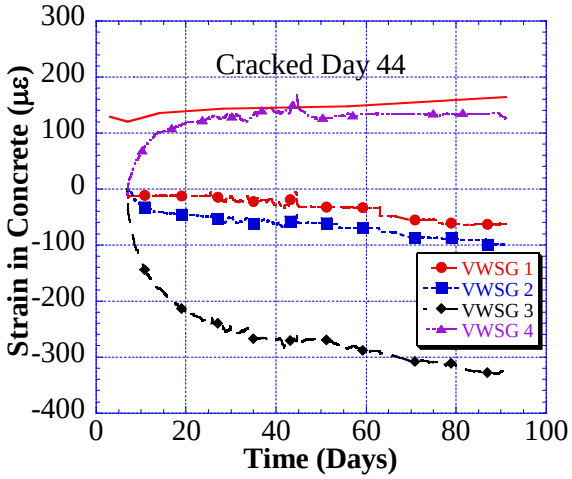

G2M1 – Specimen 2 – Concrete Strains

G2M2 – R409239

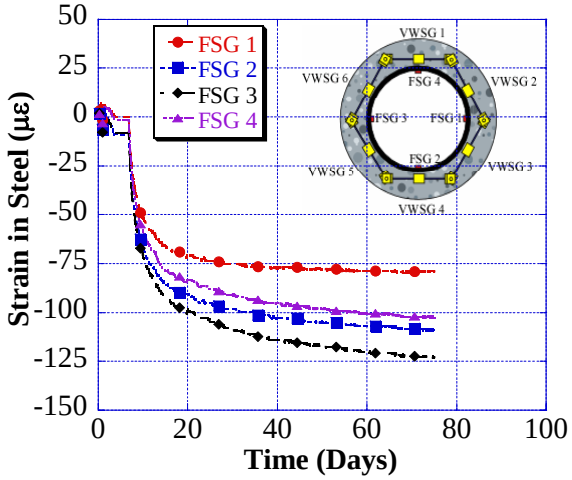

G2M2 – Specimen 1 – Steel Strains

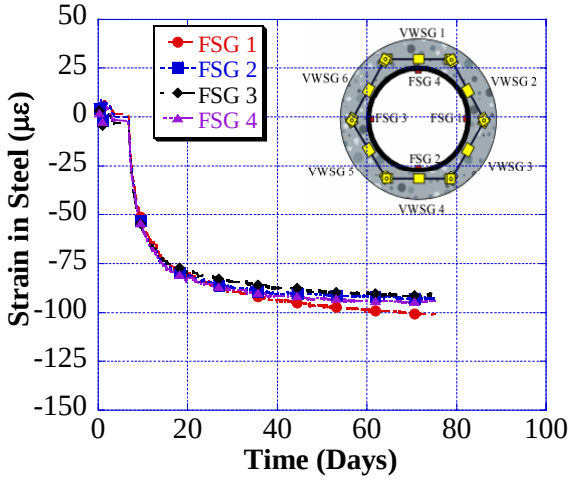

G2M2 – Specimen 2 – Steel Strains

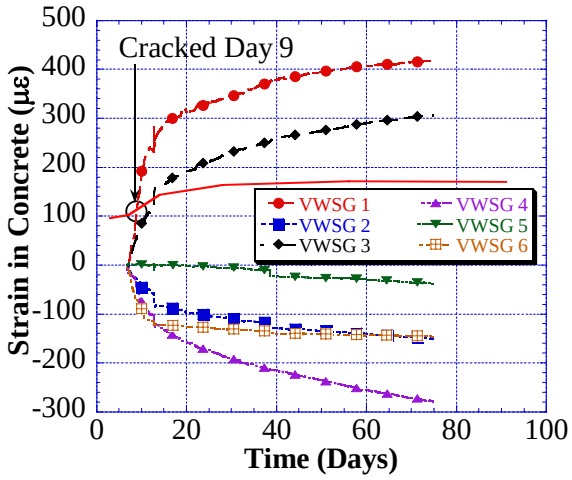

G2M2 – Specimen 1 – Concrete Strains

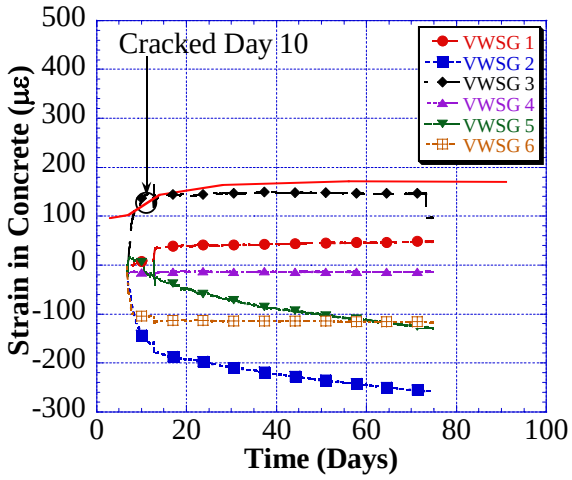

G2M2 – Specimen 2 – Concrete Strains

G2M3 – R309497

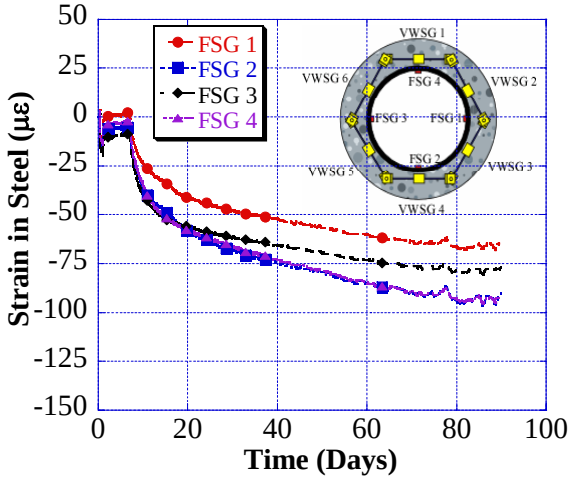

G2M3 – Specimen 1 – Steel Strains

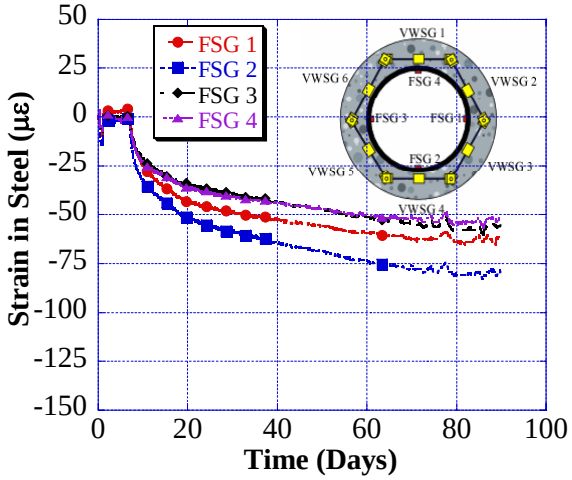

G2M3 – Specimen 2 – Steel Strains

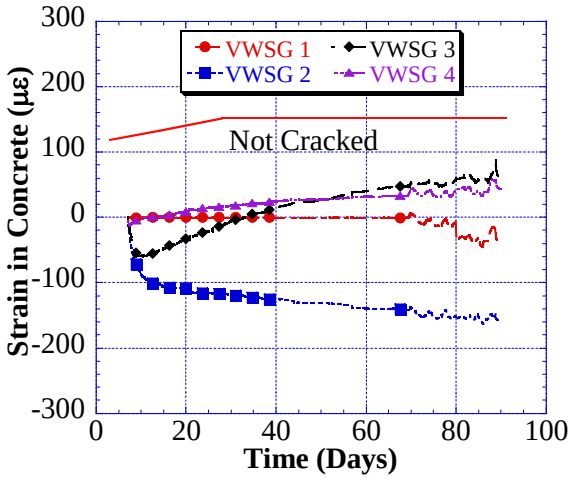

G2M3 – Specimen 1 – Concrete Strains

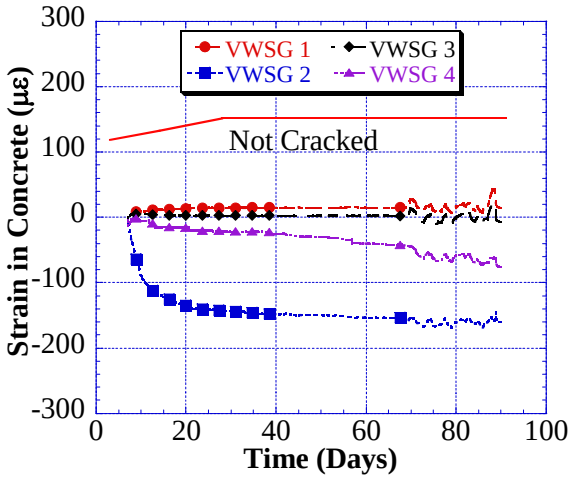

G2M3 – Specimen 2 – Concrete Strains

G2M4 – R310682

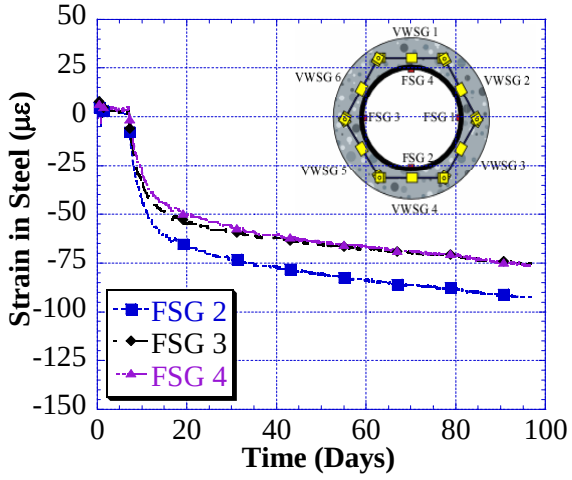

G2M4 – Specimen 1 – Steel Strains

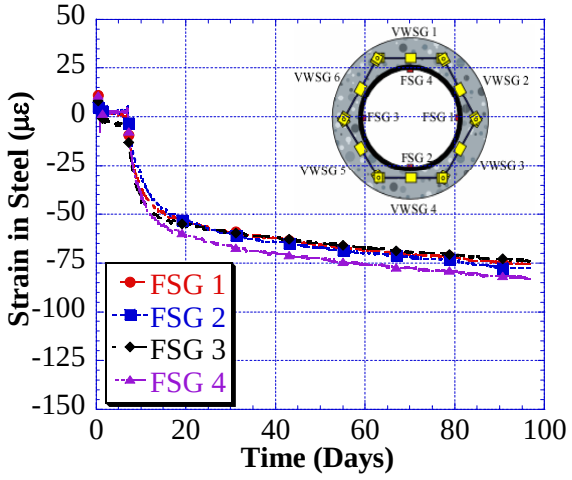

G2M4 – Specimen 2 – Steel Strains

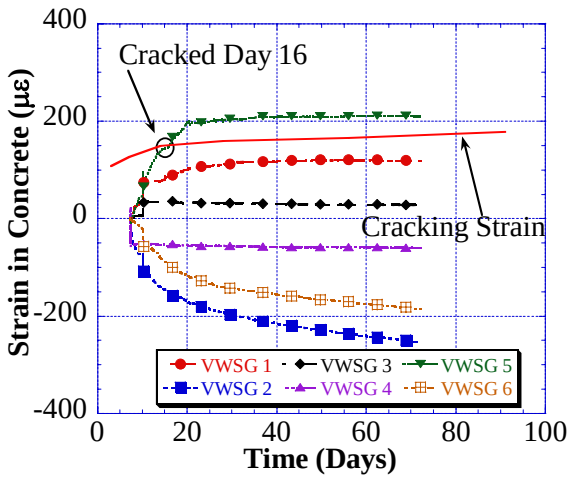

G2M4 – Specimen 1 – Concrete Strains

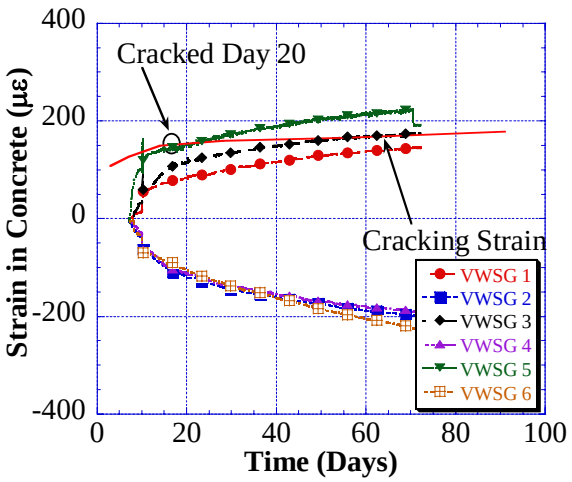

G2M4 – Specimen 2 – Concrete Strains

G2M5 – R200626S

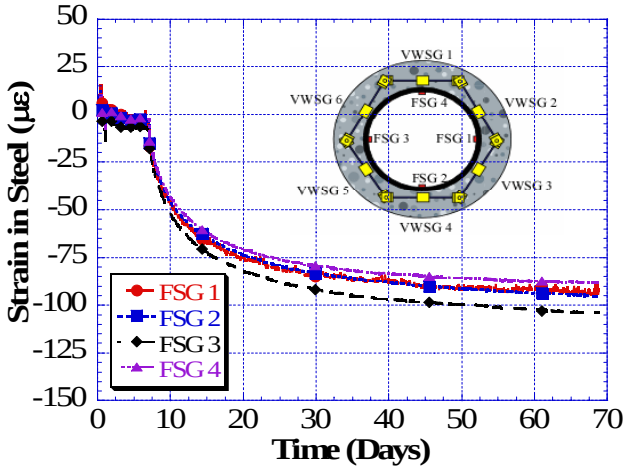

G2M5 – Specimen 1 – Steel Strains

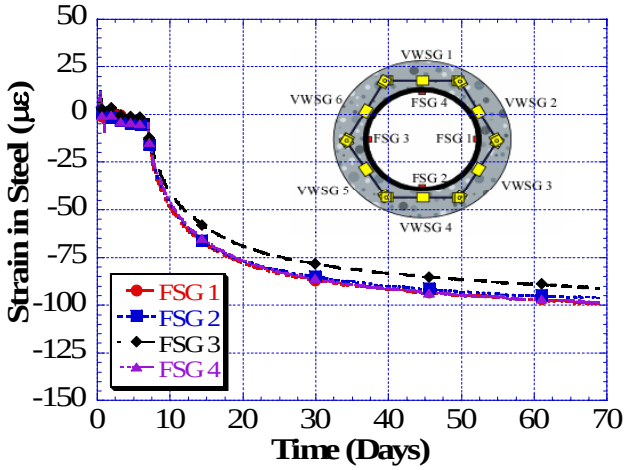

G2M5 – Specimen 2 – Steel Strains

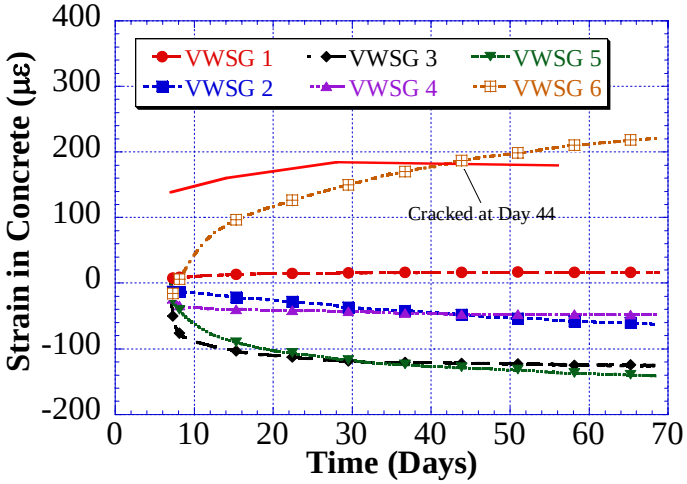

G2M5 – Specimen 1 – Concrete Strains

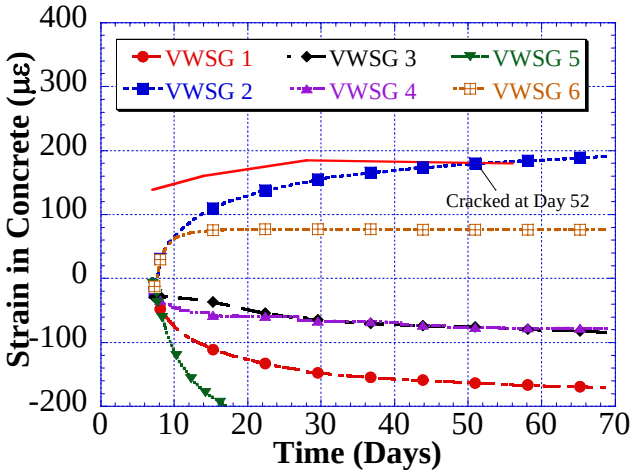

G2M5 – Specimen 2 – Concrete Strains

G2M6 – R200633S

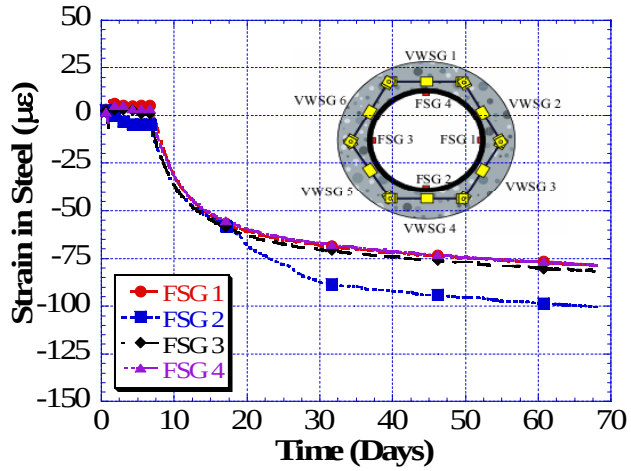

G2M6 – Specimen 1 – Steel Strains

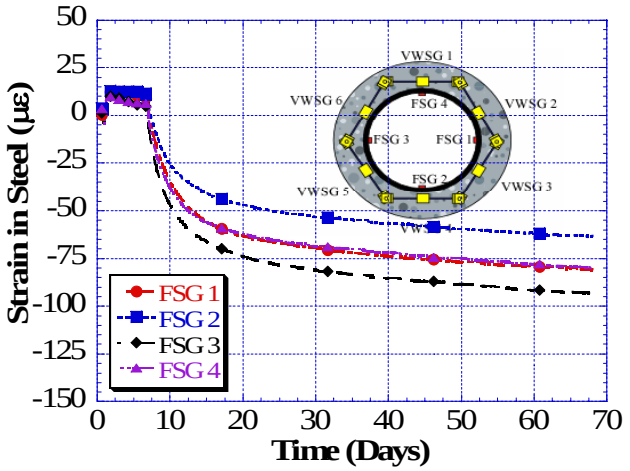

G2M6 – Specimen 2 – Steel Strains

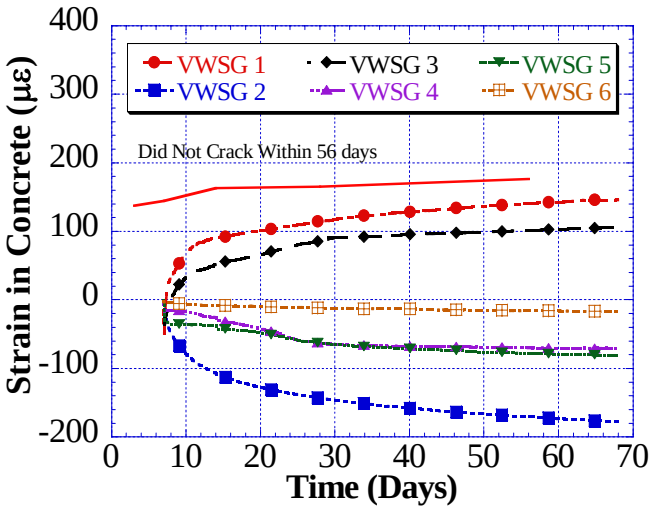

G2M6 – Specimen 1 – Concrete Strains

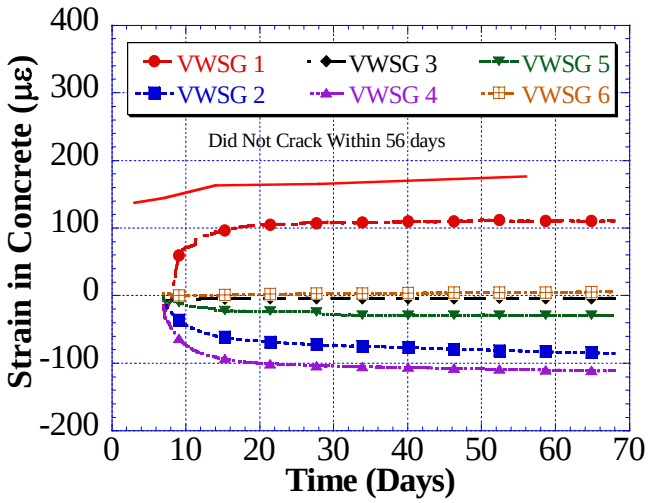

G2M6 – Specimen 2 – Concrete Strains

GROUP 3 MIXES

G3M1 – R308163

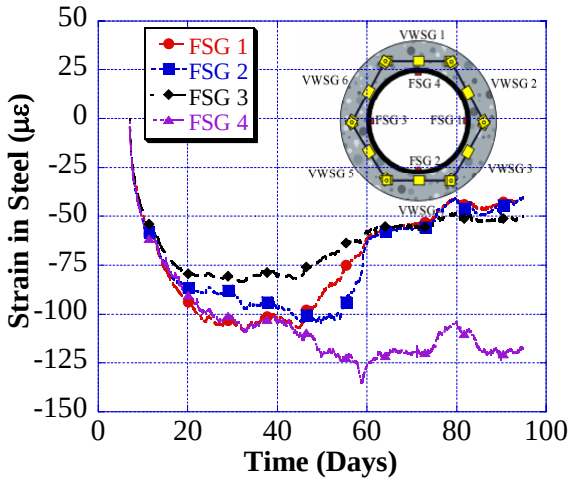

G3M1 – Specimen 1 – Steel Strains

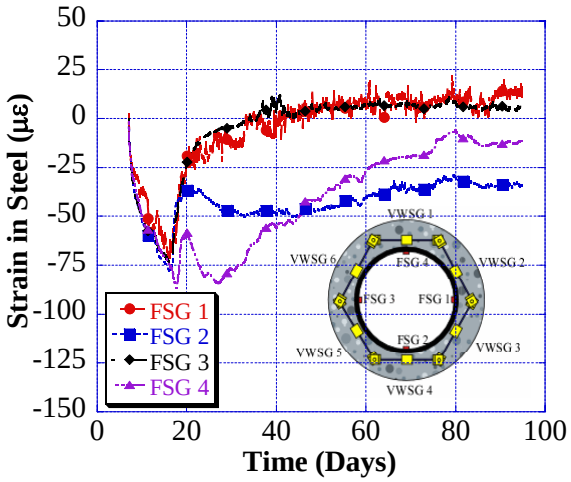

G3M1 – Specimen 2 – Steel Strains

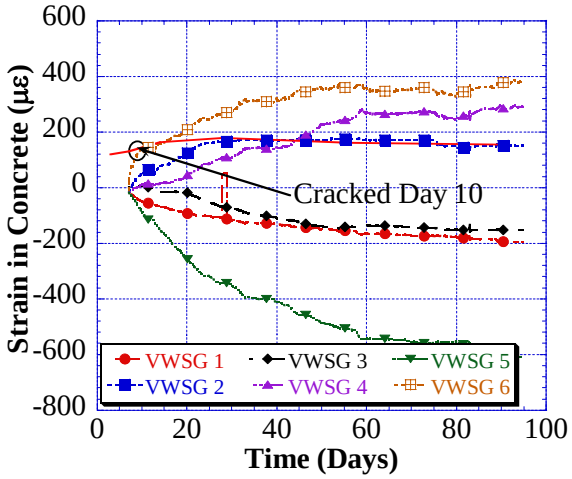

G3M1 – Specimen 1 – Concrete Strains

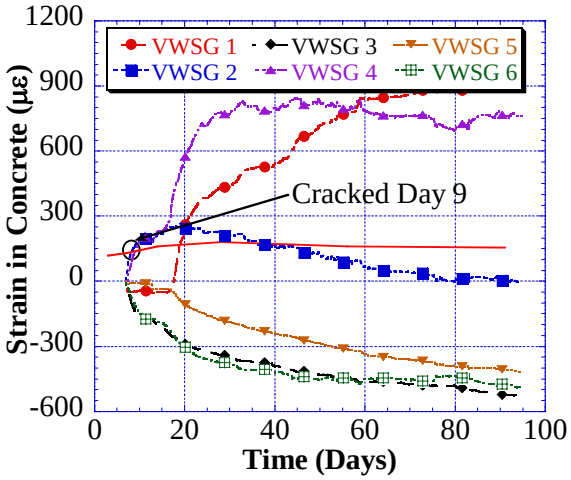

G3M1 – Specimen 2 – Concrete Strains

G3M2 – R308278

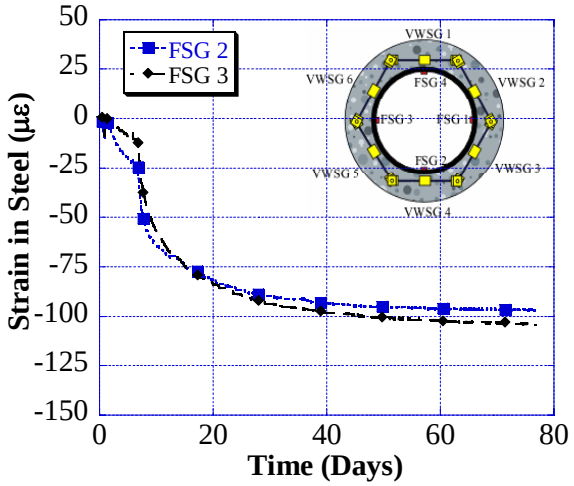

G3M2 – Specimen 1 – Steel Strains

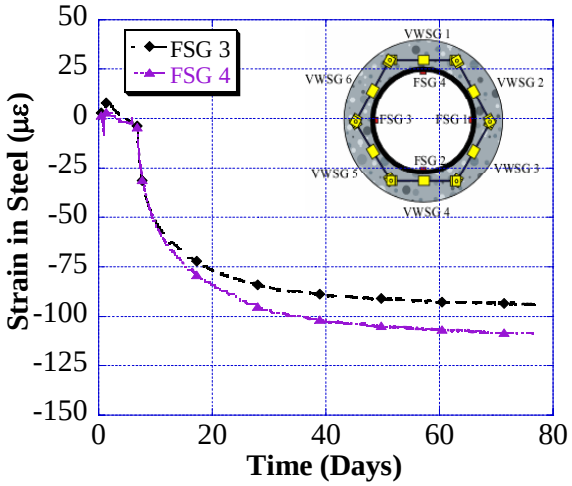

G3M2 – Specimen 2 – Steel Strains

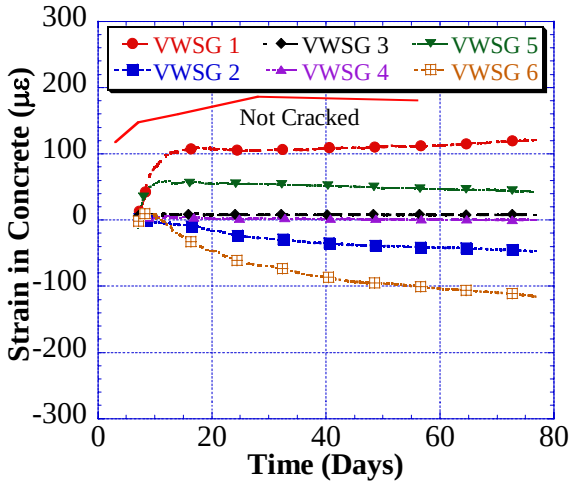

G3M2 – Specimen 1 – Concrete Strains

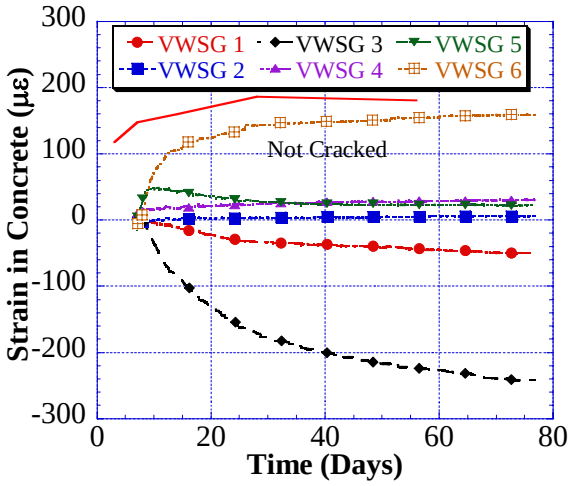

G3M2 – Specimen 2 – Concrete Strains

GROUP 4 MIXES

G4M1 – R309495

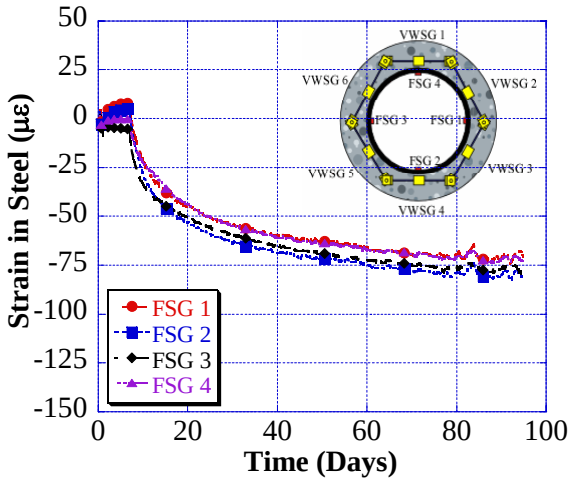

G4M1 – Specimen 1 – Steel Strains

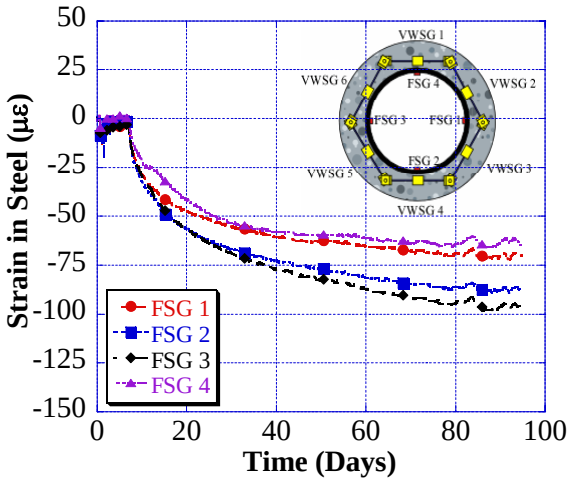

G4M1 – Specimen 2 – Steel Strains

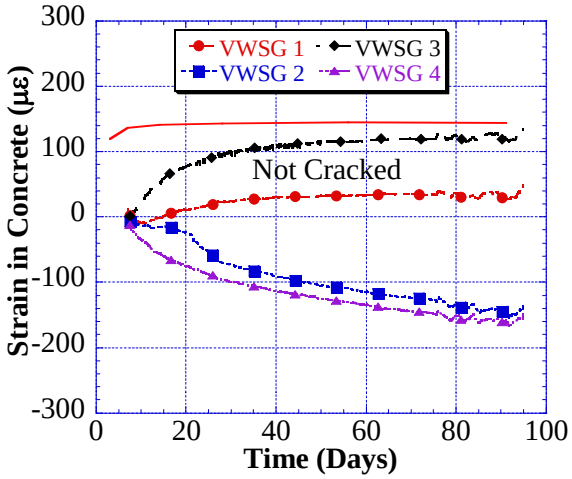

G4M1 – Specimen 1 – Concrete Strains

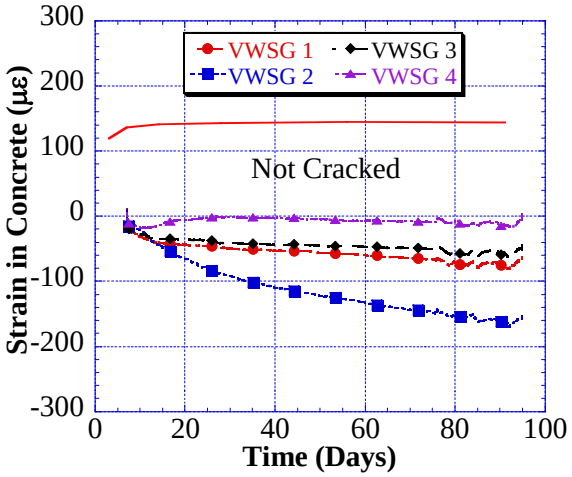

G4M1 – Specimen 2 – Concrete Strains

G4M2 – R408844

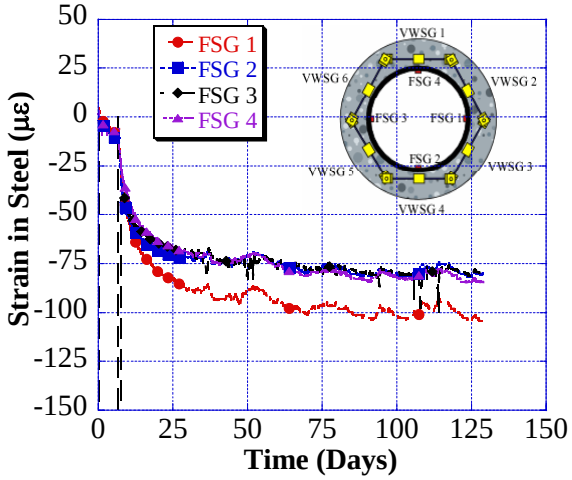

G4M2 – Specimen 1 – Steel Strains

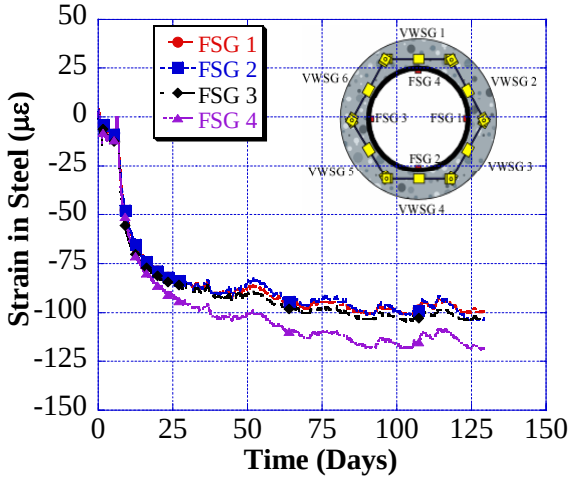

G4M2 – Specimen 2 – Steel Strains

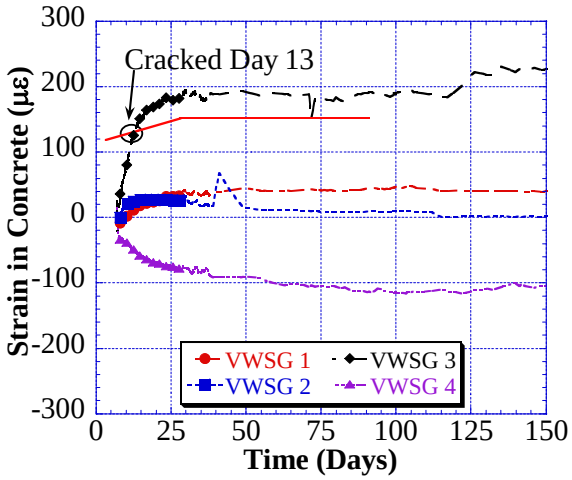

G4M2 – Specimen 1 – Concrete Strains

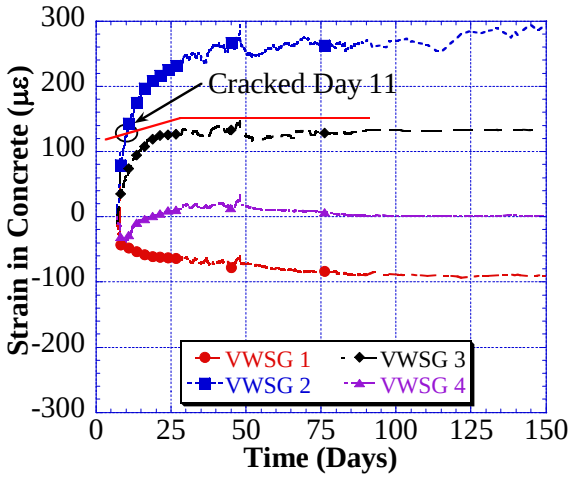

G4M2 – Specimen 2 – Concrete Strains

G4M3 – R309496

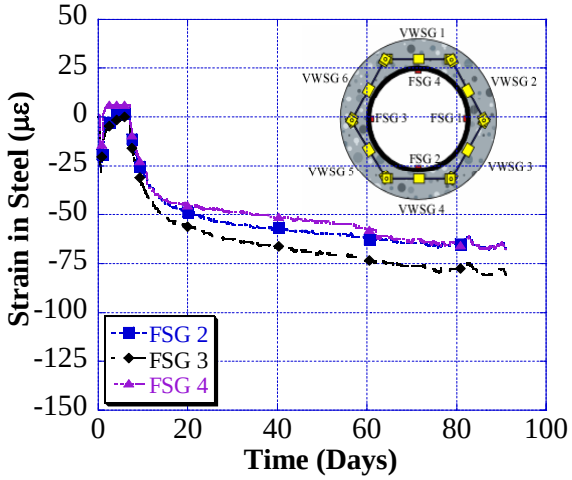

G4M3 – Specimen 1 – Steel Strains

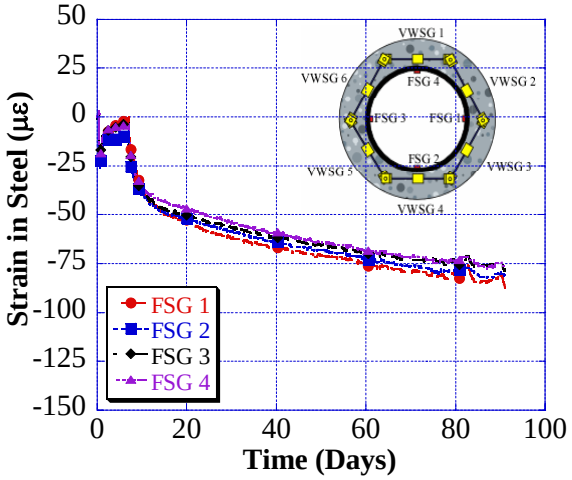

G4M3 – Specimen 2 – Steel Strains

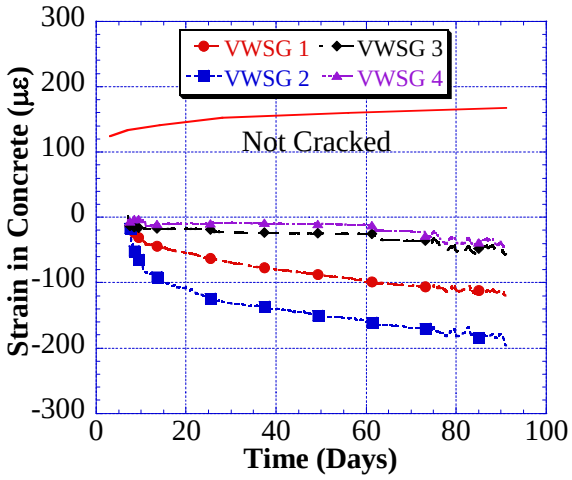

G4M3 – Specimen 1 – Concrete Strains

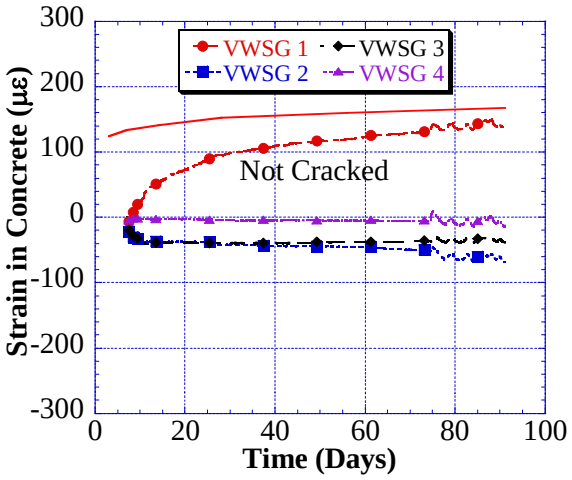

G4M3 – Specimen 2 – Concrete Strains

G4M4 – R408694

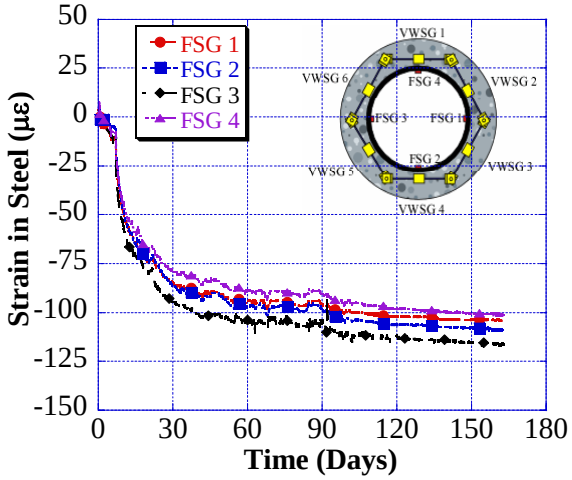

G4M4 – Specimen 1 – Steel Strains

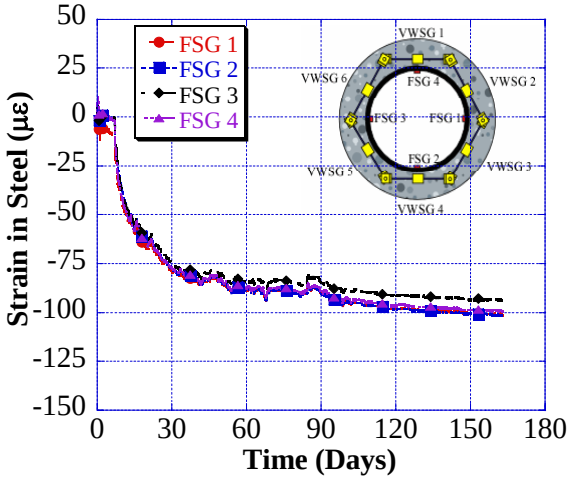

G4M4 – Specimen 2 – Steel Strains

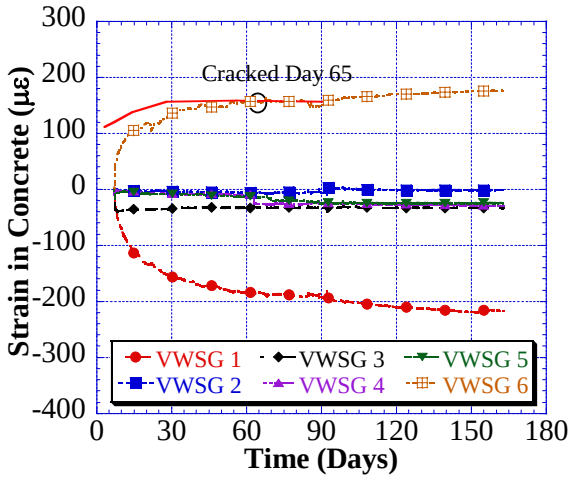

G4M4 – Specimen 1 – Concrete Strains

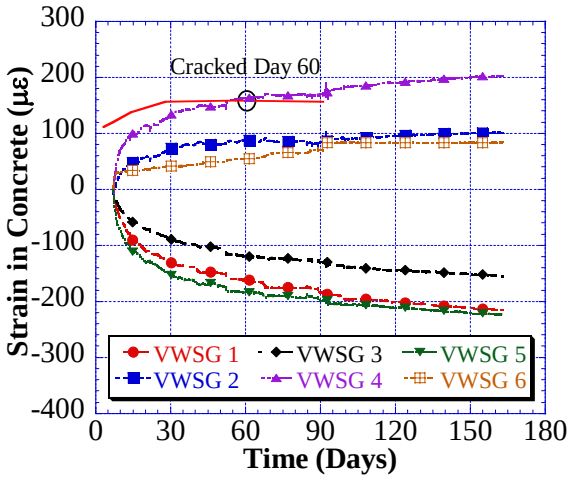

G4M4 – Specimen 2 – Concrete Strains

APPENDIX C

RING CRACK DRAWINGS

GROUP 1 MIXES

G1M1 – R311266

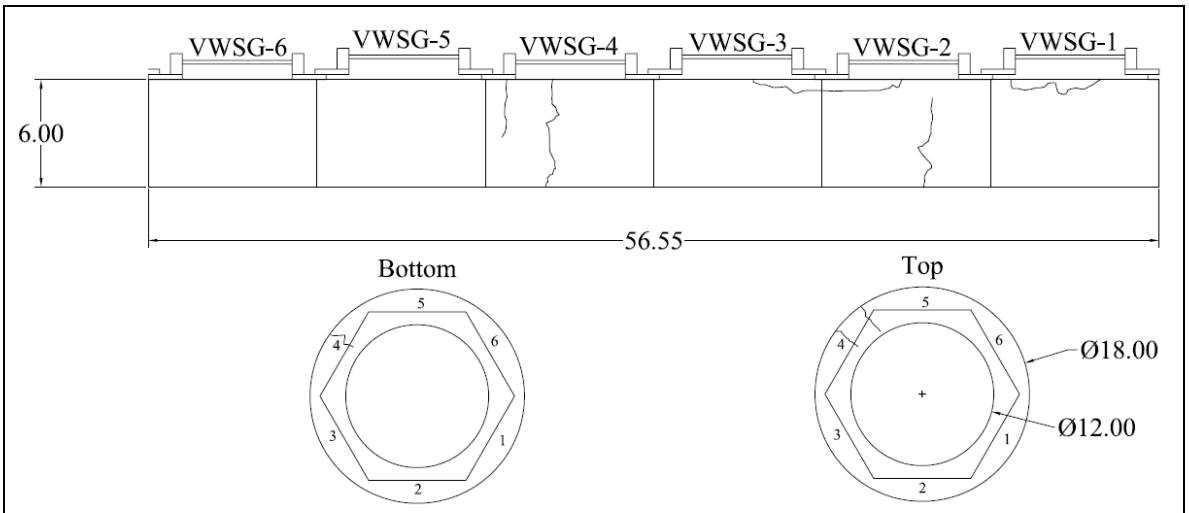

G1M1 – Ring Specimen 1 – Crack Drawings

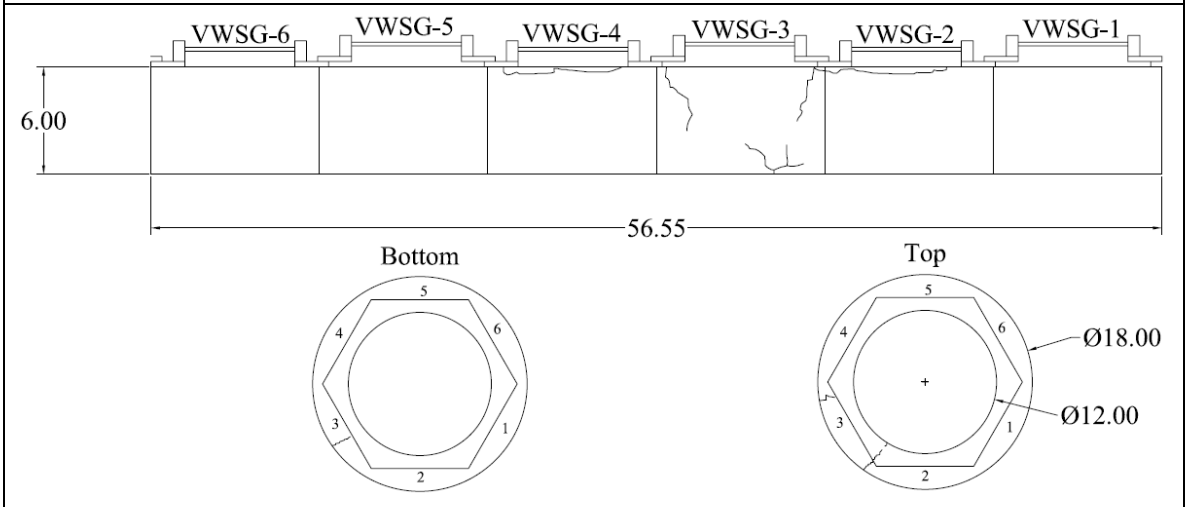

G1M1 – Ring Specimen 2 – Crack Drawings

G1M2 – R408847

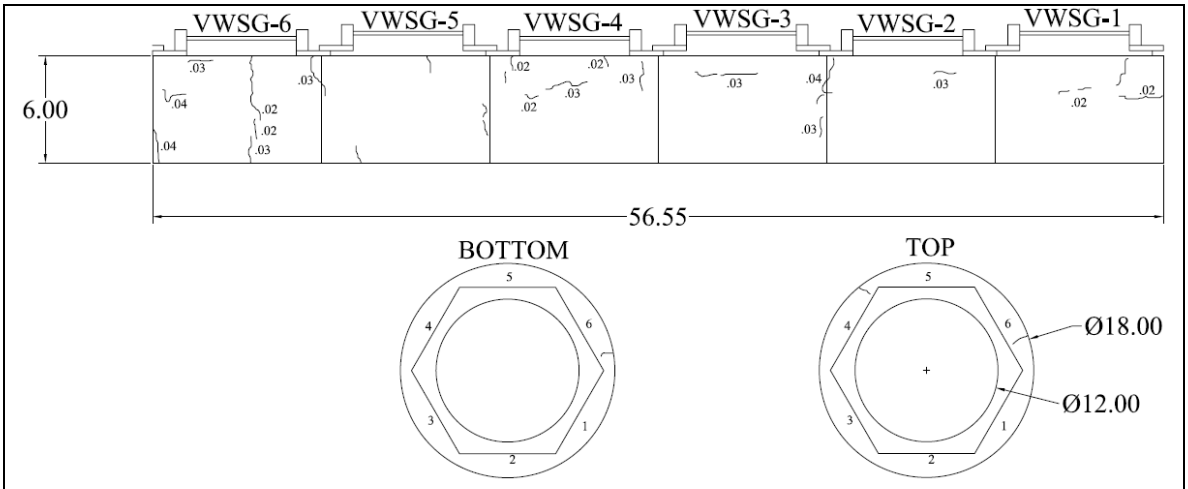

G1M2 – Ring Specimen 1 – Crack Drawings

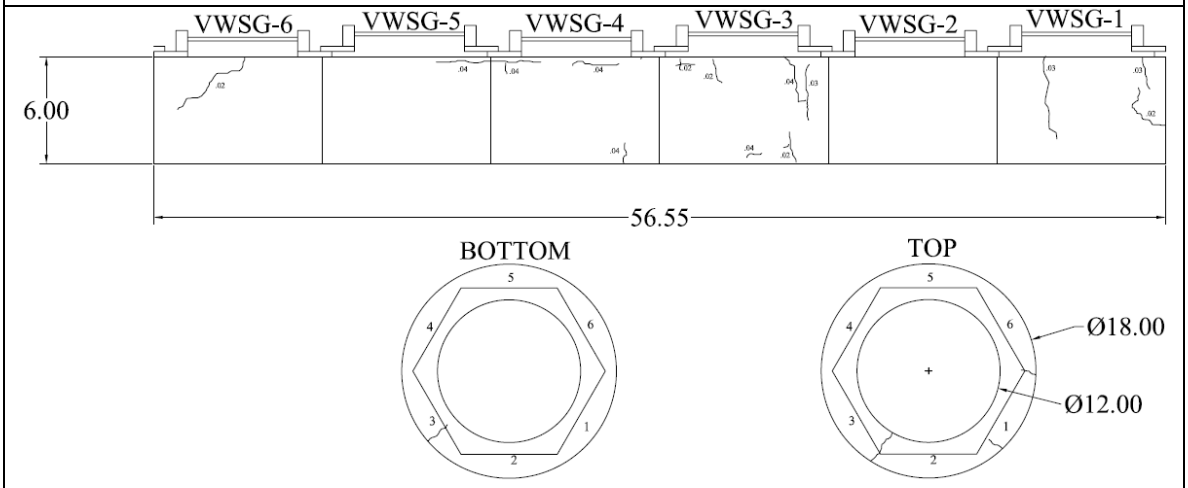

G1M2 – Ring Specimen 2 – Crack Drawings

G1M3 – R200578S

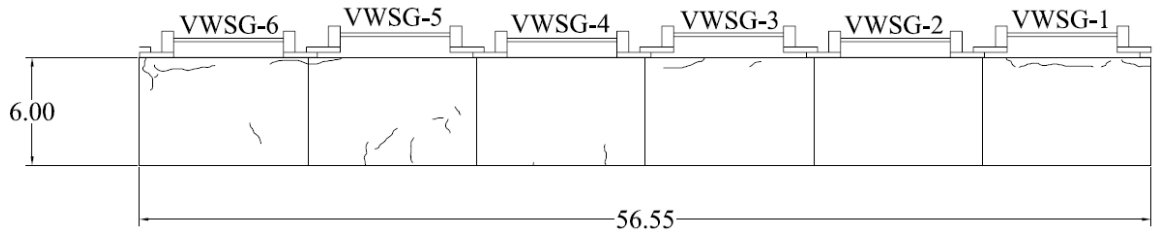

G1M3 – Ring Specimen 1 – Crack Drawings

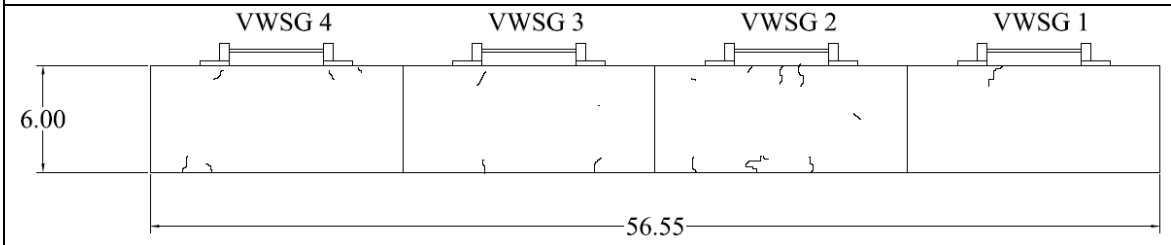

G1M3 – Ring Specimen 2 – Crack Drawings

GROUP 2 MIXES

G2M1 – R408850

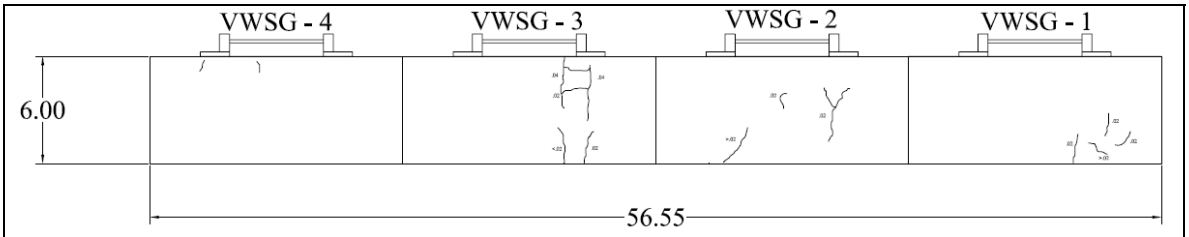

G2M1 – Ring Specimen 1 – Crack Drawings

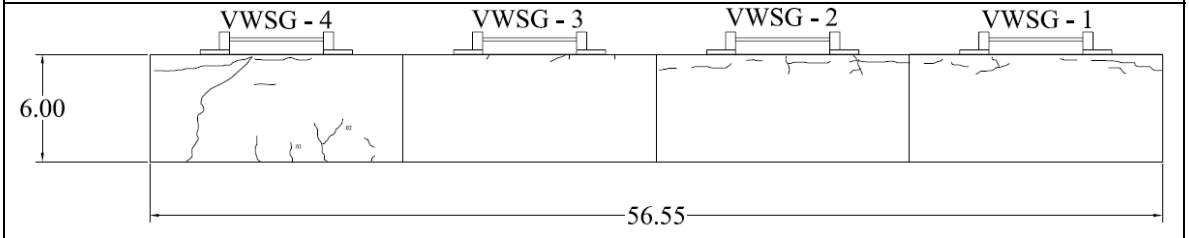

G2M1 – Ring Specimen 2 – Crack Drawings

G2M2 – R409239

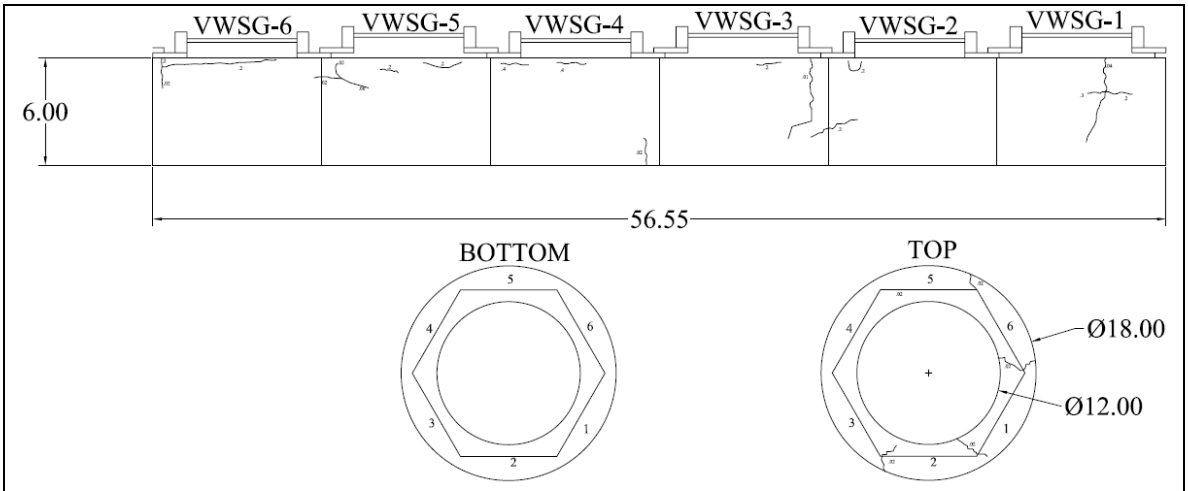

G2M2 – Ring Specimen 1 – Crack Drawings

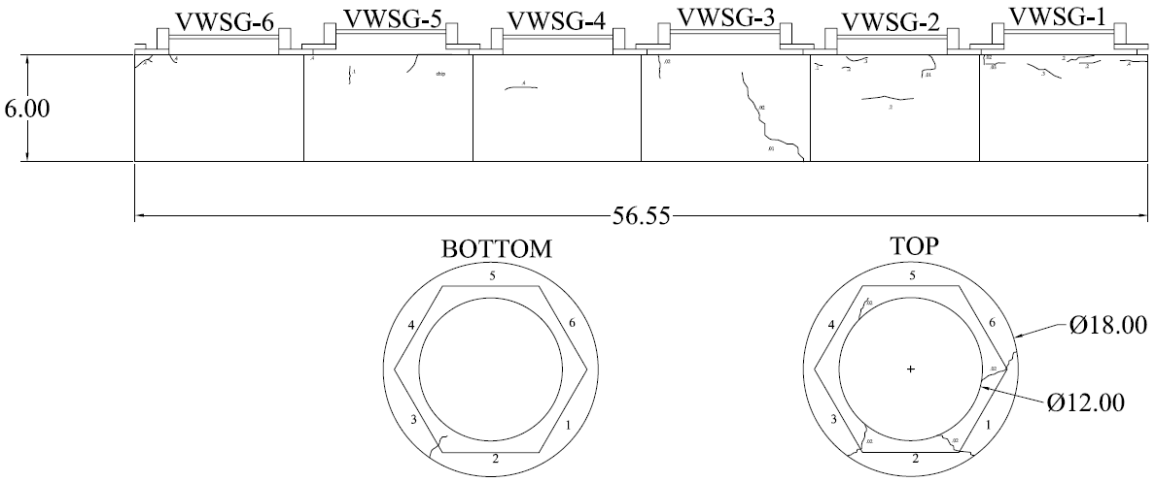

G2M2 – Ring Specimen 2 – Crack Drawings

G2M3 – R309497

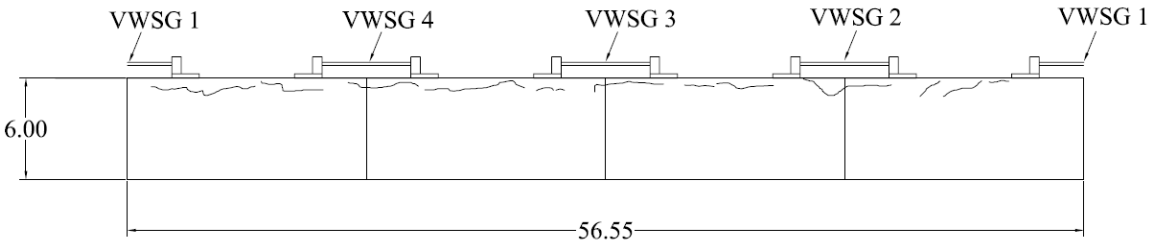

G2M3 – Ring Specimen 1 – Crack Drawings

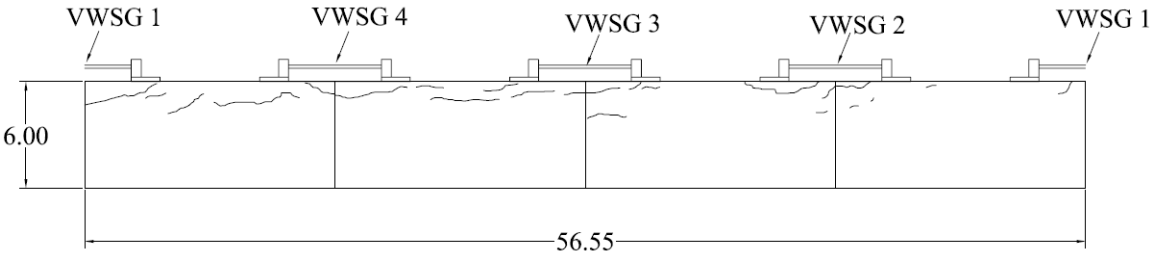

G2M3 – Ring Specimen 2 – Crack Drawings

G2M4 – R310682

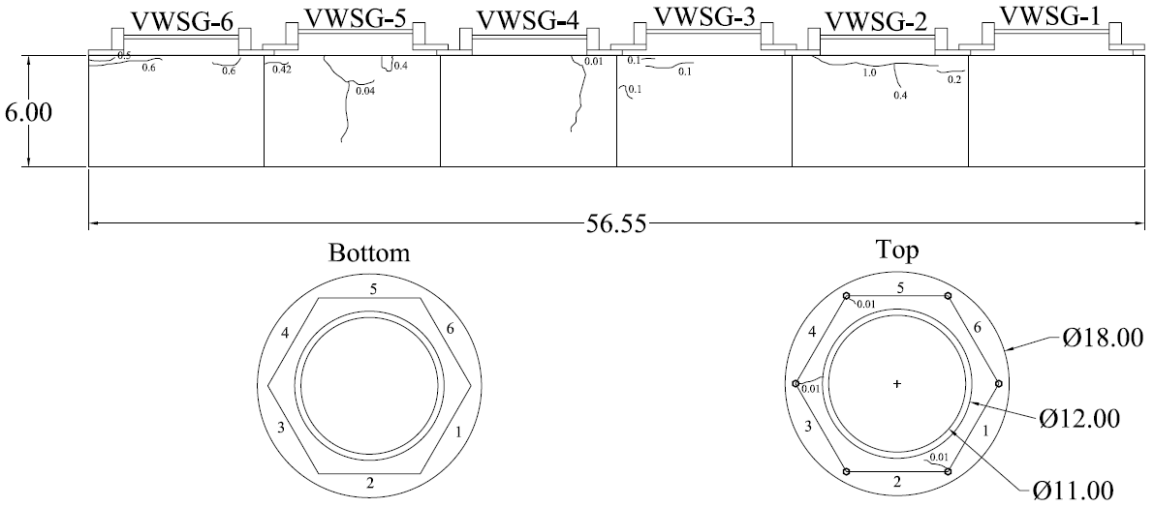

G2M4 – Ring Specimen 1 – Crack Drawings

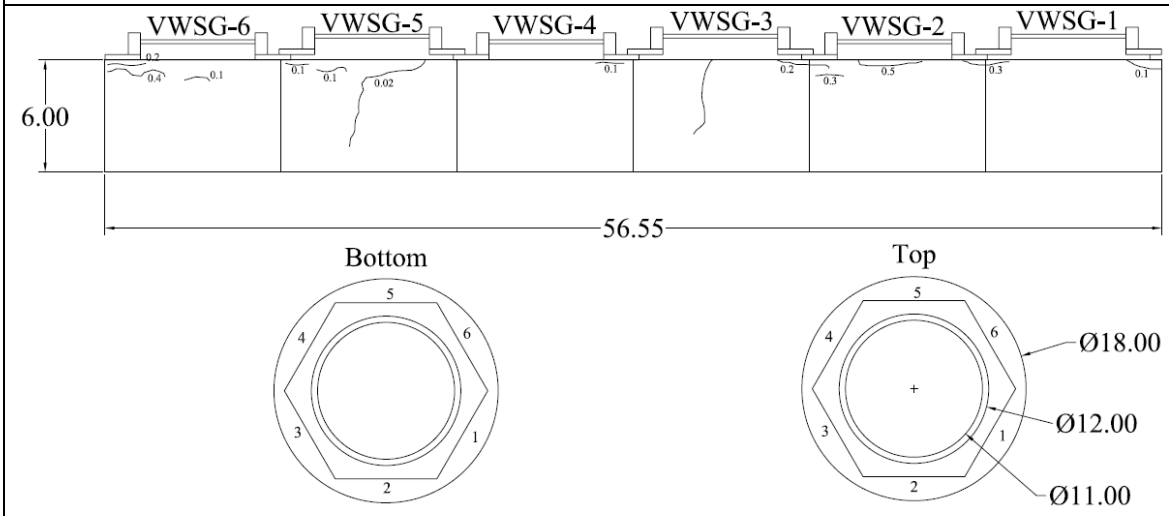

G2M4 – Ring Specimen 2 – Crack Drawings

G2M5 – R200626S

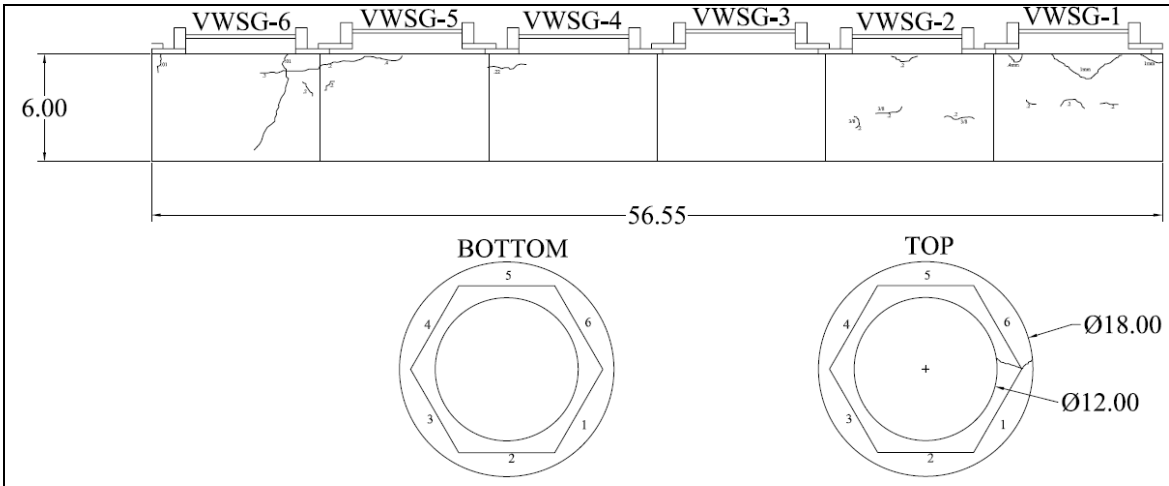

G2M5 – Ring Specimen 1 – Crack Drawings

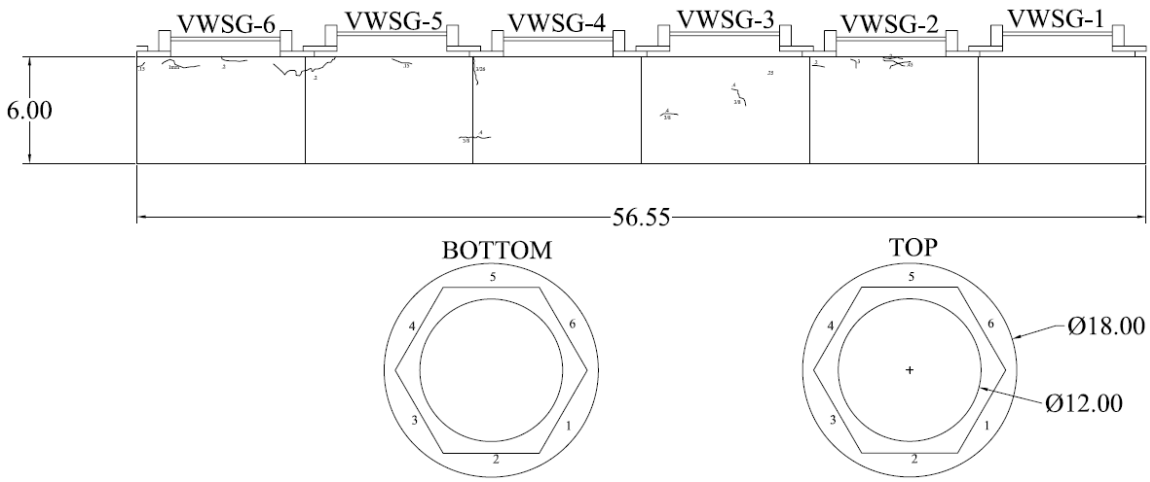

G2M5 – Ring Specimen 2 – Crack Drawings

G2M6 – R200633S

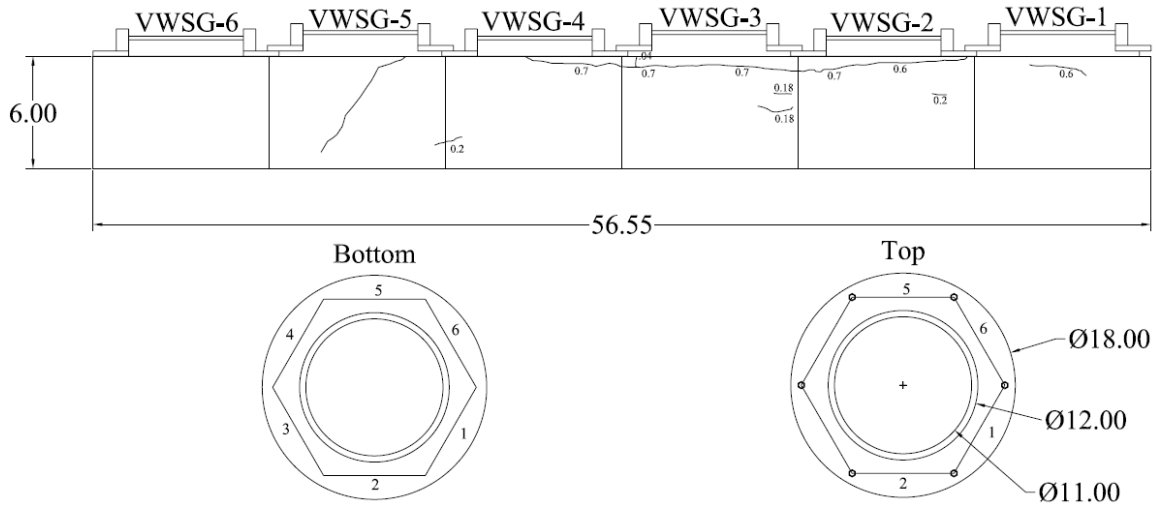

G2M6 – Ring Specimen 1 – Crack Drawings

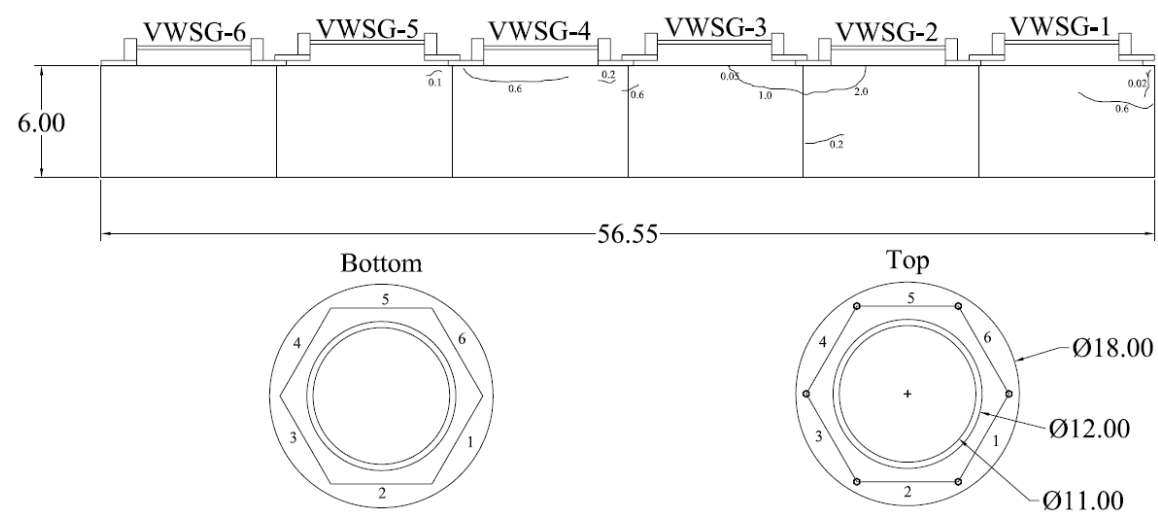

G2M6 – Ring Specimen 2 – Crack Drawings

GROUP 3 MIXES

G3M1 – R308163

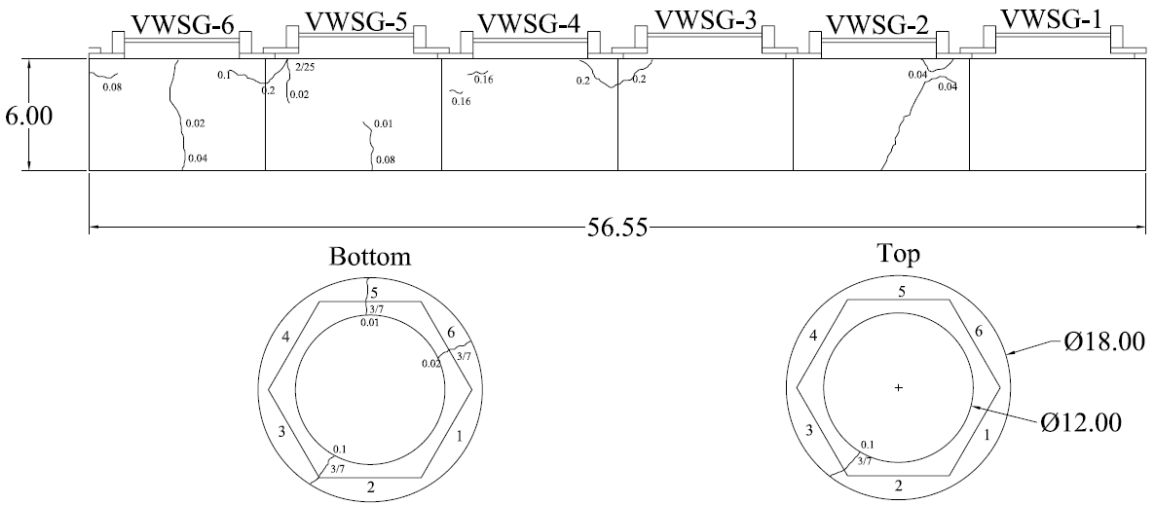

G3M1 – Ring Specimen 1 – Crack Drawings

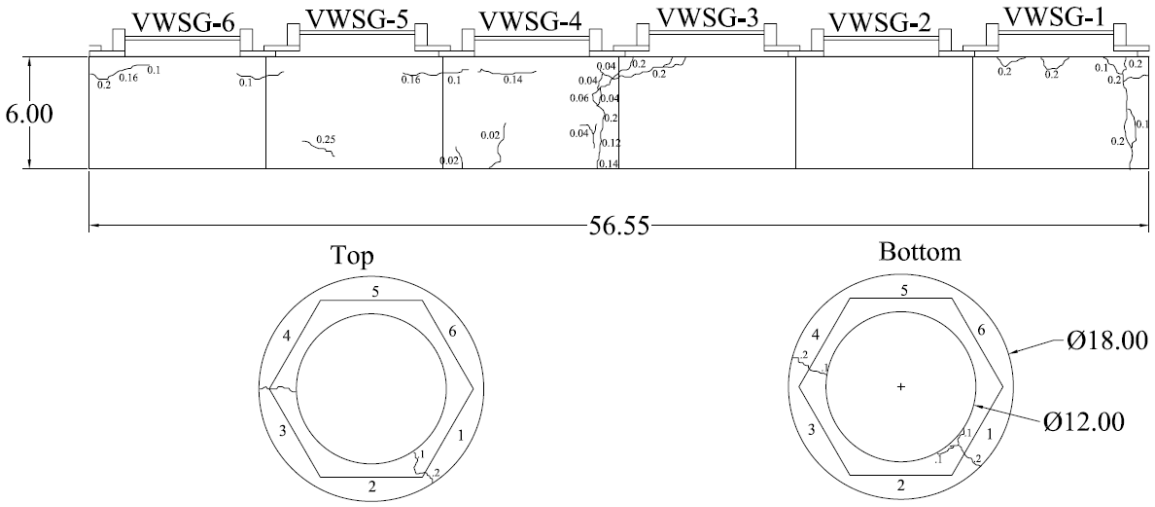

G3M1 – Ring Specimen 2 – Crack Drawings

G3M2 – R308278

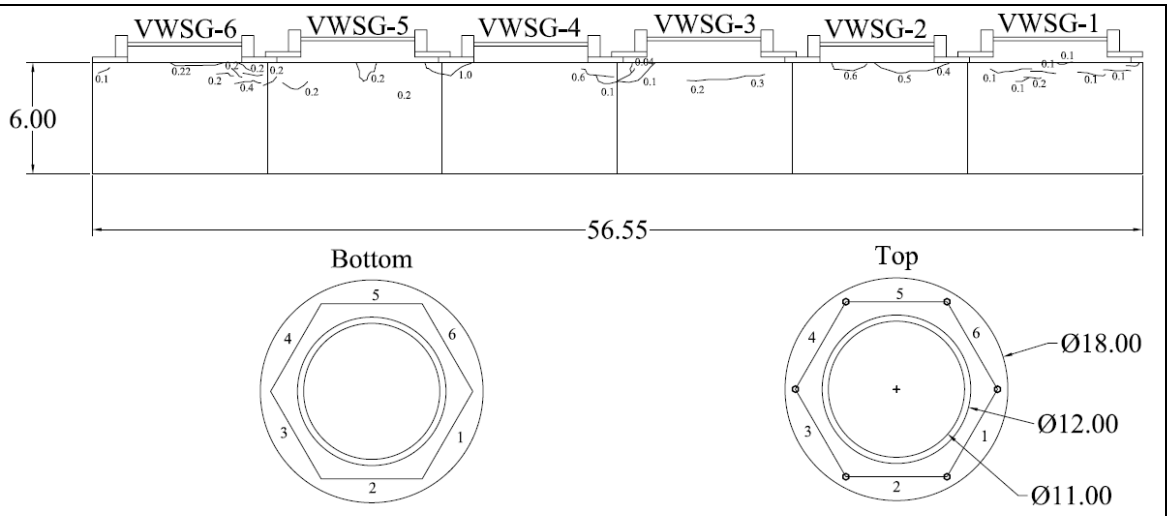

G3M2 – Ring Specimen 1 – Crack Drawings

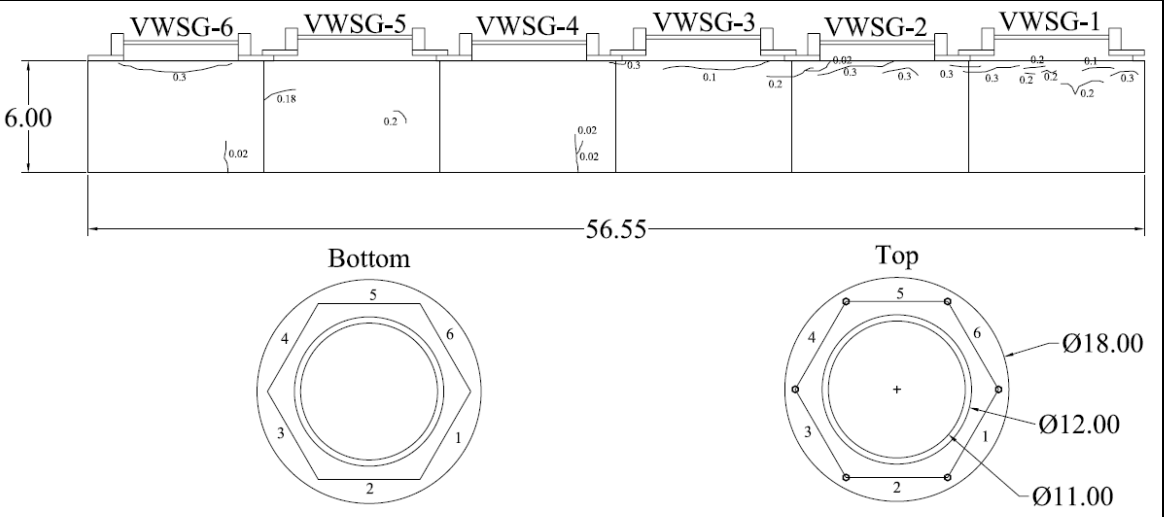

G3M2 – Ring Specimen 2 – Crack Drawings

GROUP 4 MIXES

G4M1 – R309495

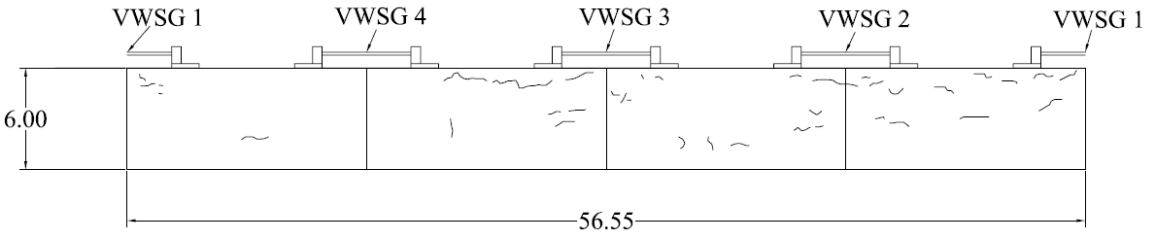

G4M1 – Ring Specimen 1 – Crack Drawings

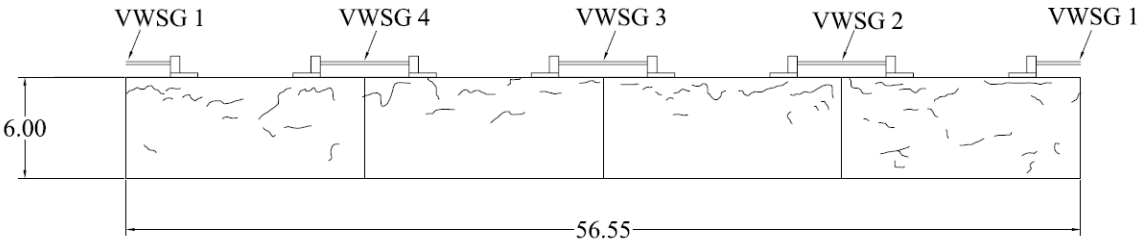

G4M1 – Ring Specimen 2 – Crack Drawings

G4M2 – R408844

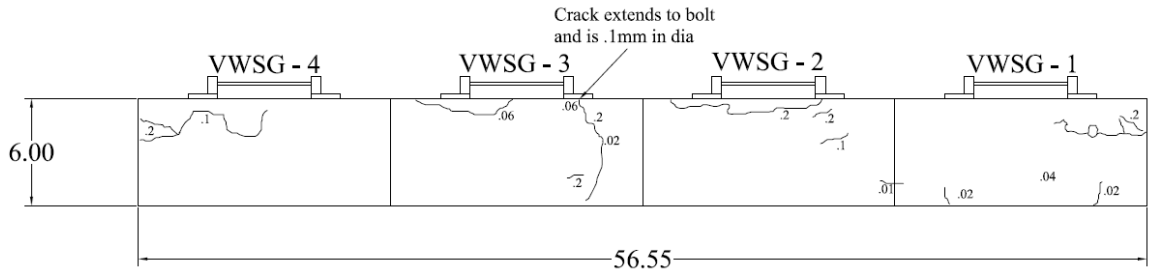

G4M2 – Ring Specimen 1 – Crack Drawings

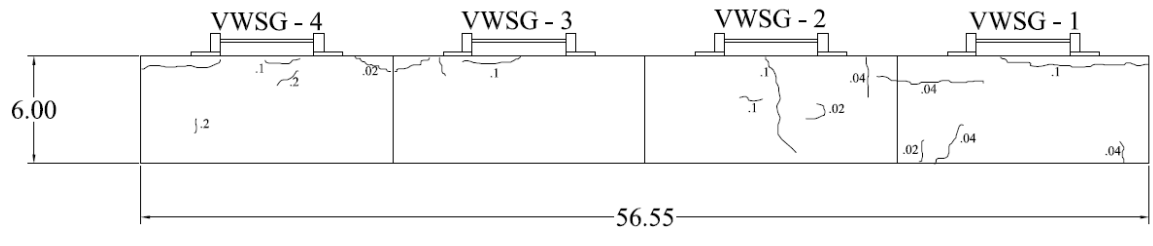

G4M2 – Ring Specimen 2 – Crack Drawings

G4M3 – R309496

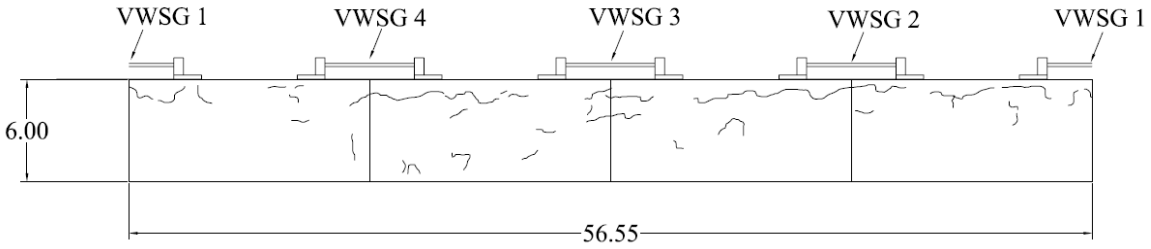

G4M3 – Ring Specimen 1 – Crack Drawings

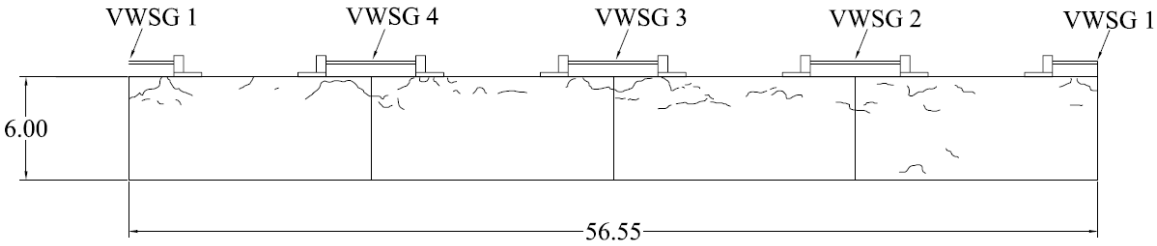

G4M3 – Ring Specimen 2 – Crack Drawings

G4M4 – R408694

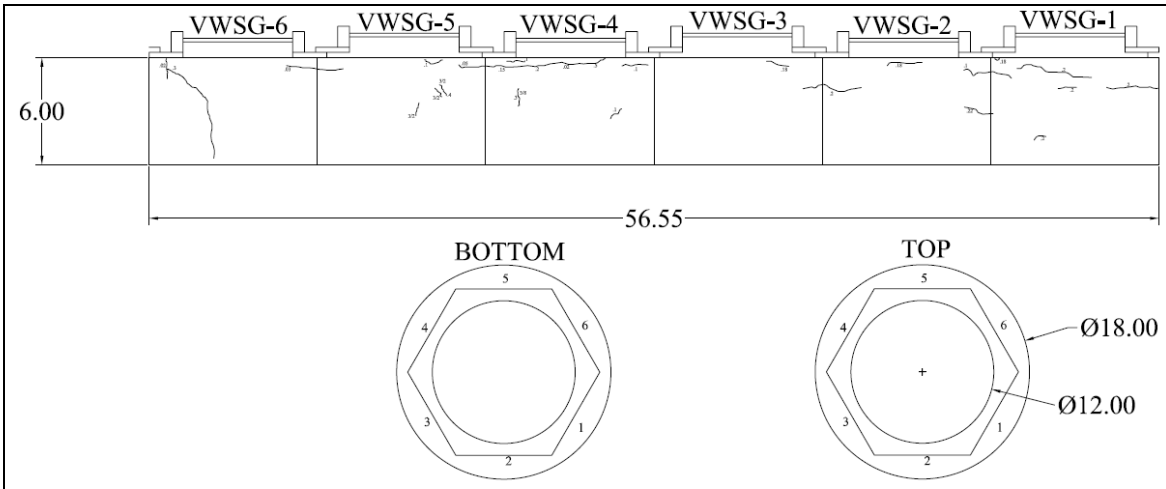

G4M4 – Ring Specimen 1 – Crack Drawings

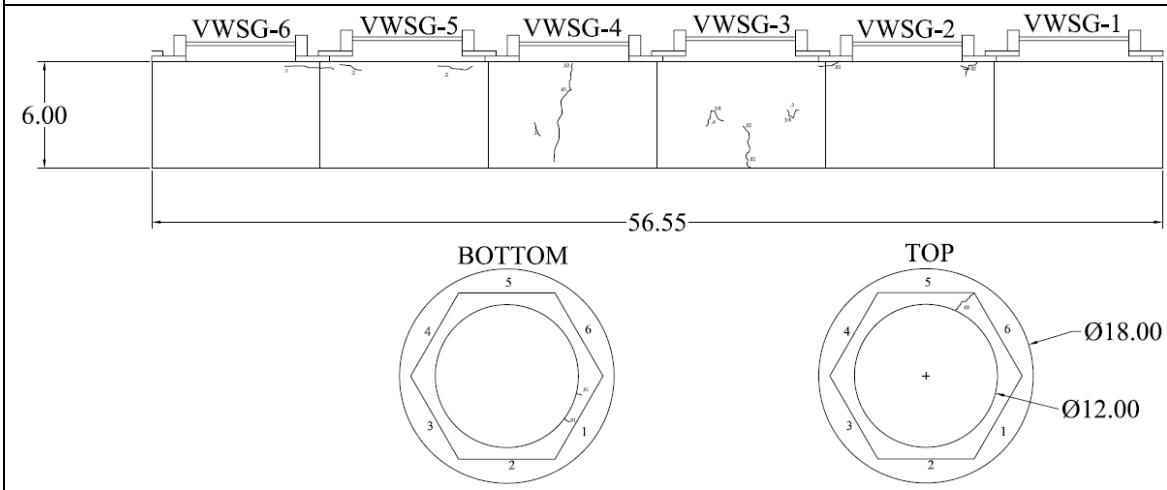

G4M4 – Ring Specimen 2 – Crack Drawings